# Control of Process Operations and Monitoring of Product Qualities through Generic Model-based Framework in Crystallization Processes

**Abdul Samad, Noor Asma Fazli Bin; Gani, Rafiqul; Gernaey, Krist V.; Sin, Gürkan**

*Publication date:*
2012

*Document Version*
Publisher's PDF, also known as Version of record

# Control of Process Operations and Monitoring of Product Qualities through Generic Model-based Framework in Crystallization Processes

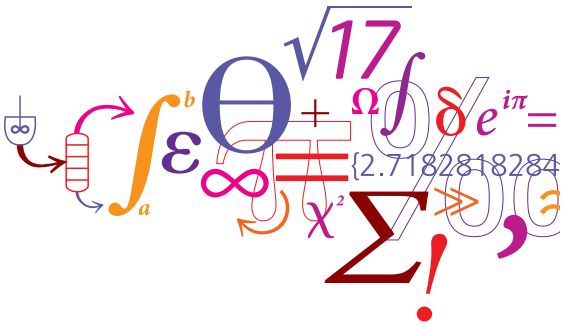

**Noor Asma Fazli Bin Abdul Samad**

Ph.D. Thesis

August 2012

DTU Chemical Engineering
Department of Chemical and Biochemical Engineering

# Control of Process Operations and Monitoring of Product Qualities through Generic Model-based Framework in Crystallization Processes

Ph. D. Thesis

Noor Asma Fazli Bin Abdul Samad

31 August 2012

Computer Aided Process-Product Engineering Center
Department of Chemical and Biochemical Engineering
Technical University of Denmark

DTU Chemical Engineering
Department of Chemical and Biochemical Engineering

Address: Computer Aided Process Engineering Center
Department of Chemical and Biochemical Engineering
Technical University of Denmark
Building 229
DK-2800 Kgs. Lyngby
Denmark
Phone: +45 4525 2800
Fax: +45 4588 4588
Web: www.capec.kt.dtu.dk

Print: J&R Frydenberg A/S
København
November 2012

ISBN: 978-87-92481-87-0

# Preface

This thesis is submitted as partial fulfillment of the requirements for the degree of Doctor of Philosophy (Ph.D.) in Chemical Engineering at the Technical University of Denmark (DTU). The project has been carried out at the Computer Aided Process-Product Engineering Center (CAPEC) at the Department of Chemical and Biochemical Engineering, from January 2009 until August 2012, under the supervision of Professor Rafiqul Gani, Associate Professor Krist V. Gernaey and Associate Professor Gürkan Sin. This work has been financed by the Ministry of Higher Education (MOHE) of Malaysia and Universiti Malaysia Pahang (UMP).

First and foremost, I am highly indebted to the my supervisors, Professor Rafiqul Gani, Associate Professor Krist V. Gernaey and Associate Professor Gürkan Sin for giving me the opportunity to work on a very interesting project and for providing the guidance and support throughout this project as well as for sparing a lot of their precious time for technical discussions and invaluable suggestions. Their valuable remarks and suggestions enabled me to learn a lot about crystallization process. A special thanks to my main supervisor Professor Rafiqul Gani for his continuous guidance, motivation, patience and always keep believing in myself as well as for providing numerous travels through conferences which open my mind to the insight of the international research.

I am thankful to all my co-workers and friends from the CAPEC as well as in the PROCESS for their encouragement and help on several occasions.

Finally, I am grateful to my family in Malaysia, especially my parent, Abdul Samad and Shamsiah, for their ambitions for me to get higher education. They always encouraged

and supported me, no matter how far we are from each other. Last but not least, my special thanks to my wife Suriyati Saleh for her love, her patience and her presence in my life was the driving force towards the succesful completion of this work.

Kgs. Lyngby, August 2012

Noor Asma Fazli Bin Abdul Samad

# Abstract

A generic and systematic model-based framework for the design of a process monitoring and control system to achieve the desired crystal size distribution (CSD) and crystal shape for a wide range of crystallization processes has been developed. This framework combines a generic multi-dimensional modelling framework, tools for design of set point profiles, for design of PAT (Process Analytical Technology) systems as well as option to perform the uncertainty and sensitivity analysis of the PAT system design. Through this framework, it is possible for a wide range of crystallization processes to generate the necessary problem-system specific model, the necessary set point using the extended analytical CSD estimator and the response surface method (RSM) and a PAT system design including implementation of monitoring tools and control strategies in order to produce a desired product with its corresponding target properties. In addition the impact and influence of input uncertainties on the predicted PAT system performance can be quantified, i.e. the risk of not achieving the target specifications of the crystal product can also be investigated. The application of the systematic model-based framework is divided into three sections: a) the application of the generic multi-dimensional modelling framework are highlighted: i) the capability to develop and further extend a batch cooling crystallization model is illustrated through a paracetamol case study, supplemented by a sucrose crystallization example to demonstrate how the framework supports smooth switching between chemical systems with a minimum modelling effort; ii) a potassium dihydrogen phosphate (KDP) case study is used to demonstrate how the model complexity can be increased, that is, by switching from a one-dimensional to a two-dimensional description; b) the systematic framework is used in a case study to design a

monitoring and control (PAT) system for a potassium dichromate and KDP crystallization processes to achieve the desired target CSD respectively; and c) Based on the PAT system design in b), the application of uncertainty and sensitivity analysis is then highlighted for the potassium dichromate and KDP crystallization process both in open-loop and closed-loop operation. In the case study, the impact of input uncertainties related to parameters of the nucleation and the crystal growth model on the predicted system performance has been investigated for a one- and two-dimensional CSD and it shown the PAT system design is reliable and robust under considered uncertainties.

# Resume på Dansk

En generelt og systematisk modelbaseret ramme til design af procesovervågnings- og kontrolsystem med henblik på at opnå en ønsket krystalstørrelsesfordeling og krystalform for et bredt spektrum af krystallisationsprocesser er blevet udviklet. Denne ramme kombinerer en generel multidimensionel ramme til modellering, værktøjer til design af indstillingsværdiprofiler, design af PAT (Process Analytical Technology)-systemer samt muligheden for at udføre usikkerheds- og sensitivitetsanalyse for disse PAT-systemer. Med denne ramme er det muligt at generere de nødvendige problem- og systemspecifikke modeller for et bredt spektrum af krystallisationsprocesser, det krævede sætpunkt gennem den udvidede analytiske estimator til krystalstørrelsesfordeling og "*Response Surface Method*", samt et design til PAT-systemer, der inkluderer implementeringen af værktøjer til overvågning og kontrolstrategier til at opnå et ønsket produkt, med dets tilsvarende ønskede egenskaber. Derudover kan virkning og indflydelse af usikkerheder i input på det forhåndsbestemte PAT-systems virkningsgrad kvantificeres, dvs. risikoen for ikke at opnå de givne specifikationer for krystalproduktet tilsvarende kan undersøges. Anvendelsen af den systematisk modelbaserede ramme er inddelt i tre afsnit: a) anvendelsen af den generelle modelbaserede ramme er fremhævet: i) muligheden for at udvikle og yderligere udvide en model for batch kølingskrystallisation illustreres ved et paracetamol case study suppleret med et eksempel med sakkarose for at demonstrere hvordan rammen understøtter glidende overgang fra et kemisk system til et andet med et minimum af modelleringsarbejde; ii) et kaliumdihydrogenphosphat (KDP) case study anvendes til at vise hvordan modellens kompleksitet kan øges ved at skifte fra en endimensionel til en todimensionel beskrivelse af systemet; b) den systematiske ramme

anvendes i et case study til at designe et overvågnings- og kontrolsystem til at opnå den ønskede krystalstørrelsesfordeling i henholdsvis en kaliumdichromat og en KDP krystallisationsproces; samt c) baseret på designet af PAT-systemet i b) fremhæves anvendelse af usikkerheds- og sensitivitetsanalyse for kaliumdichromat og en KDP krystallisationsprocesserne både i åben og lukket sløjfe. I det pågældende case study er virkningen af usikkerheder i input relateret til parametre i modellerne for kimdannelse og væksten af krystallerne på systemets forhåndsbestemte præstation undersøgt for både en- og todimensionel krystalstørrelsesfordeling og det viste PAT-sytemet designet er pålidelig og robust under betragtes som usikkerheder.

# Contents

# List of Tables

# List of Figures

# 1. Introduction

The chapter begins with an introduction (section 1.1) to give an overview of challenges in crystallization processes. This leads to the definition of the objective of this work, which is the development of a generic and systematic model-based framework for the design of a process monitoring and control (PAT) system for crystallization processes. Finally, the organization of this thesis is summarized.

## 1.1 Introduction

Crystallization processes have a wide application range as a solid-liquid separation technique in the chemical, the pharmaceutical and the food industries due to the fact that high quality crystalline products can be produced. For example in the chemical industries, crystallization is usually utilized in the manufacture of polymers, high value chemicals and as a purification and separation technique in the petrochemical industry. Furthermore, the crystallization of protein is one of the most common techniques used for drug design in the pharmaceutical industry (Shi et al., 2006). Due to special bioavailability and stability reasons, some pharmaceuticals are crystallized during the preparation of various drug delivery devices (Garcia et al., 1999; Mangin et al., 2006). In the food industries, the crystallization is often used as a purification and separation technique for the production of butter, cheese, salt and sugar (Myerson, 2002).

The main specifications of the crystal product are usually given in terms of crystal size, crystal size distribution (CSD), shape and purity. A challenge, however, in

many crystallization processes is how to obtain a uniform and reproducible CSD (Wibowo & Ng, 2001; Braatz, 2002). In order to achieve this specification, considerable efforts have been put in development of detailed models of crystallization processes in order to support the development of improved operation and control strategies. In terms of the model-based approaches, each time a crystallization process is studied, one usually develops the necessary specific model to cover the effects of the various operational parameters on the behavior of the crystals. The control strategies are then implemented as well, to allow simulation-based investigation of the control of the CSD, for example by using supersaturation control or temperature control (Braatz, 2002; Fujiwara et al., 2005; Aamir et al., 2009). Finally it is then checked whether the obtained CSD matches the target. If not, then the simulation is repeated for a different set point candidate until the target CSD is obtained. Although these approaches can yield a control strategy and a set point candidate that allows obtaining the target product with the desired CSD, they face quite some challenges that are worth mentioning. These challenges must be overcome, since they stand in the way for fully exploiting the crystallization model for development of monitoring or control strategies.

A first challenge, in terms of crystallization modelling, is that the necessary balance and constitutive equations need to be collected, for example from the literature, in order to develop a crystallization model that can be used to describe the CSD during the crystallization process. However, one of the challenges here is that most models reported in the literature (Fujiwara et al., 2002; Ma et al., 2002; Puel et al., 2003; Nagy et al., 2008a,b; Aamir et al., 2010; to name a few) are problem-specific, meaning that the models were developed with a certain crystal product in mind. As a consequence, a series

of different model assumptions and model types have been reported in the literature and applied to specific crystallization case studies. The result is that the model user often experiences difficulties to select the appropriate model. There is thus an obvious need for a generic crystallization model that can describe a crystallization operation, and from which the model user can – in a well-structured and transparent way – generate a large number of specific models for studying and optimizing different crystallization processes.

Such a problem-system specific model then needs to be analyzed and extended further with appropriate monitoring and control algorithms, in order to perform simulation-based design of control strategies. However there are two challenges that need to be considered before the monitoring and control tools can be implemented. When designing control strategies of crystallization systems, one problem is the design of suitable set point profiles that need to be achieved through an appropriate control system. Two approaches could be considered: a model-based design approach and a model free (or direct design) approach. In the model-based design approach, the set point profile is obtained using optimal control (Shi et al., 2006; Zhang and Rohani, 2003, 2004; Rawlings et al., 1993). This approach requires a detailed first principle model of the system with accurate model parameters, for example, for nucleation and growth kinetics, in order to ensure the successful implementation of the optimal control trajectory. It may not, however, be possible to obtain all the necessary model parameters and the performance of this approach depends on the model accuracy (Nagy et al., 2008a). In addition, some additional set point constraints need to be considered as well. On the one hand, if the crystallization process is operated close to the metastable limit, excessive nucleation may result because of the high supersaturation. On the other hand, in case the

set point profile is too close to the solubility line, it may lead to slow growth and long batch times (Fujiwara et al., 2005), resulting in a low overall productivity.

The model free approach uses a feedback control system to maintain the operation at its set point profiles where the set point profile is designed to lie within the metastable zone. Unlike the model-based approach, a detailed first principle model is not required, and a close-to-optimal set point profiles can be obtained relatively fast (Nagy and Braatz, 2012; Nagy et al., 2008a; Fujiwara et al., 2005). For example, the approach can be used to generate concentration set point profiles in the crystallization phase diagram and maintain the set point profiles using a proportional-integral (PI) control system. The set point profiles, which in fact consists of both the supersaturation and the total batch time needed to complete the crystallization operation, can be determined using an analytical CSD estimator as highlighted in the work of Nagy and Aamir (2012) and Aamir (2010). The analytical CSD estimator originally developed by Aamir (2010) is computationally efficient and can be applied for size independent and size dependent growth for one-dimensional crystallization processes. Although the one-dimensional crystallization process is widely used in many applications, the crystal shape used is somehow limited to a spherical or cubic shape, described by only one characteristic length. However, crystal particles may exhibit other shapes also. For example, some organic crystals produced by the pharmaceutical industry typically have shapes like a tetragonal prism that is described by more than one characteristic length, represented mathematically as a two-dimensional model (Briesen, 2006).

Once a set point profile has been designed, another problem is the design of a monitoring and control system (Process Analytical Technology (PAT) system) for the

crystallization process in order to keep the process at the proposed set point profile. Here a unique model-based methodology for PAT system design has been developed (Singh et al., 2009). This methodology involves the selection of critical process variables, the selection and placement of suitable monitoring and analysis equipments, and finally the coupling of monitoring and analysis tools for a control system to ensure that the selected critical process variables can be controlled. So far the design methodology has been applied in fermentation, tablet manufacturing and cheese production. However, in order to achieve a wide application range of the PAT system design methodology, and particularly for crystallization processes, it needs to be linked to a modelling framework for efficient generation of problem-system specific models as well as PAT system design.

Another challenge is that so far in model-based PAT system design, it has been assumed that the exact value of the model parameters is known, for example in the nucleation and crystal growth rate expressions (Singh et al., 2009; Samad et al., 2012a). These parameters are usually estimated from experimental data, often with considerable measurement errors which also implies a certain error on the estimated parameters. Consequently, there is a degree of uncertainty around the values of nucleation and crystal growth model parameters, which must be taken into account to design a reliable and robust PAT system. In the crystallization process, several approaches have been taken to deal with uncertainties by incorporating robustness in the control of crystallization (Nagy & Braatz, 2003; 2004; Nagy, 2009; Saengchan et al., 2011). Nagy (2009) proposed a robust on-line model-based optimization algorithm using distributional batch nonlinear model predictive control (NMPC) which considers the nucleation parameter uncertainties in the optimization problem formulation to determine the robust operating profiles. The

Monte Carlo simulations were then performed off-line by randomly sampling the uncertain parameter space and applying the robust operating profiles. By performing this approach, the variability in the product CSD has been significantly reduced. However the uncertainties around the crystal growth parameters are not considered in their work and the impact of individual contribution in the input uncertainties on the output are not quantified. In the work of Saengchan et al. (2011), improvement of batch crystallization control on potassium sulfate crystallization given uncertain kinetic parameters has been proposed using model predictive control (MPC).

Furthermore, the impact of parameter uncertainty and control implementation inaccuracies on the performance of optimal control trajectory are quantified in the work of Ma et al. (1999). These quantitative estimates are then used to decide whether more laboratory experiments are needed to provide more accurate parameter values or to define performance objectives for control loops that implement the optimal control trajectory. As a result, a robust feedback control whether using a simple PID controller or more advanced controller such as MPC is needed to deal with uncertainties and to ensure the desired crystal product is achieved. Before deciding for an appropriate approach to deal with uncertainties in crystallization process, foremost the impact of such model parameter uncertainties on the predicted system performance needs to be quantified and evaluated. Such an evaluation is useful to find out whether uncertainties considered may lead to a situation where the target specifications of the crystal product are no longer reached. The latter situation is of course not desirable in a pharmaceutical production process. This requires expansion of model-based methods with formal uncertainty and sensitivity analysis in a comprehensive way.

## 1.2 Objective of this work

The main objective of this work is to develop a generic and systematic model-based framework for the design of a process monitoring and control (PAT) system to achieve the desired CSD and crystal shape for a wide range of crystallization processes. In order to reach the main objective, several steps had to be taken. First of all, a generic modelling framework needs to be developed with the purpose of a generating problem-system specific model in an efficient way for a wide range of crystallization processes. Once the problem-system specific model is available, then there is a need to decide where the crystallization should be operated in order to obtain the desired crystal product consistently. Therefore the appropriate techniques for efficient determination of the set point need to be available as one of the steps in the design framework as well. This design framework should furthermore be able to link with the already available tools for PAT system design (Singh et al., 2009) to ensure the monitoring and control implementation. Furthermore, the tools needed to perform the uncertainty and sensitivity analysis should be included in the steps of the overall design framework where the impact and influence of the model parameter uncertainty on the predicted system performance can be investigated. Lastly, the overall design framework should also be generic, meaning that all the tools included and models are applicable to a wide range of crystallization processes.

## 1.3 Thesis organization

This PhD-thesis is organized in six chapters including this chapter (Introduction), where the motivation and the objective of the work are presented. Chapter 2 gives a review of the literature about crystallization processes in terms of the crystallization fundamentals, modelling issues, operation and control as well as an overview of the most common techniques available for the uncertainty and sensitivity analysis. The generic multi-dimensional framework for modelling of batch cooling crystallization is presented in Chapter 3. This chapter presents the model generation procedure incorporated within the modelling framework and highlights its use through the paracetamol, sucrose and potassium dihydrogen phosphate (KDP) crystallization case studies where the different features of the framework are highlighted: (1) efficient adaptation of the generated model to another chemical system; (2) handling model complexity, where the switching between a one-dimensional and a two-dimensional model are highlighted for the same chemical system.

In Chapter 4, the generic and systematic model-based framework for the design of a process monitoring and control (PAT) system is presented. The systematic design framework contains a generic crystallizer modelling tool box, a tool for design of set point profiles, a tool for design of a process monitoring and control (PAT) system as well as a tool for implementing uncertainty and sensitivity analysis. The application is highlighted through potassium dichromate and KDP crystallization process case studies to achieve a desired crystal CSD and shape. The features of the systematic design framework to perform uncertainty and sensitivity analysis are presented in Chapter 5. Here the framework for uncertainty and sensitivity analysis is presented first where it is

embedded within the systematic design framework. Based on the PAT system designed for the potassium dichromate and KDP crystallization process in Chapter 4, the uncertainty and sensitivity analysis is then conducted in this chapter and the risk of not achieving the desired CSD and crystal shape is quantified for both processes. Finally, Chapter 6 presents conclusions and directions for future work.

# 2. Literature Review

In crystallization processes, the need to achieve the desired crystal products and consistently improve the product quality requires an understanding of the fundamentals of crystallization processes. In order to achieve this, a model of the process is typically necessary. It can be a valuable tool for process analysis, design, monitoring and control (Ramkrishna, 2000). In this chapter, an overview of crystallization processes is presented in terms of the fundamentals of the crystallization process, and is followed by a review on modelling and solution approaches for the population balance equation. A summary of the recent literature related to the monitoring and control of crystallization processes is then provided. Lastly, the methods and tools needed to perform the uncertainty and sensitivity analysis are highlighted.

## 2.1 Fundamentals of crystallization process

The crystallization process is a separation process as it produces solid particles from the liquid or from the vapor phase. The fundamental driving force for crystallization of a specific chemical from a liquid solution is supersaturation, which is defined as the state where the concentration of that chemical is above the saturation concentration. The supersaturation profile obtained during the crystallization operation determines the CSD, the shape and the solid state of the product crystals (Myerson, 2002). This supersaturation is usually achieved by cooling, evaporation, antisolvent addition or a combination of the three. The most widely used method is by cooling a solution through indirect heat

exchange. Here the supersaturation created by the cooling method can be represented by a phase diagram as shown in Figure 2.1.

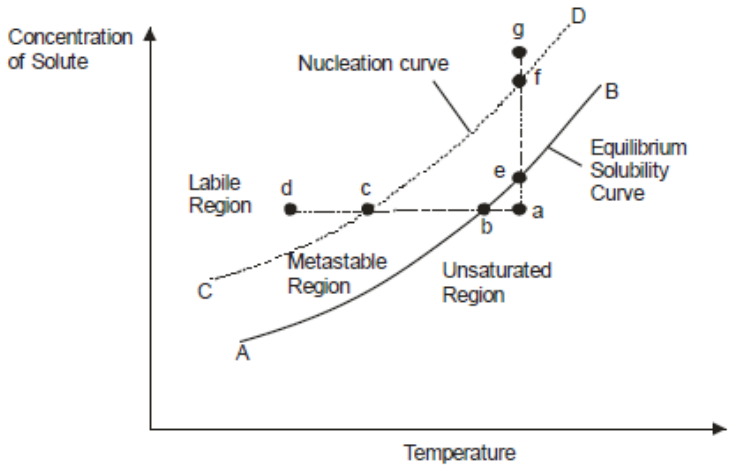


Figure 2.1 Supersaturation in crystallization processes (Smith, 2005)

Based on Figure 2.1, there are two curves, i.e. the solubility curve, also known as saturation curve (indicated as AB), and the metastable curve, also called the nucleation curve (represented as CD). In a cooling crystallization process, the solution initially starts in the unsaturated region at point 'a'. The solution is then cooled until it reaches the solubility curve at point 'b'. Now the solution becomes saturated. Further cooling is needed to cool the solution past the solubility curve, where it enters the metastable region. The solution is now in the supersaturated state. The metastable region is bounded by the solubility curve and the metastable curve. This is the region where the crystals will start to grow. Basically the solute in the solution is transferred to the crystal particles and thus the crystals will grow into larger particles. However, it is essential to keep the crystallization to operate within the metastable zone. If the solution is cooled until it

reaches point ‘c’ and the labile region at point ‘d’, then the solution will nucleate spontaneously. Here an excessive nucleation will occur which will result into the production of relatively small crystals which is not preferable in most crystallization processes.

Another method to generate a supersaturation is by using evaporation. Unlike the cooling method where the crystals will grow by capturing solute molecules from the solution, the solvent in the solution is removed gradually in the evaporation method and as a consequence the solute concentration is increased. This can be shown in Figure 2.1 where the solution originally at point ‘a’, reaches saturation at point ‘e’ and finally enters the metastable region by slowly removing the solvent by evaporation. The same concept used in the cooling crystallization is applied where the solution must be kept in the metastable region to avoid excessive nucleation occurring beyond point ‘f’.

In the antisolvent addition method, the supersaturation can be created by adding an extraneous substance (antisolvent) into the solution. Here the solute is crystallized from a primary solvent by the addition of a second solvent (antisolvent) in which the solute is relatively insoluble. Usually the antisolvent is selected based on several criteria such as: (1) the ability to be miscible with the primary solvent; (2) the ability to change the solubility of the solute in the primary solvent; and (3) the ability to modify the polarity where it should be different from the primary solvent polarity. Usually the antisolvent crystallization is conducted under low operating temperature which is important for thermally sensitive products. However, there are disadvantages using this technique which include the added unit for the separation of this extraneous material which can add complexity to the solution as well as increase cost.

Once the solution has reached the supersaturation condition, the solution starts to crystallize where there are two phenomena occurring which are nucleation and crystal growth. The nucleation is considered as a birth of new crystals and the crystal growth involves the growth of these crystals to larger sizes. In addition, there are also other phenomena which serve the same purposes as nucleation and crystal growth. The first one is called agglomeration, where the crystal may merge together with other crystal particles which results into larger crystal sizes. The other one is breakage which can occur due to the collision of crystals with each other. These are the phenomena that are very important to understand when developing a model of a specific crystallization process.

### 2.1.1 Nucleation

Usually the nucleation is classified into primary and secondary nucleation. The primary nucleation occurs in the absence of crystalline surfaces and is more prevalent in the unseeded crystallization (Myerson, 2002). The primary nucleation can also be categorized into homogeneous and heterogeneous primary nucleation. The homogeneous primary nucleation occurs in the pure bulk solution. It is determined by the formation of stable nuclei in a supersaturated solution, which means molecules of solute come close together to form clusters in an arranged order. Meanwhile the heterogeneous primary nucleation is usually induced by the presence of dissolved impurities. Nucleation in a heterogeneous system generally occurs at a lower supersaturation than a homogeneous nucleation (Mullin, 2001). Secondary nucleation normally occurs due to the presence of crystals in the supersaturated solution in case of the seeded crystallization. It can also be

induced by contact of crystals with an external surface (e.g. walls, impellers, etc.), initial breeding, macro-abrasion, dendritic and fluid shear. As a result, there are many efforts to model the nucleation phenomena and some of the commonly used models are shown in Table 2.1. Most of the models can be applied with both the normal and the relative supersaturation ( $S$ ).

Table 2.1 Overview of models used to represent the nucleation

| Mechanisms | Model | References | Remarks |
|---|---|---|---|
| Primary nucleation | $B_{n,1} = A_{pn} \exp\left( -\frac{B_{pn}}{\ln\left(\frac{c}{c^{sat}}\right)^2} \right)$ | Marchal et al. (1988) | |
| | $B_{n,1} = k_b S^b$ | Mullin (2001) | |
| Secondary nucleation | $B_{n,2} = k_b M_c^j S^b$ | Choong and Smith (2004) | |
| | $B_{n,2} = k_b M_c^j S^b N_{rpm}^p$ | Quintana-Hernández et al. (2004) | Effect of agitation is included |
| | $B_{n,2} = k_{b0} \exp\left(-\left(\Delta E_b / RT\right)\right) S^b M_c^m$ | Ouiazzane et al. (2008) | Temperature dependent |

### 2.1.2 Crystal growth

As mentioned earlier the new crystals will gradually develop towards larger sizes due to crystal growth phenomena. The crystal growth has a significant impact on the size of crystal particles that is achieved by the end of the crystallization operation. The growth of a crystal is often described by the change of a certain dimension, particularly the characteristic length of the crystal with time. This is called the linear growth rate and has dimensions of length per unit of time. However the most common

theory used for describing the crystal growth rate is the diffusion-reaction theory. Based on this theory, the crystal growth involves two main steps. The first step is the diffusion process whereby the solute molecules are transported from the bulk of the fluid phase to the solid phase. It is followed by the reaction phase where the solute molecules arrange themselves into the crystal lattice (Myerson, 2002). Based on these theories, Table 2.2 shows the empirical models that are widely used to represent the crystal growth.

Table 2.2 Overview of models used to represent the crystal growth

| Mechanisms | Model | References | Remarks |
|---|---|---|---|
| Size independent growth | $G = k_g S^g$ | Choong and Smith (2004) | |
| | $G = k_{g0} \exp\left(-\left(\Delta E_g / RT\right)\right) S^g$ | Ouiazzane et al. (2008) | Temperature dependent |
| | $G = k_g S^g N_{rpm}^q$ | Quintana-Hernández et al. (2004) | Effect of agitation is included |
| Size dependent growth | $G = k_g S^g \left(1 + \gamma L\right)^{pd}$ | Aamir et al. (2010) | |
| | $G = \eta_r \frac{k_g MM k_r}{3\rho_c k_v} S^g$<br>Effectiveness factor:<br>$\left[\frac{k_g}{k_d}\left(c - c^{sat}\right)^{g-1}\right]\eta_r + \eta_r^{1/g} - 1 = 0$<br>Mass transfer coefficient:<br>$k_d = \frac{D}{L}\left[2 + 0.47\left(\frac{L^{4/3}\varepsilon^{1/3}}{v}\right)^{0.62} \left(\frac{Diam}{Diam_T}\right)^{0.17} \left(\frac{v}{D}\right)^{0.36}\right]$ | Marchal et al. (1988) | Expression for the growth rate developed is based on the assumption of a film model. |

### 2.1.3 Agglomeration and breakage

Agglomeration is a particle size enlargement process by which fine particles are joined in an assembly e.g. within a suspension crystallization process (Jones, 2002). There are two main types of agglomeration, i.e. of primary and secondary agglomeration. In the primary agglomeration, the crystalline particles undergo a form of mal-growth, related to their crystallography and comprise individual crystals within a structure of parallel units, dendrites or twins. Secondly, crystals suspended in liquids may collide induced by the flow and join together i.e. aggregate to form a larger particulate entity which may subsequently be disrupted and redisperse or fuse to form a secondary agglomerate (Jones, 2002). Meanwhile, breakage is the particle formation that occurs based on the collision between crystal particles, and the collision of the crystal particles with the walls or the impeller. This collision then results into new crystal particles that are smaller and of varying size.

Some efforts have been made to model the agglomeration and breakage. The agglomeration model developed by Marchal et al. (1988) is based on the assumption that the agglomeration mechanism can be considered as a chemical reaction between particle sizes. The final agglomeration rate expression per size domain is based on the intrinsic rate, function of the number of collisions per time and volume unit and of the supersaturation. The breakage rate has also been modelled similar to agglomeration, except that the crystals are supposed to break up only into two smaller ones. In the work of Quintana-Hernández et al. (2004), the production-reduction term has been used to represent the agglomeration and breakage. This term is based on the empirical model to measure the global effect of birth and death of crystals due to agglomeration and

breakage and represented as a function of a kinetic constant, the supersaturation, the total mass of crystals formed and the agitation intensity. The models for agglomeration and breakage are summarized in Table 2.3.

Table 2.3 Overview of models used to represent the agglomeration and breakage phenomena

| Mechanisms | Model | References | Remarks |
|---|---|---|---|
| Production-reduction rate | $\alpha = k_{ab} S^{ab} M_c^k N_{rpm}^r$ | Quintana-Hernández et al. (2004) | Represent the birth and death rates generated by agglomerati-on and breakage of crystals. |
| Agglomerati-on rate | $B_{Agg,i} = \sum_{l=1}^{N(N+1)/2} \nu_{est(l,i)} r(l)$<br>Overall stoichiometric coefficient:<br>$\nu_{est(l,i)} = \left( \frac{S_m^3 + S_n^3}{S_q^3} \right) \delta_{i,q} - \left( \delta_{i,m} + \delta_{i,n} \right)$<br>Intrinsic rate of agglomeration of rank *l*:<br>$r(l) = k_a^{'} S_m \left( 1 + \frac{S_n}{S_m} \right)^2 N_{rpm} Diam.$<br>$f\left( \frac{S_n}{S_m} \right) \left( 1 - \frac{\left( S_n + S_m \right)^2}{\lambda_e^2} \right) k_d \left( c - c^{sat} \right)$<br>$\times N_n N_m \left( S_m - \delta \right) H \left( \lambda_e - S_n - S_m \right)$<br>Relative shape function of crystals:<br>$f\left( \frac{S_n}{S_m} \right) = \frac{4\left( 1 + S_n/S_m - \sqrt{\left( S_n/S_m \right)^2 - 1} \right)}{1/3 + S_n/S_m - \sqrt{\left( S_n/S_m \right)^2 - 1}}$ | Marchal et al. (1988); Costa et al. (2005) | The net rate of particle production by agglomerati-on in the $i^{th}$ class |

| | | | |
|---|---|---|---|
| | $-\left(S_n/S_m-\sqrt{(S_n/S_m)^2-1}\right)^2$<br>$\times\left(2(S_n/S_m)/3+\sqrt{(S_n/S_m)^2-1}/3\right)$<br>Lagrangian microscale:<br>$\lambda_e=0.3\pi N_{rpm}Diam\left(\frac{60v}{10\varepsilon}\right)^{0.5}$ | | |

## 2.2 Modelling of crystallization process

In order to represent the crystallization process for analysis, design, monitoring and control, appropriate models covering the effects of the various operational parameters on the behaviour of the crystal particles are necessary. Crystallization models generally involve three types of dynamic balance equations: population, mass and energy. These balance equations are combined with a set of constitutive equations describing phenomena such as, the nucleation, crystal growth as well as saturation equilibria and mass and heat transfer involved with the crystallization process. The type of population balance equation (PBE) employed is usually a hyperbolic partial differential equation, which also includes the crystallization kinetic phenomena. For a well-mixed batch crystallizer in which the crystals have two characteristic lengths, the process is described by a two-dimensional PBE (Hulburt and Katz, 1964; Randolph and Larson, 1988):

$$\frac{\partial f_n(L_x,L_y,t)}{\partial t}=-\frac{\partial f_n(L_x,L_y,t)G_x(L_x,L_y,c,T)}{\partial L_x}-\frac{\partial f_n(L_x,L_y,t)G_y(L_x,L_y,c,T)}{\partial L_y}+(B-D) \tag{2.1}$$

Where $f_n$ is the CSD, $L_x$ and $L_y$ refer to characteristic length and width scales, $G_x$ and $G_y$ represent the crystal growth rate for each characteristic length and width scale, $c$ is the solute concentration and $T$ is the crystallizer temperature. The terms $B$ and $D$ in Equation (2.1) are the birth and death rate of crystals that can be represented as:

$$(B-D) = B_{nuc} + B_{agg} - D_{agg} + B_{br} - D_{br} \tag{2.2}$$

Where $B_{nuc}$, $B_{agg}$ and $B_{br}$ are the birth rates due to nucleation, agglomeration and breakage respectively, while $D_{agg}$ and $D_{br}$ represent the death rates caused by agglomeration and breakage. Equation (2.1) can be transformed into a one-dimensional form if the crystals only have one characteristic dimension (characteristic length). In this case, Equation (2.1) takes the form:

$$\frac{\partial f_n(L_x,t)}{\partial t} = -\frac{\partial f_n(L_x,t) G_x(L_x,c,T)}{\partial L_x} + (B-D) \tag{2.3}$$

Equations (2.1) and (2.3) represent the generic equations for a two- and a one-dimensional PBE, respectively. Usually the solution of the generic PBE is computationally expensive and requires complex numerical solution techniques. Numerous solution techniques have been introduced in the literature and a review of the numerical solution methods of the PBE is provided by Ramkrishna (2000) and Costa et al. (2006). The most common of these can be classified into two categories: standard

method of moments and discretization (method of classes) techniques. The standard method of moments reported by Hulburt and Katz (1964) and later by Randolph and Larson (1988) is very popular, and its application has been reported by many researchers (Fujiwara et al., 2002; Shi et al., 2006; Paengjuntuek et al., 2008; Nagy et al., 2008b; to name a few). This method converts the partial differential equation (PDE) representing the population balance into a set of coupled ordinary differential equations (ODEs) for the *n* moments considered. The advantage of this method is the ease of solution, as ODE solvers are readily available. Moreover, the method can be applied in one- or two-dimensional forms (Hulburt and Katz, 1964). With the standard method of moments, however, the population balances carrying size dependent growth functions as well as agglomeration and breakage terms may cause convergence problems because of closure problems with the respective moment equations (Gimbun et al., 2009). The latter can be avoided by employing instead, any of the different forms of the quadrature method of moments (Gimbun et al., 2009, Aamir et al., 2010).

Another technique to solve the PBEs is based on discretization, where the partial differential equations are sectioned along the size domains into finite classes. This method overcomes the problems encountered with the standard method of moments as it permits the discretization of the growth functions along the size domains. Furthermore, this method allows phenomena such as agglomeration and breakage to be incorporated within the solution of the PBEs. This method is pioneered by the works of Hounslow et al. (1988) and Marchal et al. (1988). In their work, Marchal et al. solved the PBEs representing the adipic acid crystallization taking into account the nucleation, size dependent growth and agglomeration. A disadvantage of this method is that the accuracy

of the simulated behaviour is dependent on the accuracy of the numerical solution which in turn is dependent on the selected number of discretization points and therefore, also on the computational effort required to solve the system of equations. However, with the availability of faster computers and more efficient numerical solvers, this problem can be overcome (Puel et al., 2003; Costa et al., 2005; and Abbas & Romagnoli, 2007).

Although the development of PBE based solution approaches has made a significant contribution to the modelling of crystallization processes, a comprehensive generic model capable of representing a wide range of crystallization processes cannot yet be found. Current literature points to many attempts to model different crystallization operations with emphasis on different issues such as CSD or crystallization kinetics. Also, most of the literature reporting on crystallization processes described by population balance models makes the underlying assumptions that attrition, breakage, agglomeration and aggregation of crystals could be neglected (Farrell & Tsai, 1994; Hu et al., 2005; Paengjuntuek et al., 2008). Some works on population balance modelling show that agglomeration and breakage can be considered in the modelling of the crystallization process (Quintana-Hernández et al., 2004; Costa et al., 2005). However, the kinetics considered in these models (Hu et al., 2005; Abbas & Romagnoli, 2007; Paengjuntuek et al., 2008) describe only the primary nucleation and size independent growth rates but do not consider the effect of agitation on crystallization. Clearly, it can be concluded that there are many different types of models with associated variations in their complexities making their selection difficult and their use confusing. Table 2.4 shows representative examples of the different model type variations that can be found.

Table 2.4 Examples of model type variations for batch cooling crystallization

| Dimension | Chemical system | Nucleation | Crystal Growth | Unseeded/Seeded | Agglomeration/Breakage | References |
|---|---|---|---|---|---|---|
| 1 | Sucrose | Secondary nucleation (effect of agitation is included) | Size independent growth | Seeded | Agglomeration and breakage | Quintana-Hernández et al. (2004) |
| 1 | Sucrose | Secondary nucleation (no agitation) | Size independent growth | Unseeded | No agglomeration | Ouiazzane et al. (2008) |
| 1 | Paracetamol | Secondary nucleation (no agitation) | Size independent growth | Unseeded | No agglomeration | Fujiwara et al. (2005) |
| 1 | Adipic acid | Secondary nucleation | Size dependent growth | Seeded | Agglomeration rate | Costa et al. (2005) |
| 1 | Potassium dichromate | Secondary nucleation | Size dependent growth | Seeded | No agglomeration | Aamir et al. (2010) |
| 2 | Potassium dihydrogen phosphate (KDP) | Secondary nucleation | Size dependent and independent growth | Seeded | No agglomeration | Ma et al., (2002); Qamar et al. (2007) |
| 2 | Hydroquinone | Primary and secondary nucleation | Size dependent growth | Seeded | No agglomeration | Puel et al. (2003) |

Based on the example in Table 2.4, it can be demonstrated that many attempts have been made to model the one-dimensional crystallization process. Only a few researchers have made an effort to model the crystallization process in the two-dimensional case. For example, Puel et al. analyzed the transient behavior of hydroquinone crystallization. They characterized each individual crystal as a parallelepiped with its length and then an identical width and depth. They used the method of classes to solve the two-dimensional population balance and further extended their work by including nucleation and crystal growth kinetics (Puel et al., 2003). By using the same particle shape characterization concept as Puel et al., the two-dimensional population balance for potassium dihydrogen phosphate (KDP) has been studied in the work of Ma et al. (2002), Briesen (2006) and Qamar et al. (2007). However, the main focus of their work is solely to develop an efficient solution technique to solve the two-dimensional population balance equations.

The main advantage of implementing the two-dimensional model is the ability to consider more complex crystal shapes compared to the one-dimensional model. In one-dimensional models, the population balance equations only consider one inner variable which represents the characteristic length as a measure for crystal size. This approach is undoubtedly used to obtain a required CSD but is limited only to the description of spherical or cubic crystals, i.e., crystal shapes that can be described by a single characteristic length. Organic crystals, however, have many crystal shapes that need to be described by more than one characteristic length (Briesen, 2006). Thus, in order to fully represent such crystal particles, higher dimensional models are necessary. That is, a

multi-dimensional population balance modelling approach, where two – or even three – characteristic lengths of a crystal can be considered, is needed.

Based on the review of the crystallization modeling field, it appears that no attempt has been made to model a one- and two-dimensional crystallization process for the same chemical system. All the work that has been reported so far has either been focused on the one- or the two-dimensional case study only. This is one of the gaps within crystallization modelling. The availability of a one- and a two-dimensional model for the same chemical system offers more opportunities to study the crystallization process. First, the comparison of crystal products can be done in terms of CSD and shapes. Here, the evolution of the CSD in the one- and two-dimensional case, and the size of the resulting crystal shapes can be observed and compared for both cases. Furthermore, the accurate information in terms of the total mass of solute that has been transferred from the solution to the crystal particles can be obtained and compared for the one- and the two-dimensional model.

## 2.3 Operation and control

The operation of crystallization processes is usually conducted within the metastable zone which is bounded by the solubility curve and the metastable curve as shown in Figure 2.2. The metastable zone specifies the default region for operating the crystallization process in order to avoid the occurrence of nucleation and produces acceptable crystals. The main challenge here is the determination of set point profiles for the supersaturation or temperature controller. The set point needs to be carefully designed in order to avoid the occurrence of excessive nucleation if the process is operated close to

the metastable limit or to prevent slow growth in case the process is operated near the solubility curve.

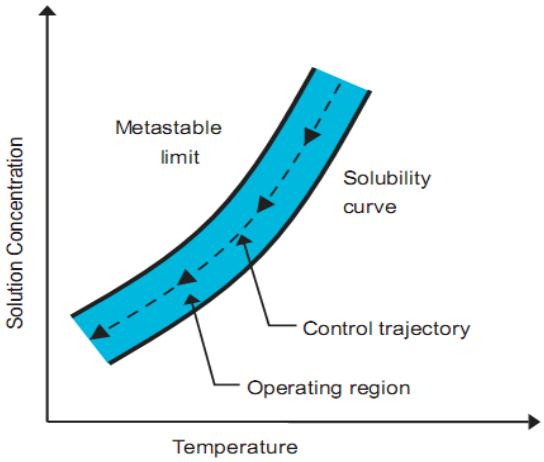


Figure 2.2 Operating region for a crystallization process (Fujiwara et al., 2005)

In the work of Aamir (2010) and Aamir et al. (2010), effort have been made to design the set point profile for a supersaturation controlled crystallization process which produces the target CSD at the end of the batch. Here the set point, which in fact consists of both the supersaturation set point and the total batch time, has been determined using an analytical CSD estimator. It is practical efficient considering that the initial seed distribution and growth kinetics for the crystallization process are known, the target CSD can be predicted easily. However the use of analytical CSD estimator is limited to the one-dimensional crystallization process only. Therefore, in order to have a wide application range the estimator needs to be extended to cover the two-dimensional case as well.

In order to keep the process at the proposed set point profile and achieve the desired crystal products, the critical variables need to be monitored and controlled. Therefore suitable monitoring tools are needed to monitor the critical variables and the controller needs to be available to control the critical variables by manipulating the necessary manipulated variables. Such tools are available in the model-based methodology for Process Analytical Technology (PAT) system design developed by Singh et al. (2009). The design procedure consists of 9 hierarchical steps involving the selection of critical process variables, selection of suitable monitoring tools/techniques and the implementation of control strategies to ensure that the selected critical process variables can be controlled in order to ensure the final product quality.

The methodology has been implemented into a software known as ICAS-PAT (Singh et al., 2010). An overview of the ICAS-PAT software is shown in Figure 2.3 where the knowledge base and the model library act as supporting tools. The knowledge base contains information on the process variables involved, the corresponding manipulated variables (actuators) and the list of the equipments used for measurement of data. Specifically for crystallization processes, the example of part of the knowledge base is shown in Figure 2.4. Meanwhile the model library contains a set of mathematical models for different types of processes, sensors and controllers. However, in order to achieve a wide application range of the PAT system design methodology, it needs to be linked to a modelling framework for efficient generation of problem-system specific models. Furthermore the creation of a larger model library and knowledge base for crystallization processes particularly, could play an important role in process control and product property monitoring.

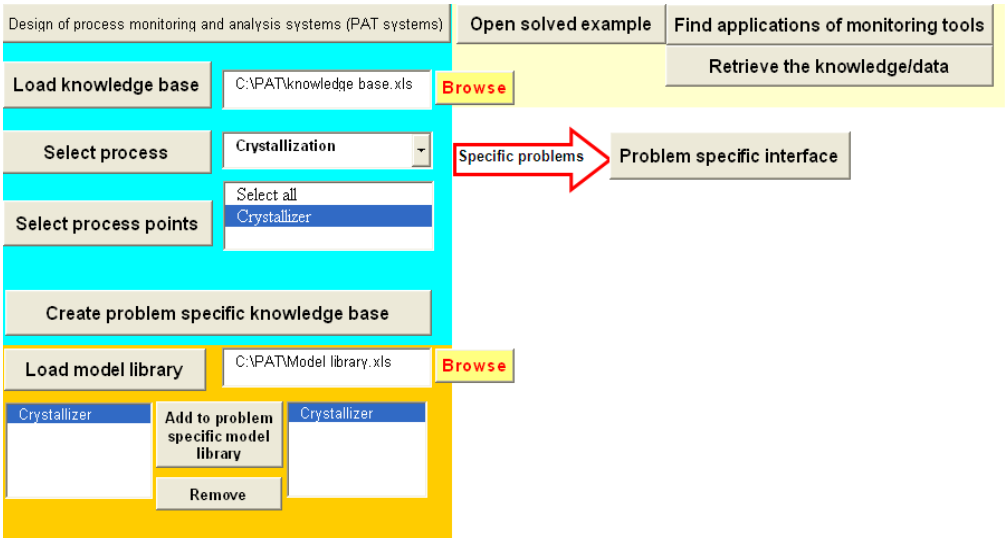


Figure 2.3 ICAS-PAT software overview

| Process | Process point | Process variables | Monitoring techniques | Monitoring tools | Accuracy | Precision | Lower operati | Upper operat | Respons | Resolutic | Sensitivit |
|---|---|---|---|---|---|---|---|---|---|---|---|
| Crystallization | Crystallizer | Particle size distribution (CSD) | FBRM | FBRM® C35 [171] | 0.010000 %' | 0.010000 % | 3.000000 µm | 3000.000000 µm | 1.000000 s | | |
| | | | | Lasentec® S400E | | | | | | | |
| | | | | Lasentec® D600L | | | | | | | |
| | | | | Lasentec® D600R | | | | | | | |
| | | | PVM | Lasentec® V819 with PVM® technology [172] | | | 2.000000 µm | 1000.000000 µm | | 2.000000 µm | |
| | | | LDS (Laser diffraction spectrometry) | LDS (Laser diffraction spectrometry) | | | | | 60.000000 min | | |
| | | | Ultrasonic spectroscopy | Ultrasonic spectroscopy | | | 0.010000 µm[68] | 1000.000000 µm | [68] | | |
| | | | Raman spectroscopy | Raman spectroscopy | | | | | | | |
| | | | Diffusing wave spectroscopy (DWS) | Diffusing wave spectroscopy (DWS) | | | | | | | |
| | | | Frequency-domain photon migration (FDPM) | Frequency-domain photon migration (FDPM) | | | | | | | |
| | | | Electroacoustic effects [65] | Electroacoustic effects [65] | | | | | | | |
| | | | Acoustic attenuation of sound waves [65] | Acoustic attenuation of sound waves [65] | | | | | | | |
| | | Supersaturation | ATR-FTIR [86] | ATR-FTIR [86] | | | | | | | |
| | | | NIR | AvaSpec-NIR256-1.7 | 0.170000 nm | 0.170000 nm | 900.000000 nm | 1750.000000 nm | 0.001100 s | 50.000000 n | 350.000000 |
| | | | | AvaSpec-NIR256-2.2 | 0.170000 nm | 0.170000 nm | 1000.000000 nm | 2200.000000 nm | 0.001100 s | 60.000000 n | 250.000000 |
| | | | | AvaSpec-NIR256-2.5 | 0.170000 nm | 0.170000 nm | 1000.000000 nm | 2500.000000 nm | 0.001100 s | 90.000000 n | 200.000000 |
| | | | | EPP 2000 Fiber Optic Spectrometer-NIR | 0.200000 nm | 0.200000 nm | 500.000000 nm | 1200.000000 nm | 0.002000 s | 0.800000 nm | |
| | | | | EPP 2000 Fiber Optic Spectrometer-NIR2 | 0.100000 nm | 0.100000 nm | 600.000000 nm | 1000.000000 nm | 0.002000 s | 0.400000 nm | |
| | | | | EPP 2000 Fiber Optic Spectrometer-NIR2b | 0.100000 nm | 0.100000 nm | 785.000000 nm | 1200.000000 nm | 0.002000 s | 0.400000 nm | |
| | | | | Antaris target blend analyzer | | | 1350.000000 nm | 1800.000000 nm | | 1.600000 nm | |
| | | | | NIR 256-2.1 | | | 900.000000 nm | 2100.000000 nm | 0.001000 s | 12.000000 nm | |
| | | | | NIR 256-2.5 | | | 900.000000 nm | 2550.000000 nm | 0.001000 s | 7.500000 nm | |
| | | | ATR-MIR [67] | ATR-MIR [67] | | | | | | | |
| | | | Ultrasonics | Ultrasonics | | | | | | | |
| | | Particle shape (morphology) | Lasentic's PVM (process vision measurement) | Lasentic's PVM (process vision measurement) | | | | | | | |
| | | | Video microscopy | video microscopy | | | | | | | |
| | | Stirrer speed | NIR | AvaSpec-NIR256-1.7 | 0.170000 nm | 0.170000 nm | 900.000000 nm | 1750.000000 nm | 0.001100 s | 50.000000 n | 350.000000 |
| | | | | AvaSpec-NIR256-2.2 | 0.170000 nm | 0.170000 nm | 1000.000000 nm | 2200.000000 nm | 0.001100 s | 60.000000 n | 250.000000 |
| | | | | AvaSpec-NIR256-2.5 | 0.170000 nm | 0.170000 nm | 1000.000000 nm | 2500.000000 nm | 0.001100 s | 90.000000 n | 200.000000 |
| | | | | EPP 2000 Fiber Optic Spectrometer-NIR | 0.200000 nm | 0.200000 nm | 500.000000 nm | 1200.000000 nm | 0.002000 s | 0.800000 nm | |
| | | | | EPP 2000 Fiber Optic Spectrometer-NIR2 | 0.100000 nm | 0.100000 nm | 600.000000 nm | 1000.000000 nm | 0.002000 s | 0.400000 nm | |
| | | | | EPP 2000 Fiber Optic Spectrometer-NIR2b | 0.100000 nm | 0.100000 nm | 785.000000 nm | 1200.000000 nm | 0.002000 s | 0.400000 nm | |
| | | | | Antaris target blend analyzer | | | 1350.000000 nm | 1800.000000 nm | | 1.600000 nm | |
| | | | | NIR 256-2.1 | | | 900.000000 nm | 2100.000000 nm | 0.001000 s | 12.000000 nm | |
| | | | | NIR 256-2.5 | | | 900.000000 nm | 2550.000000 nm | 0.001000 s | 7.500000 nm | |
| | | Homogeneity | NIR | AvaSpec-NIR256-1.7 | 0.170000 nm | 0.170000 nm | 900.000000 nm | 1750.000000 nm | 0.001100 s | 50.000000 n | 350.000000 |
| | | | | AvaSpec-NIR256-2.2 | 0.170000 nm | 0.170000 nm | 1000.000000 nm | 2200.000000 nm | 00.001100 s | 60.000000 n | 250.000000 |
| | | | | AvaSpec-NIR256-2.5 | 0.170000 nm | 0.170000 nm | 1000.000000 nm | 2500.000000 nm | 00.001100 s | 90.000000 n | 200.000000 |
| | | | | EPP 2000 Fiber Optic Spectrometer-NIR | 0.200000 nm | 0.200000 nm | 500.000000 nm | 1200.000000 nm | 00.002000 s | 0.800000 nm | |
| | | | | EPP 2000 Fiber Optic Spectrometer-NIR2 | 0.100000 nm | 0.100000 nm | 600.000000 nm | 1000.000000 nm | 00.002000 s | 0.400000 nm | |

Figure 2.4 Crystallization knowledge base

## 2.4 Uncertainty and sensitivity issues

Basically the uncertainty and sensitivity analysis can be applied in order to quantify the uncertainties and minimize the risk of not achieving the target specifications. This is actually a part of good modeling practice (GMoP) to allow improvement of the usage and the reliability of the model within PAT applications (Sin et al., 2009a). In general, uncertainty analysis is concerned with propagation of the various sources of uncertainty (e.g., data, parameters, kinetics, etc.) to the model output (e.g., performance index). The uncertainty analysis leads to probability distributions of model predictions, which are then used to infer the mean, variance and percentiles of model predictions. The sensitivity analysis, on the other hand, aims at identifying and quantifying the individual contributions of the uncertain inputs to the output uncertainty. Uncertainty and sensitivity analysis are usually (and preferably) performed in tandem with each other (Sin et al., 2009b).

Uncertainty analysis associated with the predictions of simulation models is generally classified as: a) stochastic uncertainty that arises from stochastic components of a simulation model required to describe a stochastic system; b) subjective (or input) uncertainty that represents incomplete knowledge about the fixed values used as input to the model for example process parameters; and c) structural uncertainty that relates to the mathematical formulation or the model structure (Helton and Davis, 2003). Basically there are numerous techniques to perform the uncertainty analysis including linear error propagation (Omlin and Reichert, 1999), the Monte Carlo procedure (Helton and Davis, 2003; Flores-Alsina et al., 2009; Sin et al., 2009b; etc.) and fast probability integration (FPI) (Haskin et al., 1996).

In the differential analysis technique, a Taylor series is developed to represent the model under consideration. Based on the Taylor series approximation, variance propagation formulas can be used to determine the output uncertainty that results from the input distributions. The main advantage of the differential analysis technique is that uncertainty as well as sensitivity analysis can be implemented easily once the Taylor series approximation is obtained. However, this technique is inherently local, implementation is difficult and a large computational time is required.

The response surface methodology (RSM) is another technique that can be used for the propagation of uncertainty. The RSM involves Design of Experiment (DoE) to select the model input. The DoE can be designed using factorial, fractional factorial or central composite design to cover all the model inputs (Myers et al., 2009). The RSM offers a complete control over the structure of the model input based on the selected designs in the DoE and thus a reliable response surface model can be produced to represent the original model which subsequently can be used in the uncertainty and sensitivity analysis. However, the most difficult part in the RSM is to develop an appropriate response surface. This is due to the fact that a large number of design points are needed to cover all the considered factors to produce a reasonable response surface where only a limited number of values for each input variable are available. Furthermore, there are some difficulties using the RSM technique when there are correlations and restrictions between input variables.

Monte Carlo techniques are based on the use of a probabilistic procedure to select model input and result in a mapping between inputs and analysis outputs that is then used to produce uncertainty analysis results. The advantages of Monte Carlo analysis

is the extensive sampling from the ranges of the uncertain variables, and a surrogate model is not needed to obtain the uncertainty results unlike the other uncertainty techniques such as Taylor series in differential analysis or RSM. A variety of sensitivity analysis techniques are available to complement the uncertainty analysis based on Monte Carlo and the approach is conceptually simple, widely used and easy to explain (Helton and Davis, 2003).

Alternatively, the fast probability integration (FPI) can be employed to propagate input uncertainty. The technique is based on the use of analytical procedures to evaluate distribution functions (Haskin et al., 1996). In this technique, only the estimation of the tails of a distribution is needed compared to another technique such as the differential analysis which requires the estimation of full distributions. This unique feature allows this technique to require less computational time compared to the other techniques. However, the underlying mathematics is rather complicated, and therefore hard to explain, which limits practical application. Furthermore, the approach is implemented only to uncertainty analysis and there is a lack of sensitivity analysis techniques to complement the uncertainty analysis.

Sensitivity analysis is complimentary to uncertainty analysis and can be viewed as an analysis of variance, in which the aim is to decompose the output variance with respect to input parameters (Helton and Davis, 2003; Saltelli et al., 2006). Based on the variance in model predictions, the input parameters will then be ranked as a parameter significance ranking where the top in the ranking reveals the input parameter explaining most of the variance. The main purpose of this parameter ranking obtained from the sensitivity analysis is that the efforts can then be focused on reducing the uncertainty in

the most influential parameters, whereas the parameters that have little or no influence on the model output can be neglected. Examples of sensitivity analysis based ranking include the standardized regression coefficient method (SRC) and Morris screening.

The SRC method is one of the global sensitivity analysis techniques where the effect on the output of a factor can be estimated when all the other factors are varying, thus enabling the identification in non-linear and/or non-additive models (Cariboni et al., 2007). Since the SRCs basically are built on regression analysis, and are also based on Monte Carlo simulation, the method reflects the shape of the probability distribution of each factor. Regression analysis allows also for the estimation of the coefficient of determination, $R^2$, which represents the fraction of the output variance explained by the regression. However, since we typically work with non-linear models, the SRC method is only considered valid for assessing the factor importance when $R^2 > 0.7$. If the $R^2$ is below 0.7, then the method cannot be considered as a reliable sensitivity measure (Cariboni et al., 2007), i.e. indicating that the effect of the parameters on the model output cannot be represented by a linear regression. The coefficients from the regression model are then scaled using the standard deviations of model input and output to provide the sensitivity measures, $\beta_{jk}$, which will then be ranked in order of importance.

Another method to test the sensitivity of the model is the Morris screening method (Morris, 1991). The method is based on calculating a number of incremental ratios for each input, called elementary effects (EE), from which basic statistics are computed to derive sensitivity information. Based on the EE, two sensitivity measures are computed for each input: the mean (μ), which assesses the overall influence of the factor on the output, and the standard deviation (σ), which estimates the ensemble of the

factor's higher order effects. The ranking can then be determined based on the values of μ.

## 2.5 Conclusion

Crystallization is often applied in the production of pharmaceutical product and the crystallization step is an essential part of the manufacturing process for many chemicals-based products. Although the literature reports on many significant contributions within the modelling of crystallization processes, a comprehensive generic model still remains a task for the future. Current literature points to many attempts to model crystallization operations with emphasis on different issues such as CSD or crystallization kinetics. Therefore, there is a need for a generic crystallization model from which a large number of specific models for different crystallization processes can be generated. It is essential to maintain the crystallization operation at the designated set point where supersaturation or temperature control can be applied to drive the process within the metastable zone and thereby enhance the control of the CSD. Although this approach has been shown to produce high quality crystals, the set point operating profiles for the controller are usually chosen arbitrarily or by trial-and-error. Therefore there is a need for a systematic procedure to generate set points that guarantees that the target CSD can be achieved.

Furthermore, to control and monitor the crystallization operations and to ensure that the desired CSD is achieved, the developed PAT system needs to be linked with the modelling framework as well. In order to minimize the risk of not obtaining the target crystal products, an uncertainty and sensitivity analysis need to be carried out. Here a

number of procedures have been discussed for the propagation of uncertainty. Based on the analysis, the Monte Carlo procedure has been chosen to implement the uncertainty analysis. This is due to the fact that it is generally accepted as computationally effective and reliable. In order to complement the Monte Carlo-based uncertainty analysis, the SRC method and Morris screening are chosen as techniques for sensitivity analysis. As a consequence, a model-based framework that allows the study of different crystallization operational scenarios, and has the ability to generate the set point profiles and to design the PAT system as well as conducting the uncertainty and sensitivity analysis will be developed and applied in the following chapters of this thesis.

# 3. A generic multi-dimensional model-based framework for crystallization processes

In this chapter, a generic model for multi-dimensional PBEs (within a modelling framework) from which a large number of "problem-system" specific models for different crystallization processes can be created, is presented. The term "problem" refers to different crystallization operational scenarios, while the term "system" refers to different chemical systems. The generality of the framework and the developed modelling approach allow the further development and adaptation of the crystallization model to reflect changing product monitoring schemes (such as, monitoring of crystal properties) and/or process conditions (such as, temperature and/or agitation profiles). The chapter presents a model generation procedure incorporated within the modelling framework and highlights its use through two case studies where the creation (generation) of appropriate models needed for different modelling objectives is considered. In the first case study, one-dimensional models are generated and their simulated results analyzed for the crystallization of paracetamol and sucrose, respectively. In the second case study, one- as well as two-dimensional models are generated and solved with standard method of moments and method of classes for potassium dihydrogen phosphate (KDP) crystallization.

## 3.1 Generic multi-dimensional model-based framework

A generic multi-dimensional framework for modelling of batch cooling crystallization (Figure 3.1) and related operations (solvent based crystallization and/or continuous crystallization) has been developed (Samad et al., 2010, 2011a,b). This modelling framework helps to generate problem-system specific models describing various crystallization processes through a generic crystallization model. As shown in Figure 3.1, the problem-system specific model generation procedure consists of four main steps. It should be noted that this model generation procedure combines selection criteria related to theory or "what is the correct model structure" with data-based empiricism or "can the model parameters be estimated realistically ". The latter obviously depends on the data availability and quality and that is why the model generation procedure includes a regression step, if necessary.

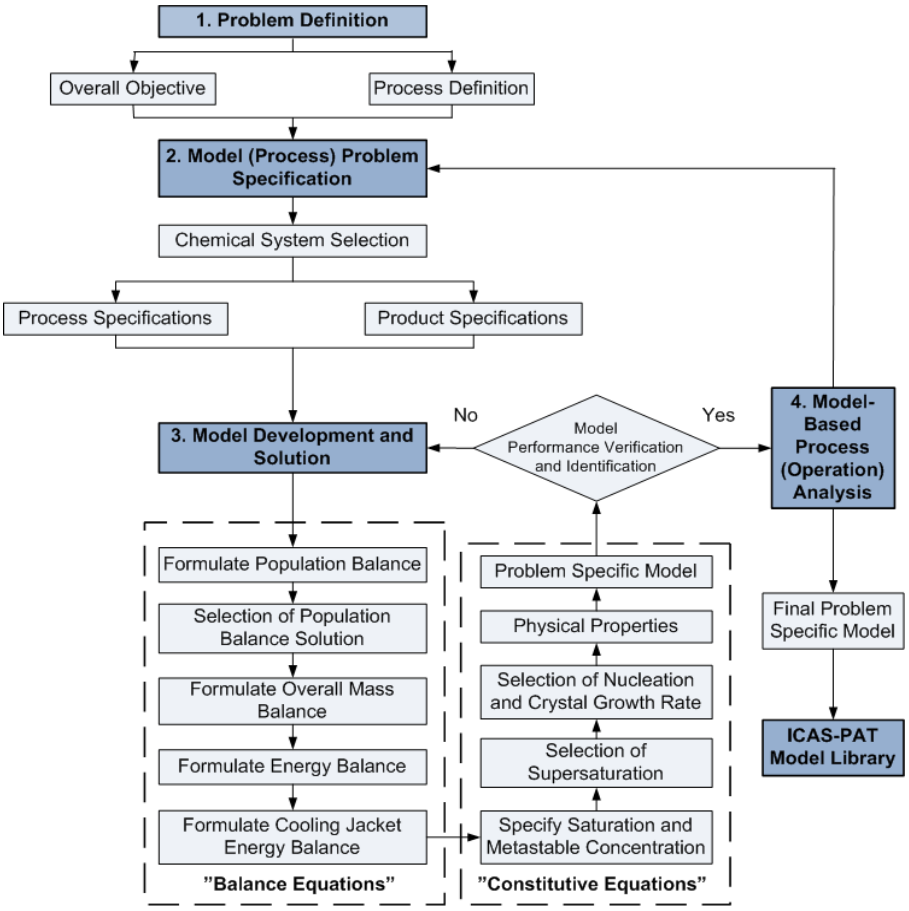


Figure 3.1 Generic crystallization modelling framework (Note that the selection of constitutive equations also includes model parameter estimation)

## 3.2 Problem definition (Step 1)

The modelling framework starts with the problem definition for the crystallization process under study in terms of the overall modelling objective and details of the crystallization process to be studied. For example, the overall objective could be to study properties of the crystal particles (CSD, mean crystal size), the evolution of the CSD or to generate information related to the crystallization operation (such as,

concentration-temperature profiles). The process details could be operational characteristics such as unseeded versus seeded operation; size dependent or independent growth; temperature of operation and many more. Furthermore, decisions related to the dimensions of the model need to be made in this step. Note that the dimension of the model is related to the crystal morphology (single versus multiple dimensions) that would be studied.

## 3.3 Model (process) problem specification (Step 2)

The problem specification starts with the selection of the chemical system that is to be investigated and the collection of the information about its process and product specifications. For example, this information could be a list of chemicals involved, such as the solute and solvent(s) and equipments used in the process (batch crystallizer, jacketed tank, etc.). Information on the solute-solvent saturation solid-liquid equilibrium (saturation) data – generated experimentally or by simulation with a model (Thomsen et al., 1998); crystal growth kinetics data; etc., help in the selection of the appropriate constitutive models in the next step.

## 3.4 Model development and solution (Step 3)

This step is concerned with the listing of the necessary balance and constitutive equations involved in the crystallization process. The balance equations library consists of population, overall mass and energy balances for a defined crystallization volume supplemented with energy balance equations for external heating/cooling, for example, a

cooling jacket. The constitutive model equations library contains a set of models describing nucleation, crystal growth rate, supersaturation, saturation concentration, metastable concentration, agglomeration, breakage and physical properties corresponding to different types of chemical systems found in the literature on crystallization processes. Based on the modelling objectives (step 1) and the problem specification details (step 2), the appropriate problem-system specific model equations are retrieved from the generic model.

### 3.4.1 Population balance equation (PBE) formulation and selection of solution method

The generic PBEs for the one- and two-dimensional case as listed in Table 3.1 are transformed to a system of ODEs by applying the standard method of moments in the case of unseeded/seeded, size independent growth and nucleation or the method of classes for unseeded/seeded, size dependent as well as size independent growth, agglomeration and breakage, as shown in Figure 3.2. The method of classes (adopted from Costa et al. (2005) and Puel et al. (2003)) is employed based on the assumption that the number of particles in the size domain (class) is constant. In order to avoid artificial diffusion, small size of class width is chosen and the integrator must be carefully selected. The accuracy of this method is depending on the the number of classes meaning that the greater number of classes, the better is the accuracy in this method. In this work, the Backward Differentiation Formulas (BDF) is chosen as an integrator to solve the method of classes. The decisions (see Figure 3.2) are based on the process definition (step 1). Tables 3.2 and 3.3 list the generic PBEs corresponding to each solution technique.

Table 3.1 Generic equations for the PBE

| Dimension | Equation | Description |
|---|---|---|
| 1D | $\frac{\partial f_n(L_x,t)}{\partial t} = -\frac{\partial f_n(L_x,t) G_x(L_x,c,T)}{\partial L_x} + (B-D)$<br><br>Where<br><br>$(B-D) = B_{nuc} + B_{agg} - D_{agg} + B_{br} - D_{br}$ | This is a general PBE for the x-direction only ($0 \rightarrow L_x$) |
| 2D | $\frac{\partial f_n(L_x,L_y,t)}{\partial t} = -\frac{\partial f_n(L_x,L_y,t) G_x(L_x,L_y,c,T)}{\partial L_x}$<br><br>$-\frac{\partial f_n(L_x,L_y,t) G_y(L_x,L_y,c,T)}{\partial L_y} + (B-D)$<br><br>Where<br><br>$(B-D) = B_{nuc} + B_{agg} - D_{agg} + B_{br} - D_{br}$ | This is a general PBE for the x and y-direction only ($0 \rightarrow L_x; 0 \rightarrow L_y$) |

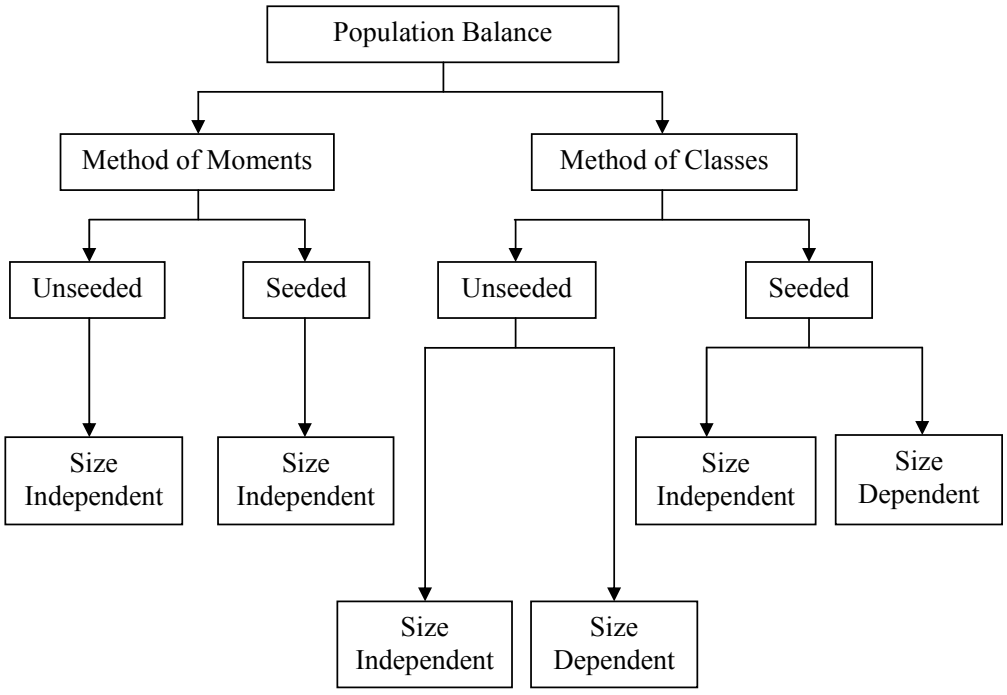


Figure 3.2 PBE solution techniques based on process operation characteristics

Table 3.2 Solution techniques for one-dimensional PBEs

| Solution | Cases | Equations |
|---|---|---|
| Method of moments | Size independent growth | $\frac{d\mu_0}{dt} = B_{nuc}$<br>$\frac{d\mu_m}{dt} = mG_x\mu_{m-1} + B_{nuc}L_0^m; \quad m = 1,\ldots,4$ |
| Method of classes | Size independent growth | For $i = 1$;<br>$\frac{dN_1}{dt} + \frac{G_x}{2\Delta Cl_1}N_1 = B_{nuc} + B_{agg,1} - D_{br,1}$<br>For $1 < i < n$;<br>$\frac{dN_i}{dt} + \frac{G_x}{2\Delta Cl_i}N_i - \frac{G_x}{2\Delta Cl_{i-1}}N_{i-1} = B_{agg,i} - D_{br,i}$<br>For $i = n$;<br>$\frac{dN_n}{dt} + \frac{G_x}{2\Delta Cl_n}N_n - \frac{G_x}{2\Delta Cl_{n-1}}N_{n-1} = B_{agg,n} - D_{br,n}$ |
| | Size dependent growth | For $i = 1$;<br>$\frac{dN_1}{dt} + \frac{G_x(L_{x1})}{2\Delta Cl_2}N_2 + \frac{G_x(L_{x1}) - G_x(L_{x0})}{2\Delta Cl_1}N_1$<br>$= B_{nuc} + B_{agg,1} - D_{br,1}$<br>For $1 < i < n$;<br>$\frac{dN_i}{dt} + \frac{G_x(L_{xi})}{2\Delta Cl_{i+1}}N_{i+1} + \frac{G_x(L_{xi}) - G_x(L_{xi-1})}{2\Delta Cl_i}N_i - \frac{G_x(L_{xi-1})}{2\Delta Cl_{i-1}}N_{i-1}$<br>$= B_{agg,i} - D_{br,i}$<br>For $i = n$;<br>$\frac{dN_n}{dt} + \frac{G_x(L_{xn-1})}{2\Delta Cl_n}N_n - \frac{G_x(L_{xn-1})}{2\Delta Cl_{n-1}}N_{n-1} = B_{agg,n} - D_{br,n}$ |

Table 3.3 Solution techniques for two-dimensional PBE

| Solution | Cases | Equation |
|---|---|---|
| Method of moments | Size independent growth | $\frac{d\mu_{00}}{dt} = B_{nuc}$<br>$\frac{d\mu_{mn}}{dt} = mG_x\mu_{(m-1)n} + nG_y\mu_{m(n-1)} + B_{nuc}L_{10}^m L_{20}^n; \quad m,n \neq 0$ |
| Method of classes | Size independent growth | $\frac{dN_{i,j}}{dt} + f_{i,j}(t) + f_{i,j}^{'}(t) = B - D, \quad i = 1,\ldots,n; j = 1,\ldots,m$<br>$f_{i,j}(t) = f_{i,j}^{1,O}(t) - f_{i,j}^{1,I}(t) \;\; ; \;\; f_{i,j}^{'}(t) = f_{i,j}^{2,O}(t) - f_{i,j}^{2,I}(t)$<br>$f_{i,j}^{1,O}(t) = G_x\left(a_i N_{i,j}(t) + b_i N_{i+1,j}(t)\right)$<br>$f_{i,j}^{1,I}(t) = G_x\left(a_{i-1} N_{i-1,j}(t) + b_{i-1} N_{i,j}(t)\right)$<br>$a_i = \frac{\Delta Cl_{i+1}}{\Delta Cl_i\left(\Delta Cl_{i+1} + \Delta Cl_i\right)} \;\; ; b_i = \frac{\Delta Cl_i}{\Delta Cl_{i+1}\left(\Delta Cl_{i+1} + \Delta Cl_i\right)}$<br>$f_{i,j}^{2,O}(t) = G_y\left(c_j N_{i,j}(t) + d_j N_{i,j+1}(t)\right)$<br>$f_{i,j}^{2,I}(t) = G_y\left(c_{j-1} N_{i,j-1}(t) + d_{j-1} N_{i,j}(t)\right)$<br>$c_j = \frac{\Delta Cl_{j+1}}{\Delta Cl_j\left(\Delta Cl_{j+1} + \Delta Cl_j\right)} \;\; ; d_j = \frac{\Delta Cl_j}{\Delta Cl_{j+1}\left(\Delta Cl_{j+1} + \Delta Cl_j\right)}$ |
| | Size dependent growth | $\frac{dN_{i,j}}{dt} + f_{i,j}(t) + f_{i,j}^{'}(t) = B - D, \quad i = 1,\ldots,n; j = 1,\ldots,m$<br>$f_{i,j}(t) = f_{i,j}^{1,O}(t) - f_{i,j}^{1,I}(t) \;\; ; f_{i,j}^{'}(t) = f_{i,j}^{2,O}(t) - f_{i,j}^{2,I}(t)$<br>$f_{i,j}^{1,O}(t) = G_x(S_i,t)\left(a_i N_{i,j}(t) + b_i N_{i+1,j}(t)\right)$<br>$f_{i,j}^{1,I}(t) = G_x(S_{i-1},t)\left(a_{i-1} N_{i-1,j}(t) + b_{i-1} N_{i,j}(t)\right)$<br>$a_i = \frac{\Delta Cl_{i+1}}{\Delta Cl_i\left(\Delta Cl_{i+1} + \Delta Cl_i\right)} \;\; ; b_i = \frac{\Delta Cl_i}{\Delta Cl_{i+1}\left(\Delta Cl_{i+1} + \Delta Cl_i\right)}$<br>$f_{i,j}^{2,O}(t) = G_y(S_j,t)\left(c_j N_{i,j}(t) + d_j N_{i,j+1}(t)\right)$<br>$f_{i,j}^{2,I}(t) = G_y(S_{j-1},t)\left(c_{j-1} N_{i,j-1}(t) + d_{j-1} N_{i,j}(t)\right)$<br>$c_j = \frac{\Delta Cl_{j+1}}{\Delta Cl_j\left(\Delta Cl_{j+1} + \Delta Cl_j\right)} \;\; ; d_j = \frac{\Delta Cl_j}{\Delta Cl_{j+1}\left(\Delta Cl_{j+1} + \Delta Cl_j\right)}$ |

### 3.4.2 Overall mass balance formulation

For the one-dimensional model, the overall mass balance equation is obtained, for example, by specifying the shape factor, $k_v$. For a sphere shaped crystal it is π/6, while, for a cube shaped crystal, it is 1. The overall mass balance equations for the one-dimensional generic model are listed in Table 3.4. The rate of change of the solute concentration in a crystallizer for two-dimensional models is represented by Equation (3.1) where the final form of the equation depends on the crystal shape.

$$\frac{dc}{dt} = -\frac{\rho_c}{m_w}\frac{dV_c}{dt} \tag{3.1}$$

For example, if the crystal is rod-shaped, the volume of the crystal is then given by

$$V_c = L_x L_y^2 \tag{3.2}$$

The generic overall mass balance equation for rod-shaped crystals is given by

$$\frac{dc}{dt} = -\frac{\rho_c}{m_w}\left(\int_0^\infty \int_0^\infty f_n\left(L_x, L_y, t\right)\left(G_x L_y^2 + 2G_y L_x L_y\right)dL_x dL_y + B_{nuc} L_{x0}^2 L_{y0}\right) \tag{3.3}$$

By specifying the shape of the crystals, the final equation for the overall mass balance is obtained by substituting the volume occupied by the crystal shapes. Table 3.5 lists the overall mass balance equations for the two-dimensional generic model for rod-shaped

crystals. The two-dimensional generic model for the shape of a tetragonal prism is also listed in Table 3.5.

Table 3.4 Overall mass balance equations for the one-dimensional generic model

| | |
|---|---|
| Generic equations | $\frac{dc}{dt} = -\frac{\rho_c k_v V}{m_w}\left(3\int_0^\infty G_x f_n\left(L_x,t\right) L_x^{\,2} dL + B_{nuc} L_{xo}^3\right)$ |
| Method of moments | $\frac{dc}{dt} = -\frac{\rho_c k_v V}{m_w}\left(3G\mu_2 + B_{nuc} L_{x0}^3\right)$ |
| Method of classes | $\frac{dc}{dt} = -\frac{\rho_c k_v V}{m_w}\left(\sum_{i=1}^{i=n} S_{xi}^3 \frac{dN_i}{dt}\right)$ |

Table 3.5 Overall mass balance equations for the two-dimensional generic model

| | |
|---|---|
| Generic equations | Shape: rod<br>$\frac{dc}{dt} = -\frac{\rho_c}{m_w}\left(\int_0^\infty \int_0^\infty f_n\left(L_x,L_y,t\right)\left(G_x L_y^2 + 2G_y L_x L_y\right) dL_x dL_y + B_{nuc} L_{x0}^2 L_{y0}\right)$<br>Shape: tetragonal prism<br>$\frac{dc}{dt} = -\frac{\rho_c}{m_w}\left(\int_0^\infty \int_0^\infty f_n\left(L_x,L_y,t\right)\left(2G_x\left(L_x L_y - L_x^2\right) + G_y L_x^2\right) dL_x dL_y$<br>$-\frac{2}{3} B_{nuc} L_{x0}^3 + B_{nuc} L_{x0}^2 L_{y0}\Big)$ |
| Method of moments | Shape: rod<br>$\frac{dc}{dt} = -\frac{\rho_c}{m_w}\left(G_x \mu_{02} + 2G_y \mu_{11} + B_{nuc} L_{x0}^2 L_{y0}\right)$<br>Shape: tetragonal prism<br>$\frac{dc}{dt} = -\frac{\rho_c}{m_w}\left(2G_x\left(\mu_{11} - \mu_{20}\right) + G_y \mu_{20} - \frac{2}{3} B_{nuc} L_{x0}^3 + B_{nuc} L_{x0}^2 L_{y0}\right)$ |
| Method of classes | Shape: rod<br>$\frac{dc}{dt} = -\frac{\rho_c}{m_w}\left(\sum_{i,j} S_{x,i} S_{y,j}^2 \frac{dN_{i,j}}{dt}\right)$<br>Shape: tetragonal prism<br>$\frac{dc}{dt} = -\frac{\rho_c}{m_w}\left(\sum_{i,j}\left(\frac{1}{3} S_{x,i}^3 + \left(S_{y,j} - S_{x,i}\right) S_{x,i}^2\right)\frac{dN_{i,j}}{dt}\right)$ |

### 3.4.3 Energy balance formulation

In a similar way to the mass balance, energy balance equations are derived for the one-dimensional generic model (see Table 3.6) and the two-dimensional generic model (see Table 3.7).

Table 3.6 Energy balances for the one-dimensional generic model

| | |
|---|---|
| Generic equations | $\rho V c_p \frac{dT}{dt} = -\Delta H_c \rho_c k_v V \left( 3\int_0^\infty G_x n\left(L_x,t\right) {L_x}^2 dL_x + B_{nuc} L_{xo}^3 \right) - U_1 A_1 \Delta T$ |
| Method of moments | $\rho V c_p \frac{dT}{dt} = -\Delta H_c \rho_c k_v V \left( 3G_x \mu_2 + B_{nuc} L_{x0}^3 \right) - U_1 A_1 \Delta T$ |
| Method of classes | $\rho V c_p \frac{dT}{dt} = -\Delta H_c \rho_c k_v V \left( \sum_{i=1}^{i=N} S_i^3 \frac{dN_{i,j}}{dt} \right) - U_1 A_1 \Delta T$ |

Table 3.7 Energy balances for the two-dimensional generic model

| | |
|---|---|
| Generic equations | Shape: rod<br>$\rho V c_p \frac{dT}{dt} = -\Delta H_c \rho_c k_v V \left( \left( \int_0^\infty \int_0^\infty f_n\left(L_x,L_y,t\right) \left( G_x L_y^2 + 2G_y L_x L_y \right) dL_x dL_y + B_{nuc} L_{x0}^2 L_{y0} \right) - U_1 A_1 \Delta T \right)$<br>Shape: tetragonal prism<br>$\rho V c_p \frac{dT}{dt} = -\Delta H_c \rho_c k_v V \left( \left( \int_0^\infty \int_0^\infty f_n\left(L_x,L_y,t\right) \left( 2G_x \left( L_x L_y - L_x^2 \right) + G_y L_x^2 \right) dL_x dL_y - \frac{2}{3} B_{nuc} L_{x0}^3 + B_{nuc} L_{x0}^2 L_{y0} \right) - U_1 A_1 \Delta T \right)$ |
| Method of moments | Shape: rod<br>$\rho V c_p \frac{dT}{dt} = -\Delta H_c \rho_c k_v V \left( G_x \mu_{02} + 2G_y \mu_{11} + B_{nuc} L_{x0}^2 L_{y0} \right) - U_1 A_1 \Delta T$<br>Shape: tetragonal prism<br>$\rho V c_p \frac{dT}{dt} = -\Delta H_c \rho_c k_v V \left( 2G_x \left( \mu_{11} - \mu_{20} \right) + G_y \mu_{20} - \frac{2}{3} B_{nuc} L_{x0}^3 + B_{nuc} L_{x0}^2 L_{y0} \right) - U_1 A_1 \Delta T$ |
| Method of | Shape: rod |

| | |
|---|---|
| classes | $\rho V c_p \frac{dT}{dt} = -\Delta H_c \rho_c k_v V \left( \sum_{i,j} S_{x,i} S_{y,j}^2 \frac{dN_{i,j}}{dt} \right) - U_1 A_1 \Delta T$<br>Shape: tetragonal prism<br>$\rho V c_p \frac{dT}{dt} = -\Delta H_c \rho_c k_v V \left( \sum_{i,j} \left( \frac{1}{3} S_{x,i}^3 + \left( S_{y,j} - S_{x,i} \right) S_{x,i}^2 \right) \frac{dN_{i,j}}{dt} \right) - U_1 A_1 \Delta T$ |

### 3.4.4 Cooling jacket energy balance formulation

The energy balance model for the cooling jacket is similar for one- and two-dimensional models and is applicable to both the standard method of moments and the method of classes (see Table 3.8).

Table 3.8 Energy balance model for the cooling jacket

| | |
|---|---|
| Generic equations | $\rho_w V_w c_{pw} \frac{dT_w}{dt} = \rho_w F_{win} c_{pw} \left( T_{win} - T_w \right) + U_1 A_1 \left( T - T_w \right) + U_2 A_2 \left( T_{ex} - T_w \right)$ |

### 3.4.5 Constitutive equation selection

The constitutive equations represent the models describing saturation concentration, metastable concentration, supersaturation, nucleation, crystal growth rate, agglomeration, breakage and physical properties corresponding to different types of chemical systems that may be found in the crystallization process being studied (modelled). The selection of the constitutive equations (from the model library) starts with the specification of the saturation concentration. The dependence of the saturation concentration and the metastable concentration on temperature is approximated by a third order polynomial expression (see Table 3.9). The coefficients in the saturation and

metastable polynomial expression depend on the solubility of the chemical system being investigated, which can be obtained from a database of experimental data (Abildskov, 2005) or solid solubility models (Modaressi et al., 2008). There are two main types of supersaturation, normal supersaturation and relative supersaturation. The nucleation and crystal growth rate equations are determined based on the supersaturation selection. Here the effect of agitation is included as an option as well. Furthermore two different growth kinetic models can be incorporated - size dependent or size independent, depending on the selection of the crystal growth rate model (see step 1). For the two-dimensional case, two crystal growth rates (one per dimension) need to be considered.

The parameters needed to perform the calculation of saturation concentration, metastable concentration, heat of crystallization, nucleation rate and crystal growth rate are obtained from the literature, from a database or regressed through available experimental data. This modelling framework is also integrated with model identification and data handling frameworks where a model parameter regression and translation procedure for raw experimental data can be implemented (Samad et al., 2012c). Due to the importance of appropriately validated constitutive models, this cannot be disregarded as the performance of the full model largely depends on the quality of the parameters of the selected constitutive models, which in turn depends on the quality of the available data. However, the features are beyond the contribution of this work and are not highlighted in this thesis. In this work, the model parameters for the selected constitutive models are taken from published data (retrieved from the model library). Table 3.9 lists a representative set of constitutive models for the different phenomena considered in this work.

Table 3.9 List of constitutive models

| Constitutive Equations | General Equations | | Selection Criteria |
|---|---|---|---|
| Saturation Concentration | $c^{sat} = a_{i1} + b_{i1}T + c_{i1}T^2 + d_{i1}T^3$ | | The coefficients depend on chemical system solubility data |
| Metastable Concentration | $c^{met} = a_{i2} + b_{i2}T + c_{i2}T^2 + d_{i2}T^3$ | | The coefficients depend on chemical system solubility data |
| Heat of Crystallization | $\Delta H_c = a_{i3} + b_{i3}T + c_{i3}T^2 + d_{i3}T^3$ | | The coefficients depend on the chemical system |
| Supersaturation | Normal, $S$ | $\frac{c}{c^{sat}}; \frac{x}{x^{sat}}; \frac{m}{m^{sat}}$ | Depends on unit selection and if $c - c^{sat} > 1$ |
| | | $\Delta c = c - c^{sat}$ | Selected if $c - c^{sat} < 1$ |
| | Relative, $\sigma$ | $\sigma = S - 1$ | Ideal solution assumption and depends on the unit selection. Compare with the saturated reference. Valid only at $\sigma << 1$ |
| | | $\sigma = S\xi - 1$<br><br>Where:<br>$\xi = \frac{\gamma_m}{\gamma_{m,eq}} = \frac{\gamma_x}{\gamma_{x,eq}} = \frac{\gamma_c}{\gamma_{c,eq}}$ | Non-ideal solution assumption and depends on the unit selection. Compare with saturated reference. The symbol ζ is the activity coefficient ratio used in the relative supersaturation. If the solution is assumed ideal then the activity coefficient is 1. If the solution is not ideal, then the activity coefficient |

| | | | |
|---|---|---|---|
| | | | ratio must be calculated in the supersaturation equation. The ζ can be calculated using the given equation depending on the unit selection (molar, mass fraction or mass concentration): |
| Nucleation rate | Primary nucleation:<br>$B_{n,1} = A_{pn} \exp\left( -\frac{B_{pn}}{\ln\left(\frac{c}{c^{sat}}\right)^2} \right)$<br>Secondary nucleation:<br>$B_{n,2} = k_b M_c^j S^b N_{rpm}^p$ or $B_{n,2} = k_b M_c^j \sigma^b N_{rpm}^p$<br>For temperature dependent:<br>$k_b = k_{b0} \exp\left(-\left(\Delta E_b / RT\right)\right)$ | | Depends on data availability. If the data for primary nucleation (Marchal et al., 1998) are not available then only secondary nucleation (Quintana-Hernández et al., 2004) should be used.<br>Effect of agitation and temperature dependent are included as an option.<br>Selection of nucleation rate equations is depending on the choice of the supersaturation. |
| Crystal growth rate<br>(for two-dimensional systems, there will be two crystal growth rates) | Size independent growth:<br>$G_x = k_{gx} S^{gx} N_{rpm}^{qx}$ or $G_x = k_{gx} \sigma^{gx} N_{rpm}^{qx}$<br>For temperature dependent:<br>$k_{gx} = k_{gx0} \exp\left(-\left(\Delta E_g / RT\right)\right)$ | | Assuming all the crystals has the same growth rate.<br>Effect of agitation and temperature dependent are included as an option.<br>Selection of crystal growth rate equations depends |

| | | |
|---|---|---|
| | | on the choice of the supersaturation (Quintana-Hernández et al., 2004) |
| | Size dependent growth:<br>$G_x = k_{gx} S^{gx} N_{rpm}^{qx} \left(1+\gamma_x L_x\right)^{px}$ or<br>$G_x = k_{gx} \sigma^{gx} N_{rpm}^{qx} \left(1+\gamma_x L_x\right)^{px}$<br><br>For temperature dependent:<br>$k_{gx} = k_{gx0} \exp\left(-\left(\Delta E_g / RT\right)\right)$ | Effect of agitation and temperature dependent are included as an option.<br>Selection of crystal growth rate equations depends on the choice of the supersaturation. |
| | Size dependent growth:<br>$G_x = \eta_r \frac{k_{gx} MM k_r}{3\rho_c k_v} S^{gx}$<br><br>Effectiveness factor:<br>$\left[\frac{k_g}{k_d}\left(c-c^{sat}\right)^{g-1}\right]\eta_r + \eta_r^{1/g} - 1 = 0$<br><br>Mass transfer coefficient:<br>$k_d = \frac{D}{L} \times$<br>$\left[2+0.47\left(\frac{L^{4/3}\varepsilon^{1/3}}{v}\right)^{0.62}\left(\frac{Diam}{Diam_T}\right)^{0.17}\left(\frac{v}{D}\right)^{0.36}\right]$ | The expression for the growth rate developed by Marchal et al. (1988) is based on the assumption of a film model.<br>This expression is supplemented with effectiveness and mass transfer coefficient equations. |
| Production-reduction rate | $\alpha = k_{ab} S^{ab} M_c^k N_{rpm}^r$ | Represent the birth and death rates generated by agglomeration and breakage of crystals. Adopted from Quintana-Hernández et al. (2004) |
| Agglomeration rate | $B_{Agg,i} = \sum_{l=1}^{N(N+1)/2} \nu_{est(l,i)} r(l)$<br><br>Overall stoichiometric coefficient: | The net rate of particle production by agglomeration in the $i^{th}$ class (Costa et al., 2005) |

| | | |
|---|---|---|
| | $$\nu_{est(l,i)} = \left(\frac{S_m^3 + S_n^3}{S_q^3}\right)\delta_{i,q} - \left(\delta_{i,m} + \delta_{i,n}\right)$$<br><br>Intrinsic rate of agglomeration of rank *l*:<br><br>$$r(l) = k_a' S_m \left(1 + \frac{S_n}{S_m}\right)^2 N_{rpm} Diam.$$<br>$$\times f\left(\frac{S_n}{S_m}\right)\left(1 - \frac{(S_n + S_m)^2}{\lambda_e^2}\right)$$<br><br>$$\times k_d\left(c - c^{sat}\right) N_n N_m (S_m - \delta) H(\lambda_e - S_n - S_m)$$<br><br>Relative shape function of crystals:<br><br>$$f\left(\frac{S_n}{S_m}\right) = \frac{4\left(1 + S_n/S_m - \sqrt{(S_n/S_m)^2 - 1}\right)}{1/3 + S_n/S_m - \sqrt{(S_n/S_m)^2 - 1}}$$<br>$$-\left(S_n/S_m - \sqrt{(S_n/S_m)^2 - 1}\right)^2$$<br>$$\times\left(2(S_n/S_m)/3 + \sqrt{(S_n/S_m)^2 - 1}/3\right)$$<br><br>Lagrangian microscale:<br><br>$$\lambda_e = 0.3\pi N_{rpm} Diam\left(\frac{60\nu}{10\varepsilon}\right)^{0.5}$$ | |

Equations for calculating the physical properties of crystal particles (such as total mass, average length of crystals, mean crystal area, etc.) for the one- and two-dimensional models are given in Tables 3.10 and 3.11, respectively. As can be noted in Tables 3.10-11, the equations used for the properties of the crystal particles depend on the specific PBE solution method used and these equations may be used to compare the simulation results obtained from the two models.

Table 3.10 Physical properties of crystal particles for the two-dimensional model

| | Method of moments | Method of classes |
|---|---|---|
| Total number of particles | $N_c = \mu_{00}$ | $N_c = \sum_{i,j} N_{i,j}$ |
| Total mass | $M_c = \rho_c \mu_{21}$ | $M_c = \rho_c \sum_{i,j} N_{i,j} S_{xi} S_{yj}^2$<br>Where $S_{xi} = \frac{L_{xi} - L_{xi-1}}{2}$ |
| Average length of a crystal | $\bar{L}_1 = \frac{\mu_{10}}{\mu_{00}}$ | Not available |
| Average width of a crystal | $\bar{L}_2 = \frac{\mu_{01}}{\mu_{00}}$ | Not available |

Table 3.11 Physical properties of crystal particles for the one-dimensional model

| | Method of moments | Method of classes |
|---|---|---|
| Total number of particles | $N_c = \mu_0$ | $N_c = \sum_i^N N_i$ |
| Total length | $L_c = k_L \mu_1$ | $L_c = k_L \sum_i^N S_i N_i$ |
| Total area | $A_c = k_A \mu_2$ | $A_c = k_A \sum_i^N S_i^2 N_i$ |
| Total mass | $M_c = \rho_c k_v \mu_3$ | $M_c = \rho_c k_v \sum_i^N S_i^3 N_i$ |
| Mean crystal size | $S[1,0] = \frac{\mu_1}{\mu_0}$ | $S[1,0] = \frac{\sum_i^N S_i N_i}{\sum_i^N N_i}$ |
| Mean crystal area | $A[2,0] = \frac{\mu_2}{\mu_0}$ | $A[2,0] = \frac{\sum_i^N S_i^2 N_i}{\sum_i^N N_i}$ |

| | | |
|---|---|---|
| Mean crystal volume | $V[3,0]=\frac{\mu_3}{\mu_0}$ | $V[3,0]=\frac{\sum_i^N S_i^3 N_i}{\sum_i^N N_i}$ |
| Mean size diameter | $D[4,3]=\frac{\mu_4}{\mu_3}$ | $D[4,3]=\frac{\sum_i^N S_i^4 N_i}{\sum_i^N S_i^3 N_i}$ |
| Population number density | - | $n(L_i)=\frac{\frac{N_i}{\Delta Cl_i}+\frac{N_{i+1}}{\Delta Cl_{i+1}}}{2}$ |
| Where $S_i=\frac{L_i-L_{i-1}}{2}$ | | |

### 3.4.6 Generation of problem-system specific models

Based on the selection of the balance and constitutive equations, a process and/or chemical system specific model is generated through the modelling framework by applying the step by step approach outlined in Figure 3.1 (highlighted for the two case studies in section 3.6 and 3.7).

## 3.5 Model-based process (operation) analysis (Step 4)

The complete set of equations representing a problem-system specific model is analyzed numerically and then solved according to an appropriate solution strategy (equation ordering, selection of numerical solver, etc.). The independent set of equations representing the model is listed and the associated variables are classified as scalars, vectors and/or matrices. An incidence matrix of all the equations and the associated variables is then developed, and ordered to obtain a lower triangular form (if feasible) for the algebraic equations (AEs). If the triangular form is obtained, then the resulting AEs

are decomposed and solved sequentially. Otherwise, they are solved simultaneously (Gani et al., 2006).

Appropriate simulation strategies are developed based on the operation scenario (phase), the form of the constitutive models as well as the form of the generated specific model. For example, the operations of a batch cooling crystallizer could be divided into three phases, where for example, phase 1 represents cooling to reach the saturation point (in this case, nucleation and crystal growth models are not needed); phase 2 represents the nucleation phase of the operation and involves cooling until supersaturation is reached (the specific model includes overall mass and energy balance equations together with a model for nucleation and a model for the cooling jacket); phase 3 represents the crystal growth rate (all the model equations are now solved).

This means that starting from the same generic model it is possible to generate each of the specific operation phase models and there is a smooth transfer of data from one phase of operation to the next. The solution strategy therefore depends on the specific sets of equations representing a specific operation and is connected to different solvers available in ICAS-MoT including the Backward Differentiation Formulas (BDF) method (Sales-Cruz, 2006). When the generated specific model is found to give satisfactory results, it is then included in a model library of the modelling framework. In this way, the generated model is each time adapted to reflect a specific case study and thereby allows the user to analyze various crystallization operations and conditions.

## 3.6 Application of the modelling framework: paracetamol crystallization process – a one-dimensional modelling case study

The application of the modelling framework is demonstrated through two case studies involving the generation and use of various types of models and complexities. The first case study involves one-dimensional models. A paracetamol crystallization process model (adopted from Fujiwara et al., 2002; Fujiwara et al., 2005; Nagy et al., 2008b) without the description of agglomeration and breakage is generated first. The extension of this model to include the effects of agglomeration and breakage is then highlighted (by simply adding the corresponding constitutive models). Furthermore the option to adapt the generated model for another chemical system by simply changing the corresponding constitutive models (and/or model parameters) is illustrated for a sucrose crystallization process (adopted from Ouiazzane et al., 2008).

### 3.6.1 Paracetamol without agglomeration and breakage

The model for paracetamol without the effects of agglomeration and breakage is generated from the generic multi-dimensional model by following the steps (see Figure 3.1) of the modelling framework.

#### 3.6.1.1 Problem definition (Step 1)

The overall objective for this modelling task is to observe the one-dimensional crystallization for size independent growth based on concentration and temperature

profiles as well as to describe the properties of the crystal particles, and especially, the total crystal mass and the mean size diameter.

### 3.6.1.2 Model (process) problem specification (Step 2)

The chemical system being studied consists of paracetamol (solute) and water (solvent). The equipment involved is a jacketed batch crystallizer.

### 3.6.1.3 Model development and solution (Step 3)

For the generation of the problem-system specific model, the process conditions and assumptions as reported by others (Fujiwara et al., 2002; Fujiwara et al., 2005; Nagy et al., 2008b) have been used. First the balance equations to be used are selected (formulated). In the PBE formulation, the assumption for this model is size independent growth of the one-dimensional PBE. Also, the agglomeration and breakage phenomena are not considered. This one-dimensional PBE is solved (in step 4) using the standard method of moments. The operation is unseeded, the solution is ideal and the initial crystal size is neglected in the overall mass and energy balance equation. In the selection of the constitutive equations, secondary nucleation is assumed while the effect of agitation is neglected in the nucleation and crystal growth rate equations. Based on the above information, the necessary balance equations are created from the generic model (see Tables 3.3, 3.5, 3.7 & 3.8) and the necessary constitutive equations are retrieved from the constitutive models library (see Tables 3.9 & 3.11). The generated model is listed in Table 3.12.

Table 3.12 List of model equations for paracetamol crystallization

| Equations | No. | Number of Equations |
|---|---|---|
| $\frac{d\mu_0}{dt} = B_{nuc}$ | 1 | 1 |
| $\frac{d\mu_1}{dt} = G_x\mu_0$ | 2 | 1 |
| $\frac{d\mu_2}{dt} = 2G_x\mu_1$ | 3 | 1 |
| $\frac{d\mu_3}{dt} = 3G_x\mu_2$ | 4 | 1 |
| $\frac{dc}{dt} = -3\rho_c k_v G_x \mu_2$ | 5 | 1 |
| $\rho V c_p \frac{dT}{dt} = -\Delta H_c \rho_c k_v V \left(3G_x\mu_2\right) - U_1 A_1 \left(T - T_w\right)$ | 6 | 1 |
| $\rho_w V_w c_{pw} \frac{dT_w}{dt} = \rho_w F_{win} c_{pw} \left(T_{win} - T_w\right) + U_1 A_1 \left(T - T_w\right) + U_2 A_2 \left(T_{ex} - T_w\right)$ | 7 | 1 |
| $c^{sat} = a_{i1} + b_{i1}T + c_{i1}T^2 + d_{i1}T^3$ | 8 | 1 |
| $S = c - c^{sat}$ | 9 | 1 |
| $M_c = \rho_c k_v \mu_3$ | 10 | 1 |
| $B_{nuc} = k_b S^b$ | 11 | 1 |
| $G_x = k_{gx} S^{gx}$ | 12 | 1 |
| $S[1,0] = \frac{\mu_1}{\mu_0}$ | 13 | 1 |
| $A[2,0] = \frac{\mu_2}{\mu_0}$ | 14 | 1 |
| $V[3,0] = \frac{\mu_3}{\mu_0}$ | 15 | 1 |
| **Total number of equations = 15** | | |

**Total number of variables = 39**

**DOF = 39 - 15 = 24**

### 3.6.1.4 Model-based process (operation) analysis (Step 4)

The generated problem-system specific model is first analyzed and then solved with the ICAS-MoT modelling tool to simulate the different crystallizer operation phases. As can be seen in Table 3.12, there are 7 differential and 8 algebraic equations in the generated paracetamol crystallization model. All the variables found in the equations are listed in Table 3.13, with the degrees of freedom (DOF) found to be 24.

Table 3.13 Variable types in the paracetamol crystallization model

| Variable types | Status | Symbol | Number | Total |
|---|---|---|---|---|
| Known (To be specified) | Fixed by system | $\rho_c, a_{i1}, b_{i1}, c_{i1}, d_{i1}, \Delta H_c, \rho_w, c_{pw}, \rho, c_p$ | 10 | 24 |
| | Fixed by model | $k_{gx}, k_b, k_v, g_x, b$ | 5 | |
| | Fixed by problem | $V_w, F_{win}, T_{win}, U_1, A_1, U_2, A_2, T_{ex}, V$ | 9 | |
| | Adjustable parameter | - | - | |
| Unknown variables (To be predicted) | Algebraic (Explicit) | $c^{sat}, M_c, B_{muc}, G_x, S, S[1,0], A[2,0], V[3,0]$ | 8 | 15 |
| | Differential (Dependent) | $\mu_0, \mu_1, \mu_2, \mu_3, c, T, T_w$ | 7 | |

Based on the DOF analysis, the variables are divided into a set that needs to be specified and a set that needs to be predicted, as shown in Table 3.13. The variables that need to be specified (known) are then classified as those that are fixed by the system, fixed by the problem, fixed by the model and finally the ones that are the adjustable (regressed) model parameters. The unknown variables are determined by solving the

model equations. Next the incidence matrix of the model equations is developed (highlighted for the base model (Table 3.12) in Appendix A) – note that the specified variables are not included in this matrix. The equations are ordered to obtain the lower triangular form. The shaded section of the matrix represents differential variables and differential equations. By neglecting the shaded portion, the incidence matrix shows a lower triangular form indicating that the remaining model equations (algebraic equations) can be solved sequentially (one equation at a time). Based on this analysis, the model equations were then solved in ICAS-MoT.

The simulation strategies (and the corresponding model) for this case study are different depending on the specific phase of the crystallization operation. Crystallization starts with an initial cooling operation (phase 1) where the solution is cooled from 45˚C to reach the saturation concentration. Once the saturation point is reached, the solution is further cooled to create supersaturation conditions where the solution starts to crystallize (phase 2-nucleation). In phase 2, the nucleation rate needs to be computed together with the concentration, temperature and cooling jacket temperature. The crystal nuclei then start to grow, thus necessitating (phase 3) the crystal growth rate model and continues until the end of the crystallization operation.

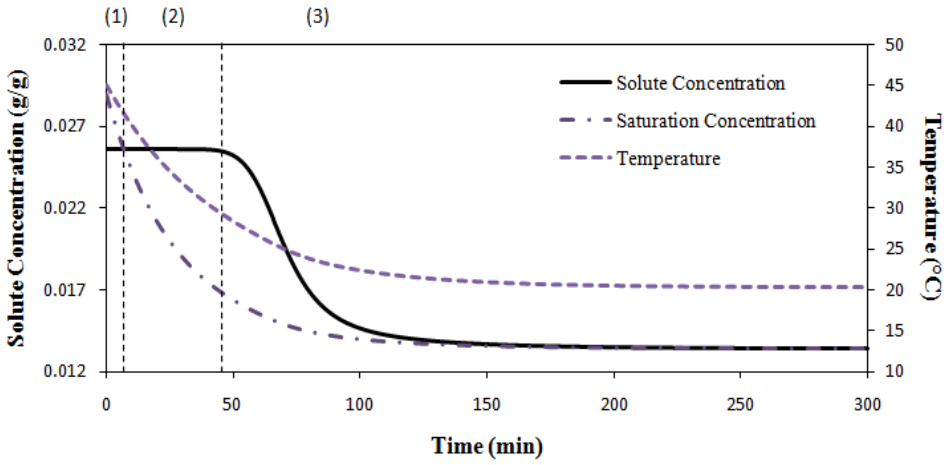


Figure 3.3 Paracetamol concentration and temperature profile for open-loop operation. Numbers above the graph refer to the different phases in the crystallization process (see text for details)

The open-loop simulation results obtained in this way are shown in Figure 3.3. According to the simulation results, a solute concentration of 0.013 g paracetamol/g water is reached at the end of the batch process when the temperature is decreased from 45 to 20˚C (see Figure 3.3). Phase 1 indicates that the simulated paracetamol concentration (initially started at 0.0256 g paracetamol/g water) is saturated at time 5.5 minutes. However the paracetamol (saturated) concentration is maintained in phase 2 because most crystal nuclei remain dissolved. In the unseeded operation, usually the crystal nuclei are generated first by the nucleation and subsequently grown by crystal growth phenomena. In order to specify the nucleation region, a threshold value has been set at 0.0255 g paracetamol/g water where the nucleation is first occurred when the paracetamol concentration is in the supersaturated condition. Once the paracetamol concentration reached this threshold value, then the crystal growth phase is started as

shown in Figure 4.3 where the paracetamol concentration starts to decrease at time 45 minutes, i.e. during phase 3, until the end of the operation at time 300 minutes.

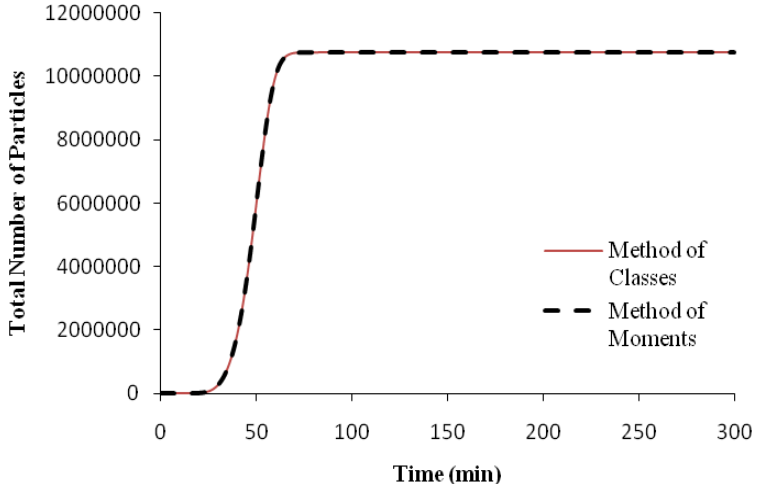


Figure 3.4 Comparison of particles simulation results for different solution methods of the PBE

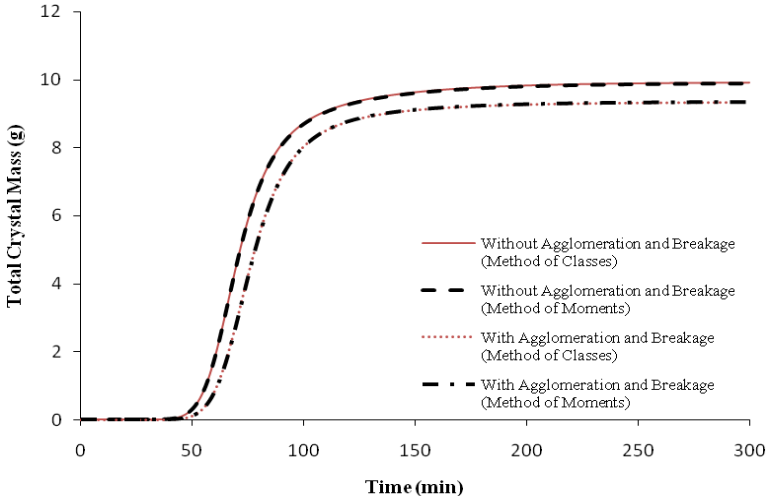


Figure 3.5 Comparison of PBE solution methods for total crystal mass simulation results with and without agglomeration and breakage

The generated paracetamol crystallization model has also been solved using the method of classes to verify that both methods of solution, in principle, give similar simulated behaviour under similar process conditions (specifications). This also validates the model generation options in the modelling framework. In this case study, the simulated behaviours by the method of classes and the standard method of moments have been found to be in good agreement. As shown in Figures 3.4 and 3.5, both methods are in agreement in terms of the total number of particles and the total crystal mass produced. In term of total crystal mass produced, it is assumed that less total number of crystal particles have been generated due to effect of agglomeration and breakage which explains the low crystal mass obtained compared to the total crystal mass generated without agglomeration and breakage. Therefore both methods can be used for one-dimensional paracetamol crystallization studies. In terms of computational details, both methods have been implemented in the ICAS-MoT modelling tool, and the calculations have been performed on a desktop PC Intel Core 2 Quad CPU, 2.66 GHz, 3.46 GB RAM. The time needed to solve the paracetamol crystallization model using the standard method of moments is 15 seconds compared to 40 seconds for the method of classes. This difference is mainly because the standard method of moments solves a smaller number of ODEs (as listed in Table 3.12), while the number of ODEs for the method of classes depends on the number of discretization points.

### 3.6.2 Paracetamol with agglomeration and breakage

An interesting and useful feature of the modelling framework is that it makes model reformulations (generating actually new models or step by step development of

models) quite easy. For example, the generated one-dimensional paracetamol crystallization model can be extended to include the effect of agglomeration and breakage. This means that the specific model generated earlier (see Table 3.12) is simply reformulated by extending the population balance equation by adding the constitutive models corresponding to agglomeration and breakage phenomena. The necessary equations are extracted from the agglomeration and breakage rate expressions, which are available in the set of constitutive models (see Table 3.9). The production-reduction term is selected from Table 3.9 without considering the agitation effects and is assumed to represent the birth and death rates generated by agglomeration and breakage. The other model equations remain unchanged. The new generated specific model for paracetamol crystallization is then analyzed and solved in ICAS-MoT to study the influence of agglomeration and breakage phenomena on the physical properties of the crystals.

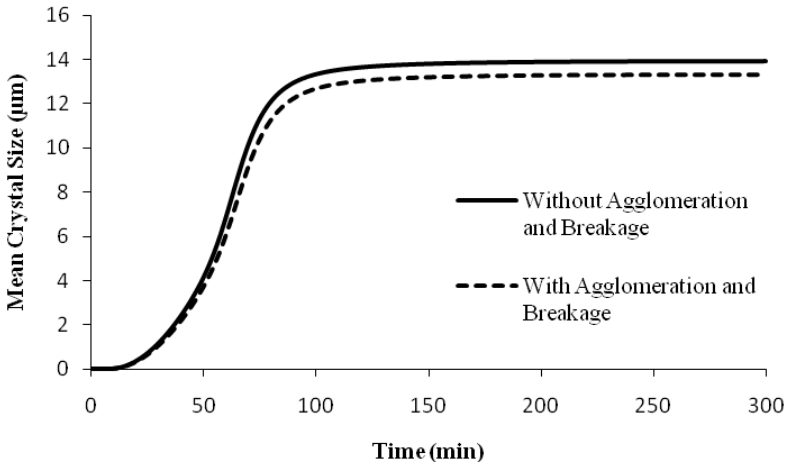


Figure 3.6 Comparison in term of mean crystal size between paracetamol crystallization model with and without agglomeration and breakage

Figures 3.5 and 3.6 show that a total paracetamol crystal mass of approximately 10 g with a mean crystal size of 14 μm is obtained when agglomeration and breakage phenomena are not considered. When agglomeration and breakage are included, the paracetamol crystallization resulted in a total crystal mass of about 9 g, with an approximate mean crystal size of 13 μm. Note that both crystal (physical) properties are rather low, especially the mean crystal size. The low value can be explained because the solute concentration is far above the saturation concentration in this case, resulting in a high supersaturation in the beginning of the crystallization process. The high supersaturation significantly increases the nucleation rate and produces many crystal particles. However by the end of the process the solute concentration operates closer to the saturation concentration indicating relatively low supersaturation. This low supersaturation leads to a low crystal growth rate contributing to a low value of the mean crystal size (diameter). These crystal properties could be further adjusted by operating the crystallizer such that the concentration is within a metastable zone. The implementation of process control and monitoring schemes to improve the crystallization operation is discussed in more detail in the Chapter 4.

### 3.6.3 Changes in the chemical system selection

Another interesting and useful modelling option is to reformulate (that is, reuse of models) an existing model by changing the set of constitutive model equations (or their parameters) suitable for another chemical system. Thus, using the generated one-dimensional paracetamol crystallization model, a model for sucrose crystallization is easily obtained, as will be demonstrated below.

For the sucrose crystallization model, the specific model generated for paracetamol (in the case without agglomeration and breakage) can be reused considering that there are no changes in the process specifications: size independent growth, unseeded and no agitation (see example in Table 2.4). Therefore, the sucrose crystallization model uses the same balances and constitutive equations as the paracetamol crystallization model. The only changes needed are that one needs to reselect the chemicals involved, which are now sucrose (solute) and water (solvent). The new chemical systems then necessitate an update of the parameters and coefficients needed to perform the calculation of the constitutive equations such as saturation concentration, nucleation rate and crystal growth rate. These are the only modifications needed to obtain the sucrose crystallization model. Moreover, a numerical analysis of the sucrose crystallization model is not needed since it has the same structure as the paracetamol model, which has already been analyzed. The sucrose crystallization model is solved in ICAS-MoT where the parameters and known variables are adopted from Quintana-Hernández et al. (2004) and Ouiazzane et al. (2008). Figure 3.7 shows the temperature profile when cooling down from 70 to 40˚C and a concentration of 2.33 g sucrose/g water is obtained by the end of the process operation. In terms of crystal properties, Figure 3.8 shows that a total crystal mass of approximately 137 g and a mean crystal size of 337 μm are obtained.

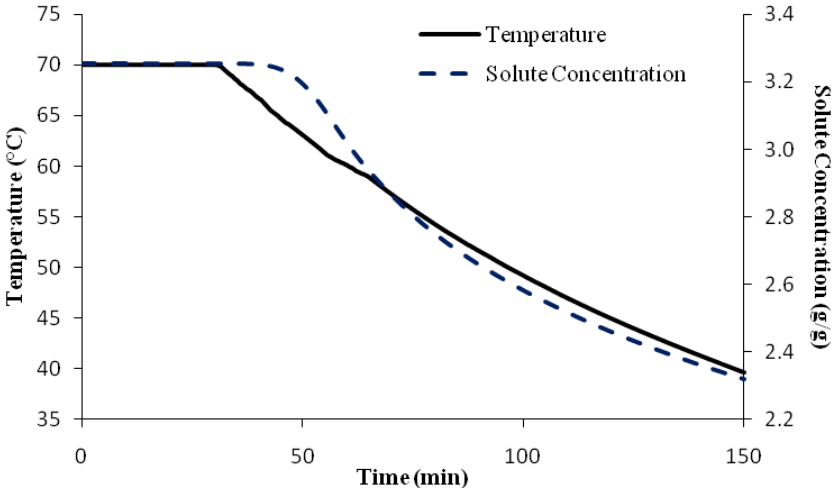


Figure 3.7 Temperature and concentration profiles for the sucrose crystallization process considering no agglomeration and breakage take place

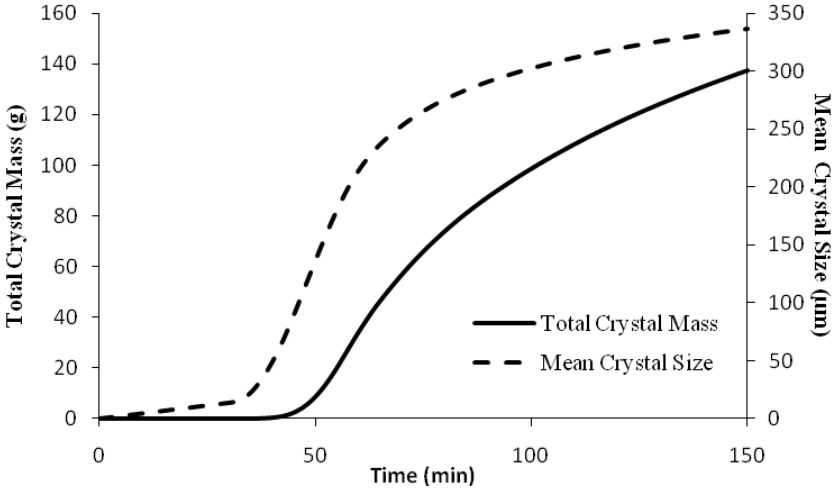


Figure 3.8 Total crystal mass and mean crystal size for the sucrose crystallization process considering no agglomeration and breakage take place

## 3.7 Application of the modelling framework: potassium dihydrogen phosphate (KDP) crystallization process – a two-dimensional modelling case study

In this section, the capability of the modelling framework to deal with increased model complexity (use of two-dimensional models) is demonstrated using the potassium dihydrogen phosphate (KDP) crystallization process (adopted from Ma et al., 2002; Gunawan et al., 2002).

### 3.7.1 Problem definition (Step 1)

The overall modelling objective in this case study is to generate models that can help to analyze the concentration and temperature profiles obtained for the one- and the two-dimensional models, as well as to predict the properties of the crystal particles, especially with respect to the total crystal mass and mean size diameter.

### 3.7.2 Model (process) problem specification (Step 2)

The chemical system that needs to be investigated is the crystallization of potassium dihydrogen phosphate (KDP) from an aqueous solution and involves KDP (solute) and water (solvent). The process equipment involved is a jacketed batch crystallizer.

### 3.7.3 Model development and solution (Step 3)

The one-dimensional KDP case study is developed first. In the PBE formulation, the assumptions for this model are size independent growth with no agglomeration and breakage phenomena considered. This one-dimensional PBE is solved using the standard method of moments. The operation is seeded and the initial crystal size is neglected in the overall mass and energy balance equation. In the constitutive models selection, the secondary nucleation is assumed. The effect of agitation is neglected in the nucleation and crystal growth rate equations, and a cube shaped crystal is assumed. Based on this information, the necessary balance and constitutive equations are extracted from the set of generic balance and constitutive equations (see Tables 3.3, 3.5, 3.7-9, 3.11).

For the same chemical system and crystallization process, the one-dimensional model can easily be transformed to a two-dimensional model. The changes needed to develop the two-dimensional KDP crystallization process model are mainly the PBE formulation where the equations now are extended to consider the growth in two directions (length and width). This two-dimensional PBE is also solved using the standard method of moments. By considering the growth in two directions, a more complex crystal shape can be considered in the two-dimensional model thus overcoming the limitation of shape selection in the one-dimensional model (e.g. cube, sphere etc.). However, the same crystal shape used in the one-dimensional model cannot be used in the two-dimensional model. In this case, a tetragonal prism-shaped crystal is assumed for the two-dimensional model. Unlike the overall mass balance equation in the one-dimensional model, where the particle shape factor is applied to represent the crystal shape, the final overall mass balance in the two-dimensional model is obtained by

substituting the volume occupied by the selected crystal shape. In the constitutive equations, two crystal growth rate equations are now added (length and width), as well as equations for calculating the average length and width of the crystals. Other than that, the same assumptions, equations and chemical properties used in the one-dimensional model, are also used here. The generated specific two-dimensional model is listed in Table 3.14.

Table 3.14 List of model equations for the two-dimensional KDP crystallization

| Equations | No. | Number of Equations |
|---|---|---|
| $\frac{d\mu_{00}}{dt} = B_{nuc}$ | 1 | 1 |
| $\frac{d\mu_{10}}{dt} = G_x \mu_{00}$ | 2 | 1 |
| $\frac{d\mu_{01}}{dt} = G_y \mu_{00}$ | 3 | 1 |
| $\frac{d\mu_{20}}{dt} = 2G_x \mu_{10}$ | 4 | 1 |
| $\frac{d\mu_{02}}{dt} = 2G_y \mu_{01}$ | 5 | 1 |
| $\frac{d\mu_{11}}{dt} = G_x \mu_{01} + G_y \mu_{10}$ | 6 | 1 |
| $\frac{d\mu_{21}}{dt} = 2G_x \mu_{11} + G_y \mu_{20}$ | 7 | 1 |
| $\frac{dc}{dt} = -\frac{\rho_c}{m_w}\left(2G_x\left(\mu_{11} - \mu_{20}\right) + G_y \mu_{20}\right)$ | 8 | 1 |
| $T = T_0 - \left(T_0 - T_f\right)\left(t / t_{batch}\right)$ | 9 | 1 |
| $c^{sat} = a_{i1} + b_{i1}T + c_{i1}T^2 + d_{i1}T^3$ | 10 | 1 |
| $S = \left(c - c^{sat}\right) / c^{sat}$ | 11 | 1 |
| $B_{nuc} = k_b S^b V$ | 12 | 1 |
| $G_x = k_{gx} S^{gx}$ | 13 | 1 |
| $G_y = k_{gy} S^{gy}$ | 14 | 1 |
| $N_c = \mu_{00}$ | 15 | 1 |
| $M_c = \rho_c \mu_{21}$ | 16 | |
| $\overline{L}_1 = \frac{\mu_{10}}{\mu_{00}}$ | 17 | 1 |
| $\overline{L}_2 = \frac{\mu_{01}}{\mu_{00}}$ | 18 | 1 |
| **Total number of equations = 18** | | |
| **Total number of variables = 34** | | |
| **DOF = 34 – 18 = 16** | | |

### 3.7.4 Model-based process (operation) analysis (Step 4)

The two-dimensional model (see Table 3.14) for the KDP crystallization process is analyzed and then solved in the ICAS-MoT modelling tool. The DOF for this specific model is 16. The complete set of variables are classified into those that need to be specified and those that need to be calculated, as listed in Table 3.15 (given only for the two-dimensional model). Next, the incidence matrix is analyzed (see Appendix B), an optimal equation-ordering is obtained (in this case also a lower-triangular form is again obtained) and based on this, the model equations are solved in ICAS-MoT.

Table 3.15 Variable types in the two-dimensional KDP crystallization model

| Variable types | Status | Symbol | Number | Total |
|---|---|---|---|---|
| Known (To be specified) | Fixed by system | $\rho_c, a_{i1}, b_{i1}, c_{i1}, d_{i1}, M_w$ | 6 | 16 |
| | Fixed by model | $k_b, b, k_{gx}, g_x, k_{gy}, g_y$ | 6 | |
| | Fixed by problem | $T_0, T_f, t, t_{batch}$ | 4 | |
| | Adjustable parameter | - | - | |
| Unknown variables (To be predicted) | Algebraic (Explicit) | $T, B_{nuc}, G_x, G_y, c^{sat}, S, N_c, M_c, \overline{L}_1, \overline{L}_2$ | 10 | 18 |
| | Differential (Dependent) | $\mu_{00}, \mu_{10}, \mu_{01}, \mu_{20}, \mu_{02}, \mu_{11}, \mu_{21}, c$ | 8 | |

For a batch time of 2 hours (for one- and two-dimensional models), the temperature is decreased linearly from 34 to 28°C until the end of the crystallization operation. The initial solute concentration of 0.308 g KDP/g water is cooled from 34°C until it reaches the saturation line after approximately 1000 seconds (phase 1). The solution is then further cooled to create the supersaturation condition. Once the

supersaturation condition is reached, 1.5 g of seed crystals are introduced into the solution to prevent a too high nucleation in the beginning (phase 2). The average size of the crystal seed in the one-dimensional case is 100 μm, while in the two-dimensional model, the average length and width of the crystal seed are also 100 μm. This seed then grows based on crystal growth phenomena until the end of the batch operation (phase 3).

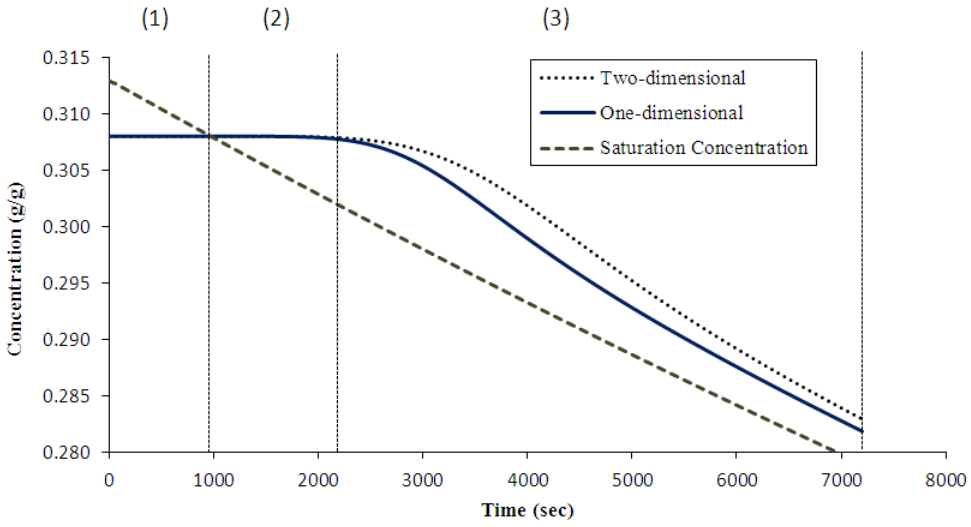


Figure 3.9 Comparison of concentration profiles for the KDP crystallization model. Numbers above the graph refer to the different phases in the crystallization process (see text for details)

This can be seen in Figure 3.9 where the solute concentration according to both models is decreasing steadily because some of the solute in the solution is transferred to the solid crystal particles until the KDP concentration reaches 0.281 g KDP/g water (one-dimensional) and 0.283 g KDP/g water (two-dimensional), when the batch operation ends. Comparing the predictions from the two models, it can be noted (see Figure 3.9) that the solute concentration profile in the one-dimensional model is decreasing more

rapidly than in the two-dimensional model. This is because the cube-shaped volume in the one-dimensional case consumes more solute from the solution than the tetragonal prism-shaped volume in the two-dimensional case.

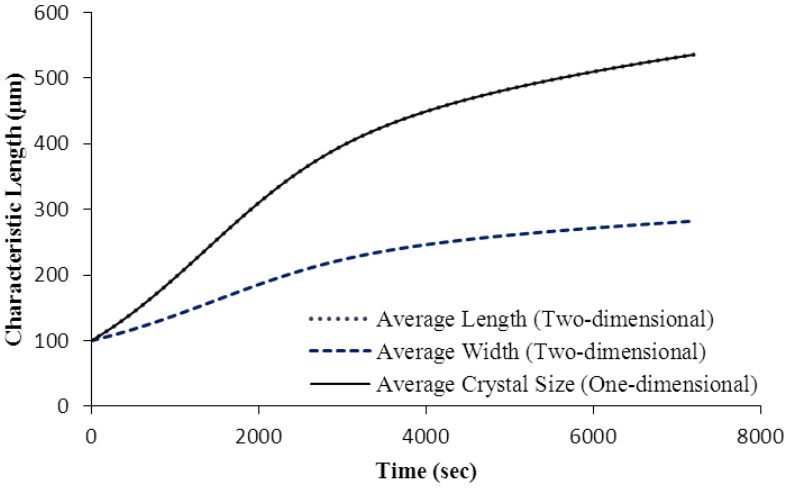


Figure 3.10 Characteristic lengths for the one- and two-dimensional KDP crystallization model

As shown in Figure 3.10, the crystal seed in the one-dimensional model has grown from 100 μm to a final average crystal size of 540 μm. The initial average length and width of the seed crystal is 100 μm for the two-dimensional case. Figure 3.10 also shows that the average length and width of the crystal increases towards the end of the process (for example, at t = 7200 seconds). The average length of the crystals grown from seeds is around 538 μm and the average width is approximately 280 μm indicating that the crystals are elongating because of two different kinetic crystal growth parameters applied to the same crystal growth model. The significance of this result is that the

volume of more complicated crystal shapes can be determined more accurately based on information on the average length and width.

The method of classes has also been applied to solve the KDP model for similar process specifications: size independent crystal growth, no agglomeration and breakage. This was done in order to compare the performance of the method of classes with the standard method of moments. As illustrated in Figures 3.11 and 3.12, results obtained from both methods are similar in terms of the total number of particles and the total crystal mass produced for the KDP process. However the total simulation time for the method of classes is 14 minutes, which is much longer than for the standard method of moments (20 seconds). In the two-dimensional case, the method of classes requires discretization in the length and width direction, resulting in a significantly higher number of ODEs.

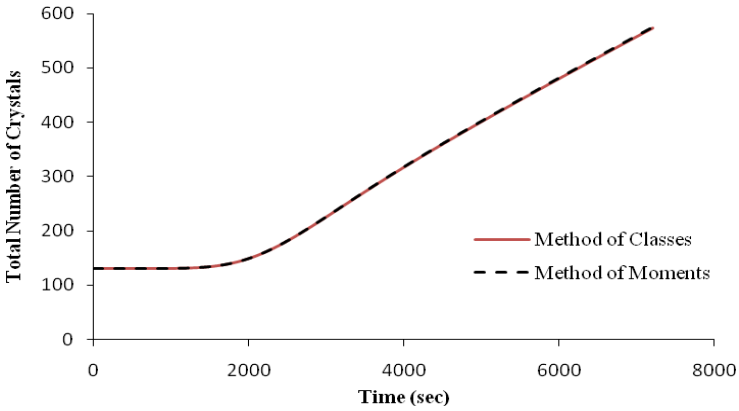


Figure 3.11 Comparison of total number of crystals for different solution methods of the PBE

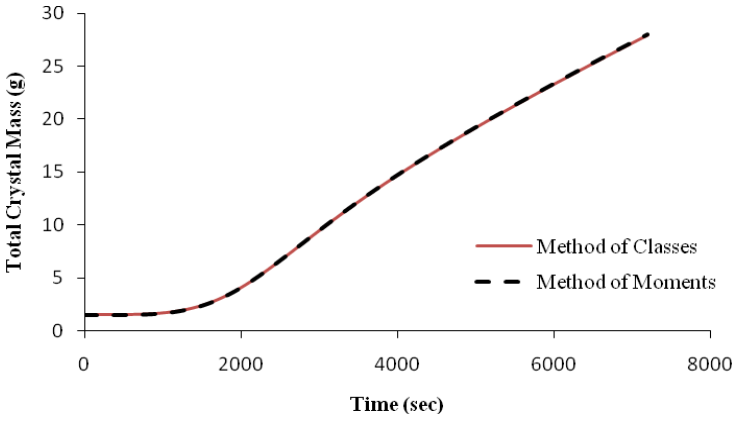


Figure 3.12 Comparison of total crystal mass for different solution methods of the PBE

## 3.8 Conclusion

A modelling framework for generating multi-dimensional batch cooling crystallization process operation models from a generic model has been presented. The generic model and the generated specific models cover different operation phases of a crystallizer. Also, by changing the constitutive models, the crystallization of a wide range of chemical systems can be studied. The application of the modelling framework has been highlighted through two case studies. In the first case study, a one-dimensional model for paracetamol crystallization was generated; the model was then extended to consider the agglomeration and breakage effects, and was then reformulated for application to sucrose crystallization. In the second case study, the feature of the modelling framework to handle different levels of model complexity, including one-dimensional and two-dimensional crystals, has been illustrated through a KDP crystallization case study. The results of the models generated with the modelling

framework have shown good agreement with the published crystallization data, validating thereby the models based on the data reported by others. These generated models are therefore ready for use in model-based design and control/-analysis of crystallization operations within model-based process monitoring and control systems (for example, Singh et al., 2009, 2010).

# 4. A systematic framework for design of a process monitoring and control (PAT) system for crystallization processes

In this chapter, the development of a generic and systematic model-based computer-aided framework for the design of a process monitoring and control system to achieve a desired CSD and crystal shape for a wide range of crystallization processes is presented. This framework combines a generic multi-dimensional modelling framework (Samad et al., 2011a), with methods and tools for generating set point profiles, for design of PAT systems (Singh et al., 2009) including methods for monitoring and control. For monitoring and control, well-known methods (Nagy et al., 2008a) have been integrated. For set point profiles generation, an extended analytical CSD estimator method and the response surface method (RSM) are employed to generate the set point profiles needed to match the desired target crystal products. The systematic framework is used to design a monitoring and control system for two systems: potassium dichromate and potassium dihydrogen phosphate (KDP) crystallization processes. In each case study, one-dimensional CSD and two-dimensional CSD modelling features of the methodology are highlighted.

## 4.1 Systematic design framework for process monitoring and control (PAT) system

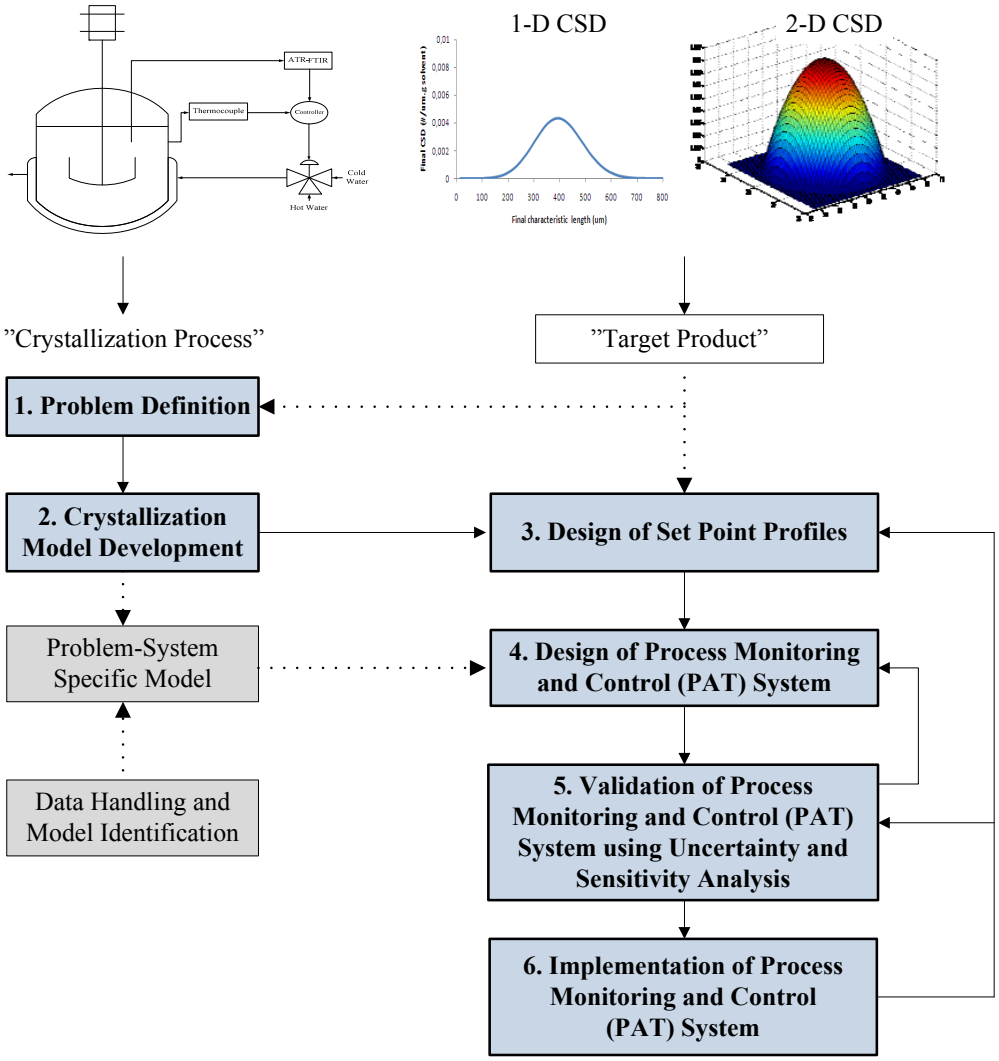


Figure 4.1 Systematic design framework for the process monitoring and control (PAT) system in crystallization processes

The main specifications of a crystal product are usually given in terms of any desired CSD, crystal size and/or shape. In order to develop an operational policy that can indeed achieve these specifications, a model-based systematic framework for design of monitoring and control systems of crystallization processes has been developed (see Figure 4.1) - it consists of 6 main steps. Each step in this framework is explained in more detail below.

## 4.2 Problem definition (Step 1) and crystallization model development (Step 2)

The first step concerns the definition of the overall design objective. For example, design a process monitoring and control system to achieve the specified (target) crystal product properties, such as, one- or two-dimensional CSD, crystal size and/or crystal shape. In the crystallization model development phase (Step 2), the necessary problem-system specific model for the chemical system under investigation is generated. For this step, although, the generic multi-dimensional crystallization modelling framework developed in Chapter 3 is adopted, in principle, the framework can allow any other modelling framework or user-specified model. This step is also connected to the practical data handling and the model identification (shown in Figure 4.1) but these features however are not highlighted in this work.

## 4.3 Design of set point profiles (Step 3)

Usually, the crystallization operation takes place within a zone bounded by the metastable limit and the solubility curve, and set point generation is based on a trial and error approach where the operation is maintained at a suggested set point trajectory until the end of the operation. It is then checked whether the obtained CSD matches the target CSD. If this is not the case, the operation is repeated using a different set point trajectory until the target CSD is matched. A major disadvantage of such an approach, apart from the fact that it can be very time consuming, is that it does not come with any guarantee that the desired target CSD will be obtained at any point. In this step of the design framework, a systematic procedure to generate the set point profiles is applied instead, by either using an extended analytical CSD estimator based method or by using the response surface method (RSM). It is also possible to supply user-specified target set point profiles.

### 4.3.1 Analytical CSD estimator

A one-dimensional analytical CSD estimator has been developed by Aamir (2010). The estimator, which is based on the assumptions of constant supersaturation throughout the entire batch operation and absence of nucleation, helps to generate set point profiles that yield a target CSD, given that the initial seed distribution and growth kinetics of the crystallization system are known. The generated set point profiles represent the supersaturation point that needs to be maintained during the entire batch operation in order to achieve the desired target CSD.

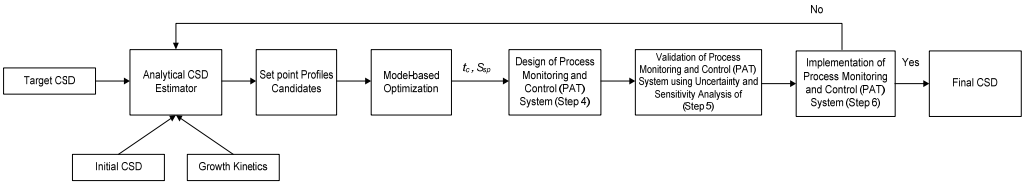


Figure 4.2 Flow chart for the generation of set point profiles to achieve a desired target CSD using the analytical CSD estimator

Figure 4.2 shows the flow chart for generating the set point profiles that allow achieving a desired target CSD using the analytical CSD estimator. In this work, the original analytical CSD estimator (Aamir, 2010) has been extended to cover one- as well as two-dimensional problems (see Table 4.1). To apply the analytical CSD estimator, three requirements need to be satisfied: (1) a target CSD is available; (2) a CSD of the initial seed crystals is known; and (3) a model representing the growth kinetics is available. The target CSD ( $f_n$ ), usually a one- or two-dimensional CSD, is specified by the users in the form of a distribution such as a normal, lognormal or bimodal (sum of two normal) distribution (Aamir, 2010). Also, the quadratic distribution can also be used as a target CSD for simulation purposes (Qamar et al., 2007; Gunawan et al., 2004). It is important to remark that although the analytical CSD estimator can be used to design the operation of crystallization systems with respect to any arbitrary target CSD, the achievable target distribution will however depend on the initial seed distribution and the growth kinetics. For example, the target distribution in the form of a normal distribution can only be attained by starting with normally distributed seed crystals and may not be attained by the use of seed crystals that follow a quadratic distribution or other distribution functions.

In order to select a feasible target CSD, the user thus needs to be aware of the distribution of the initial seed crystals. Furthermore, in the case of size independent

growth rates, the width of the distribution (based on the standard deviation for a normal and lognormal distribution) from the initial seed is not changed when compared to the target CSD, i.e., only the mean of the characteristic length is increased. In the case of a size dependent growth rate, however, a narrow initial seed size distribution may be used to attain a wider target CSD. The CSD of the initial seed ( $f_{n0}$ ) needs to be specified because it serves as a starting point for the crystals to grow from an initial characteristic length ( $L_{x0}$ ). In the proposed design framework, the CSD of the initial seed is specified (based on available experimental data or information) and/or assumed to have a normal, lognormal, bimodal or a quadratic distribution (Aamir, 2010; Qamar et al., 2007; Gunawan et al., 2004). In addition the kinetic growth parameters ( $k_{gx}, gx, \gamma_x, p_x, k_{gy}, gy, \gamma_y, p_y$ ) in the analytical CSD expressions should be available and are specific for the chemical system that is investigated. In case these parameters are not available, the modelling framework provides options to estimate them first. The estimator can handle size independent growth as well as size dependent growth (case $\left(\gamma_x = \gamma_y \neq 0;\ p_x = p_y \neq 1\right)$ or $\left(\gamma_x = \gamma_y \neq 0;\ p_x = p_y = 1\right)$ respectively).

Table 4.1 Generic analytical CSD estimator expressions

| Characteristic | Analytical Solutions |
|---|---|
| Size independent growth:<br>$G_x = k_{gx} S^{gx}$<br>$G_y = k_{gy} S^{gy}$ | Final CSD:<br>$f_n = f_{n0}$ |
| | Final characteristic length:<br>$L_x = L_{x0} + k_{gx} S_{sp}{}^{gx} t_c$ |
| | Final characteristic width:<br>$L_y = L_{y0} + k_{gy} S_{sp}{}^{gy} t_c$ |
| Size dependent growth:<br>$G_x = k_{gx} S^{gx} \left(1+\gamma_x L_x\right)^{p_x}$<br>$G_y = k_{gy} S^{gy} \left(1+\gamma_y L_y\right)^{p_y}$<br>For the case of:<br>$\left(\gamma_x = \gamma_y \neq 0;\ p_x = p_y \neq 1\right)$ | Final CSD:<br>$f_n = f_{n0}\left[\frac{\left(1+\gamma_x L_{x0}\right)^{1-p_x} + k_{gx} S_{sp}{}^{gx} \gamma_x t_c \left(1-p_x\right)}{\left(1+\gamma_x L_{x0}\right)^{1-p_x}}\right]^{\frac{p_x}{(p_x-1)}}$<br>$+ f_{n0}\left[\frac{\left(1+\gamma_y L_{y0}\right)^{1-p_y} + k_{gy} S_{sp}{}^{gy} \gamma_y t_c \left(1-p_y\right)}{\left(1+\gamma_y L_{y0}\right)^{1-p_y}}\right]^{\frac{p_y}{(p_y-1)}}$ |
| | Final characteristic length:<br>$L_x = \frac{\left[\left(1+\gamma_x L_{x0}\right)^{1-p_x} + k_{gx} S_{sp}{}^{gx} \gamma_x t_c \left(1-p_x\right)\right]^{\frac{1}{1-p_x}} - 1}{\gamma_x}$ |
| | Final characteristic width:<br>$L_y = \frac{\left[\left(1+\gamma_y L_{y0}\right)^{1-p_y} + k_{gy} S_{sp}{}^{gy} \gamma_y t_c \left(1-p_y\right)\right]^{\frac{1}{1-p_y}} - 1}{\gamma_y}$ |
| Size dependent growth<br>$G_x = k_{gx} S^{gx} \left(1+\gamma_x L_x\right)$<br>$G_y = k_{gy} S^{gy} \left(1+\gamma_y L_y\right)$<br>For the case of:<br>$\left(\gamma_x = \gamma_y \neq 0;\ p_x = p_y = 1\right)$ | Final CSD:<br>$f_n = f_{n0} \exp^{-\left(\gamma_x k_{gx} S_{sp}{}^{gx} t_c + \gamma_y k_{gy} S_{sp}{}^{gy} t_c\right)}$ |
| | Final characteristic length:<br>$L_x = \frac{\left(1+\gamma_x L_{x0}\right) \exp^{\left(\gamma_x k_{gx} S_{sp}{}^{gx} t_c\right)} - 1}{\gamma_x}$ |
| | Final characteristic width:<br>$L_y = \frac{\left(1+\gamma_y L_{y0}\right) \exp^{\left(\gamma_y k_{gy} S_{sp}{}^{gy} t_c\right)} - 1}{\gamma_y}$ |
| *Note that only one growth kinetic expression is used for the one-dimensional case, and therefore the growth term represents the additional growth kinetics in the final CSD expressions and the final characteristic width is neglected | |

Each candidate of set point profile, in essence consisting of a combination of the required supersaturation set point profiles ($S_{sp}$) and the total crystallization time ($t_c$), is generated using the analytical CSD estimator. The set point profiles are then optimized (model-based) to obtain the optimal set point profile by minimizing the sum of squares of relative errors between the predicted CSD obtained from the analytical estimator and the desired target CSD.

Minimize

$$F_{obj} = \sum_{i=1}^{n} \left( \frac{f_{n,i_{calculated}} - f_{n,i_{target}}}{f_{n,i_{target}}} \right)^2 \tag{4.1}$$

Subject to: $S_{sp}, t_c$

$$S_{sp,\min} \le S_{sp} \le S_{sp,\max} \tag{4.2}$$

$$t_{\min} \le t_c \le t_{\max} \tag{4.3}$$

$$c_{t_{batch}} \le c_{f_{\max}} \tag{4.4}$$

Where $n$ is the number of discretization points, $f_{n,i_{calculated}}$ is the predicted CSD obtained from the analytical CSD estimator and $f_{n,i_{target}}$ is the desired target CSD, $c_{t_{batch}}$ is the expected solute concentration at the end of the batch and $c_{f_{\max}}$ represents the maximum acceptable solute concentration at the end of the batch to achieve a required yield. The optimization problem consisting of Equations (4.1) to (4.4) is then constructed for either the one- or the two-dimensional case, depending on the requirements of the specific problem that is considered, and is solved using a sequential quadratic programming (SQP) based solver to obtain the optimal set point profile (combination of supersaturation

set point profile and total crystallization time). The optimal set point profile is then used in design steps (steps 4 to 6). In case a different set point profile or changes in the target specifications are desired, options to return to the analytical CSD estimator is provided (see Figure 4.2).

### 4.3.2 Response surface method (RSM)

An alternative way to generate the set point profiles to achieve desired target CSDs is to employ the response surface method (RSM) (Myers et al., 2009) as shown in Figure 3. Or in other words, design of experiments (DoE) is used for the generation of a number of suitable set point profile candidates. In the DoE, the central composite design (CCD) technique is employed to determine the required number of experiments/simulations to cover all factors. In the model-based study presented here, only simulations are considered. The number of required simulations for the CCD is estimated as $2^k + 2k + 6$ runs, where $k$ corresponds to the number of considered factors (Box and Hunter, 1957). An important reason for also including the DoE in the systematic framework is that this is a methodology that is generally used in the pharmaceutical industry when setting up experiments.

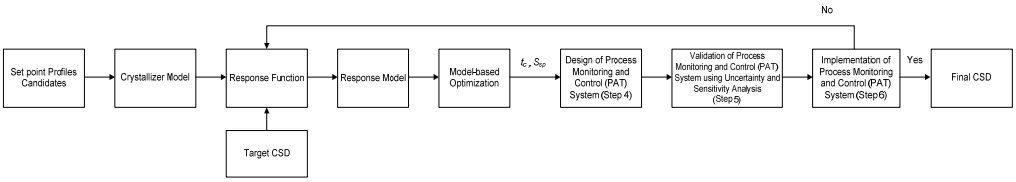


Figure 4.3 Flow chart for the generation of set point profiles to achieve a desired target CSD using the RSM

The crystallization model is then simulated for each generated set point profiles candidate in order to determine the final CSD. The final CSD corresponding to the different set point profiles candidates are then used together with the target CSD for calculating the response function (RF). The RF (Equation 4.5) is here identified as the sum of squares of relative errors between the final CSD obtained from the detailed crystallization model for each set point profiles candidate and the specified target CSD.

$$RF = \sum_{i=1}^{n} \left( \frac{f_{n,i_{calculated}} - f_{n,i_{target}}}{f_{n,i_{calculated}}} \right)^2 \tag{4.5}$$

Where $n$ is the number of discretization points, $f_{n,i_{calculated}}$ is the predicted CSD obtained from the detailed crystallization model and $f_{n,i_{target}}$ is the desired target CSD. The response model is then developed. The process factors that affect the final CSD are: a) supersaturation set point profiles, $S_{sp}$ and b) total crystallization time, $t_c$. The response model is therefore given by Equation (4.6). Based on the response data, obtained through simulations, a regression analysis is carried out to determine the coefficients of the response model $(b_0, b_1, b_2, \ldots, b_n)$.

$$RF = b_0 + b_1 S_{sp} + b_2 t_c + b_3 S_{sp} t_c + b_4 {S_{sp}}^2 + b_5 {t_c}^2 \tag{4.6}$$

The coefficients in Equation (4.6) are estimated using the least squares regression method. The $R^2$ coefficient is determined as well to assay the quality of the response

model, in order to quantify whether or not a reliable correlation is obtained. The results are evaluated by plotting the effects of the considered factors on the response through the three-dimensional response surface plots. The optimal solution is identified based on the optimal set of factors that produce a minimum response value. This is due to the fact that the lowest response value indicates that the final CSD obtained from applying the set point profiles candidates is very close to the target CSD, resulting in the lowest relative errors (response value). Similarly, the optimal set point profile is then used in the further design steps (steps 4 to 6). Again, there are options to return to the response function step if it is necessary to analyze different set point profiles candidates (see Figure 4.3).

## 4.4 Design of process monitoring and control (PAT) system (Step 4)

In this step, the process monitoring and control system is designed to achieve the desired end product properties. In order to properly design a process monitoring and control system for crystallization processes, the design methodology for PAT systems developed by Singh et al. (2009) is employed. The details of this methodology can be found in the referenced paper. In this work, the model library and the knowledge base have been supplemented with crystallization related processes.

## 4.5 Validation of process monitoring and control (PAT) system using uncertainty and sensitivity analysis (Step 5)

Another feature of the proposed framework is the ability to perform uncertainty and sensitivity analysis on the designed PAT system. In this step, the impact and influence of input uncertainties on the predicted system performance are investigated, i.e., the risk of not achieving the target specifications of the crystal product is quantified. This feature however is discussed in more detail in the Chapter 5.

## 4.6 Implementation of process monitoring and control (PAT) system (Step 6)

The developed design of the process monitoring and control system for a crystallization process is then implemented (in a rigorous simulator or an actual process) to ensure that the final product quality is satisfied with respect to the process/product specifications. The final design proposal contains the process flowsheet with the necessary monitoring tools/techniques, the model equipment data corresponding to the identified monitoring equipments for process variables (such as temperature, concentration etc.) and the graphics to illustrate the predicted evolution of the CSD (obtained in this work, by simulation). There are also options here to return to the design of the set point profiles (step 3) if a different set point profiles candidates or changes in target product specifications are considered. Furthermore, this step is also linked to the

uncertainty and sensitivity analysis step (step 5) if it is necessary to investigate the influence of uncertainty on the product properties.

## 4.7 Application of the design framework: potassium dichromate crystallization case study

The application of the developed systematic design framework to achieve a target one-dimensional CSD is demonstrated for the potassium dichromate crystallization process (adopted from Aamir et al., 2009, 2010). By defining the target CSD, the stepwise procedure in the design framework is highlighted in terms of the crystallizer model needed, the required set point generated using the analytical CSD estimator and the control strategies implementation in order to achieve the given target. The feature of the design framework to perform the uncertainty and sensitivity analysis of the Process Monitoring and Control (PAT) system (Step 5) is not highlighted in this chapter but it is the main subject of the next chapter.

### 4.7.1 Problem definition (Step 1)

The overall objective for this design task is to design a monitoring and control system for a potassium dichromate crystallization process in order to achieve a desired target one-dimensional CSD together with the mean characteristic length and total crystal mass. The target one-dimensional CSD is assumed as a normal distribution given in Equation (4.7). The mean and standard deviation of this target distribution are 490 μm

and 52 μm respectively and the desired target CSD shown in Figure 4.4 is generated using Equation (4.7).

$$f_{n,1-D}^{target} = 0.00767 \exp\left( -\frac{(L_x - 490)^2}{5408} \right) \tag{4.7}$$

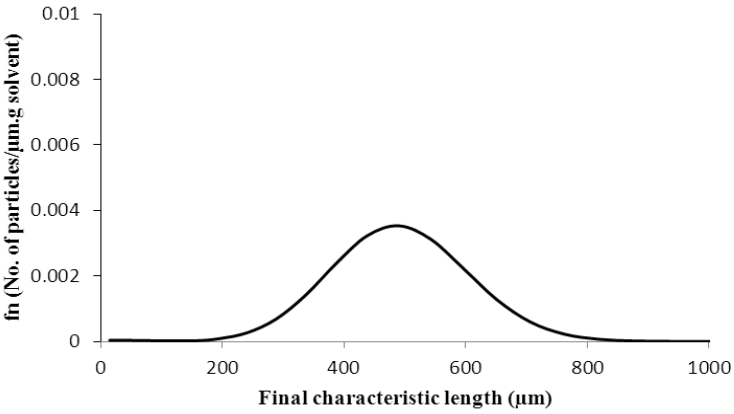


Figure 4.4 Desired target CSD

### 4.7.2 Crystallization model development (Step 2)

In order to generate a problem-system specific one-dimensional model for potassium dichromate crystallization, the generic multi-dimensional model-based framework (Samad et al., 2011a) is employed. Similar conditions and assumptions as reported in the literature (Aamir et al., 2009, 2010) are used to generate the problem-system specific model. Here the operation is seeded, and the one-dimensional case with no agglomeration and breakage is considered. Furthermore, size dependent growth and secondary nucleation are assumed while the effect of agitation is neglected in the nucleation and crystal growth rate. By using these assumptions, the set of equations

needed to represent the model is then extracted from the generic multi-dimensional model-based framework. Table 4.2 shows the complete problem-system specific model for the potassium dichromate crystallization process generated by the generic multi-dimensional model-based framework.

Table 4.2 List of model equations for the one-dimensional model of potassium dichromate crystallization

| No. | Type of equations | Equations |
|---|---|---|
| 1 | Population balance equation (size dependent growth) | For $i = 1$; $\frac{dN_1}{dt} + \frac{G_{x1}}{2\Delta Cl_2} N_2 + \frac{G_{x1} - G_{x0}}{2\Delta Cl_1} N_1 = B_{nuc}$, For $1 < i < n$; $\frac{dN_i}{dt} + \frac{G_{xi}}{2\Delta Cl_{i+1}} N_{i+1} + \frac{G_{xi} - G_{xi-1}}{2\Delta Cl_i} N_i + \frac{G_{xi-1}}{2\Delta Cl_{i-1}} N_{i-1} = 0$, For $i = n$; $\frac{dN_n}{dt} + \frac{G_{xn-1}}{2\Delta Cl_n} N_n - \frac{G_{xn-1}}{2\Delta Cl_{n-1}} N_{n-1} = 0$, |
| 2 | Overall mass balance: solute concentration | $\frac{dc}{dt} = -\frac{\rho_c k_v V}{m_w} \left( \sum_{i=1} S_{xi}^3 \frac{dN_i}{dt} \right)$ |
| 3 | Energy balance | $\rho V c_p \frac{dT}{dt} = -\Delta H_c \rho_c k_v V \left( \sum_{i=1} S_{xi}^3 \frac{dN_i}{dt} \right) - U_1 A_1 \left( T - T_w \right)$ |
| 4 | Cooling jacket energy balance | $\rho_w V_w c_{pw} \frac{dT_w}{dt} = \rho_w F_{win} c_{pw} \left( T_{win} - T_w \right) + U_1 A_1 \left( T - T_w \right) + U_2 A_2 \left( T_{ex} - T_w \right)$ |
| 5 | Saturation concentration | $c^{sat} = a_{i1} + b_{i1} T + c_{i1} T^2 + d_{i1} T^3$ |
| 6 | Supersaturation | $S = c - c^{sat}$ |
| 7 | Nucleation | $B_{nuc} = k_b S^b V$ |
| 8 | Crystal growth rate (Length direction) | $G_{xi} = k_{gx} S^{g_x} \left( 1 + \gamma_x L_{xi} \right)^{p_x}$ |
| 9 | Characteristic size | $S_{xi} = \frac{L_{xi} - L_{xi-1}}{2}$ |
| 10 | Total number of particles | $N_c = N_1 + N_2 + N_3 + \ldots + N_n$ |
| 11 | Total crystal mass | $M_c = \rho_c k_v \left( \sum_{i=1} S_{xi}^3 N_i \right)$ |
| 12 | Crystal size distribution | $f_n \left( L_{xi} \right) = \frac{\frac{N_i}{\Delta Cl_i} + \frac{N_{i+1}}{\Delta Cl_{i+1}}}{2}$ |

### 4.7.3 Design of set point profiles (Step 3)

In this step, the set point profile that yields the desired target one-dimensional CSD is generated using model-based optimization involving the analytical CSD estimator. First, the initial seed of the CSD is specified. Here the initial seed of the CSD has been generated as a normal distribution by using a mean characteristic length of 156.89 µm and a standard deviation of 43.75 µm as shown in Equation (4.8). The generated initial seed of the CSD is shown in Figure 4.5 where it served as the starting point for the seed crystal to grow until it reaches the target CSD.

$$f_{n0,1-D} = 0.00912 \exp\left( -\frac{(L_x - 156.89)^2}{3828.13} \right) \tag{4.8}$$

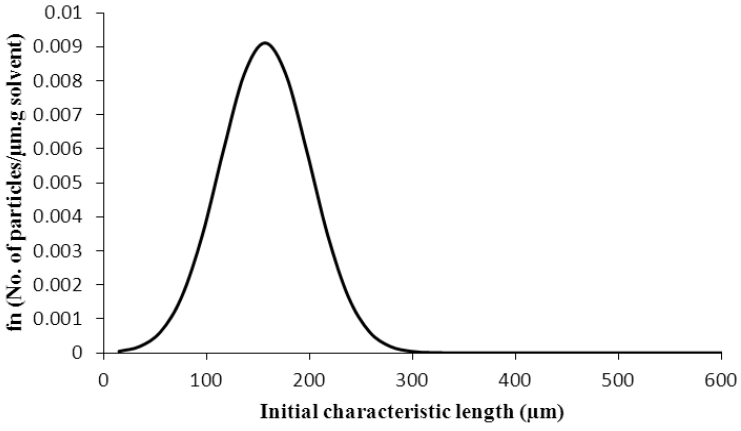


Figure 4.5 Size distribution of the initial seed of the CSD

The analytical CSD estimator for the one-dimensional and the case of size dependent growth $(\gamma_x \neq 0;\ p_x \neq 1)$ is selected as shown in Table 4.1 and the growth

parameter for the potassium dichromate system used is shown in Table 4.3 (adopted from Aamir (2010). Subsequently the analytical CSD estimator is applied to generate the set point candidates and based on these candidates, the optimal set point is obtained by solving the model-based optimization problem consisting of Equations (4.1) to (4.4) using the SQP approach implemented in the ICAS-MoT software. The lower and upper bounds set for the supersaturation set point are $1\times10^{-5}$ g solute/g water and $1\times10^{-3}$ g solute/g water, respectively. Meanwhile the lower bound of 150 minutes and upper bound of 200 minutes are set for the total crystallization time. The optimal set point profiles obtained in this way consist of the supersaturation set point of $1.25\times10^{-4}$ g solute/g water and a total crystallization time of 180 minutes.

Table 4.3 Kinetic growth parameters of potassium dichromate crystallization

| Parameter | Value | Units |
|---|---|---|
| Growth rate constant, $k_{gx}$ | 9.56 | µm/s |
| Growth constant, $\gamma_x$ | 0.0075 | 1/ µm |
| Growth constant, $p_x$ | 1.24 | - |
| Growth order constant, $g_x$ | 0.8 | - |

### 4.7.4 Design of process monitoring and control (PAT) system (Step 4)

The problem-system specific model generated in Step 2 and the set point created in Step 3 are used to design a process monitoring and control system (PAT system) for the potassium dichromate crystallization process. The objective here is to design a process monitoring and control (PAT) system for this process to achieve the desired target one-dimensional CSD. In this study, the design of a PAT system for potassium dichromate crystallization process has been performed in the ICAS-PAT software (Singh

et al., 2010). Based on the design procedure, the target product properties are potassium dichromate with the following specifications: potassium dichromate concentration: 0.137 g potassium dichromate/g water; the target one-dimensional CSD generated earlier (see Figure 4.4) with mean characteristic length: 490 μm, standard deviation of 52 μm and total crystal mass: 6.75 g. The chemical system being studied consists of potassium dichromate (solute) and water (solvent). The equipment involved is a jacketed batch crystallizer.

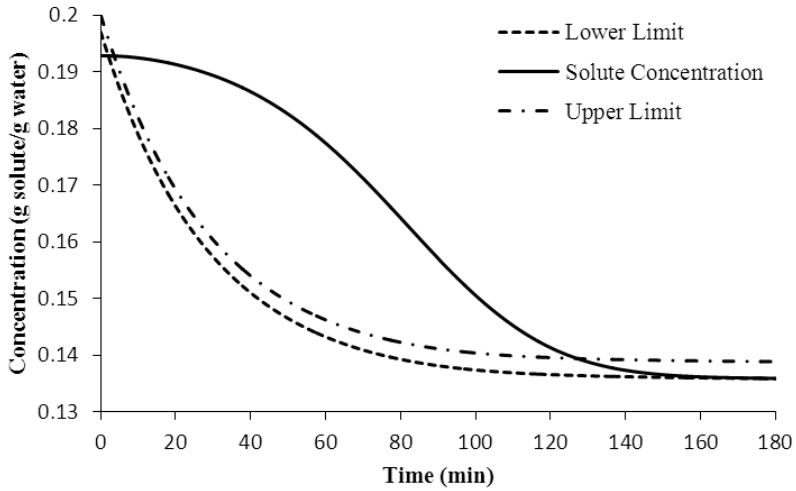


Figure 4.6 Potassium dichromate concentration profiles for open-loop simulation

The open-loop simulation is then performed in the sensitivity analysis step to identify the critical process variables. Based on the open-loop simulation as shown in Figure 4.6, the potassium dichromate concentration was found to violate the upper limit (metastable limit) specified for this process. Therefore it is concluded that the potassium dichromate concentration needs to be controlled in order to maintain the operation within

the specified limits. The analysis is then carried out for all process variables and based on the analysis it was found that the temperature also violated the specified limits and thus is listed together with the potassium dichromate concentration as a critical process variable.

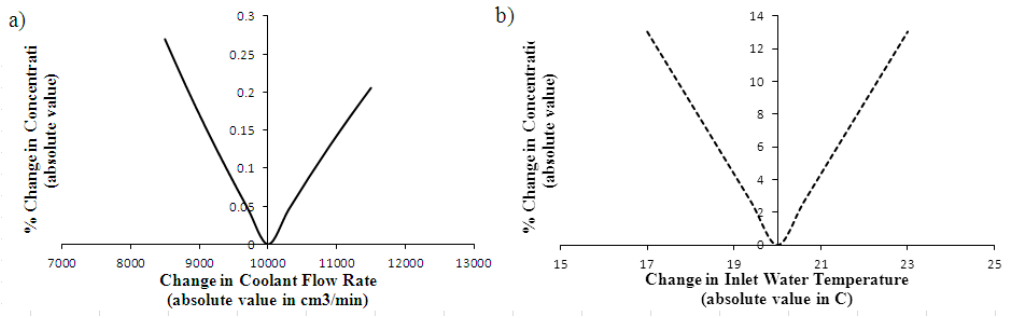


Figure 4.7 Interdependency analysis for change in potassium dichromate concentration based on a) change in coolant flow rate and b) change in inlet water temperature

The interdependency analysis is performed for each critical process variable to select a suitable actuator. The analysis is conducted for the potassium dichromate concentration and the corresponding actuator candidates (coolant flow rate and inlet water temperature) were selected for analysis. Figure 4.7 shows that the change in the inlet water temperature is more affected the potassium dichromate compare to the change in the coolant flow rate indicating thereby, the inlet water temperature is more sensitive than the coolant flow rate. Therefore, it was selected as an actuator to control the potassium dichromate concentration in the batch crystallization process. The analysis is then repeated for temperature and based on this analysis it is also concluded that the inlet water temperature is more sensitive and selected as an actuator to control the temperature. Since the objective of the control implementation in the crystallization process is usually to maintain the operation in the metastable zone, therefore only one control-loop is

applied. This can be done by implementing either supersaturation control or temperature control. In this work, the supersaturation control is used and thus the potassium dichromate concentration is controlled by manipulating the inlet water temperature.

The performance analysis of the monitoring tools is then conducted to select the appropriate monitoring tools for each measurable critical process variables. Based on the analysis, the potassium dichromate concentration, the temperature and the CSD are monitored using the attenuated total reflection fourier transform infrared (ATR-FTIR), thermocouple and laser diffraction using malvern masterisizer respectively. Based on the PAT design procedure, the process monitoring and control (PAT) system for the potassium dichromate crystallization is summarized in Table 4.4.

Table 4.4 Proposed process monitoring and analysis system for potassium dichromate crystallization

| Propose a process monitoring and control system | | | | |
|---|---|---|---|---|
| Critical process points | Critical process variables | Actuators | Monitoring techniques | Monitoring tools |
| Crystallizer | Concentration | Inlet water temperature | ATR-FTIR | ATR-FTIR probe |
| Crystallizer | Temperature | Inlet water temperature | Thermocouple | WZ-08541-28 (E20-gauge thermocouple) |
| Crystallizer | Crystal size distribution (CSD) | - | Laser diffraction | Malvern Mastersizer |

### 4.7.5 Implementation of process monitoring and control (PAT) system (Step 6)

A closed-loop simulation is then performed to validate the proposed PAT system. Here a proportional-integral (PI) controller has been developed in order to control the concentration at the desired set points where the generated set point profile is used as a supersaturation set point for the controller. Based on the closed-loop simulation result, where the potassium dichromate concentration initially started at 0.1928 g potassium dichromate/g water, it can be concluded that once the concentration set point was reached the concentration was successfully maintained at the set point using the PI controller. In Figure 4.8, approximately 0.1377 g potassium dichromate/g water remains by the end of the operation.

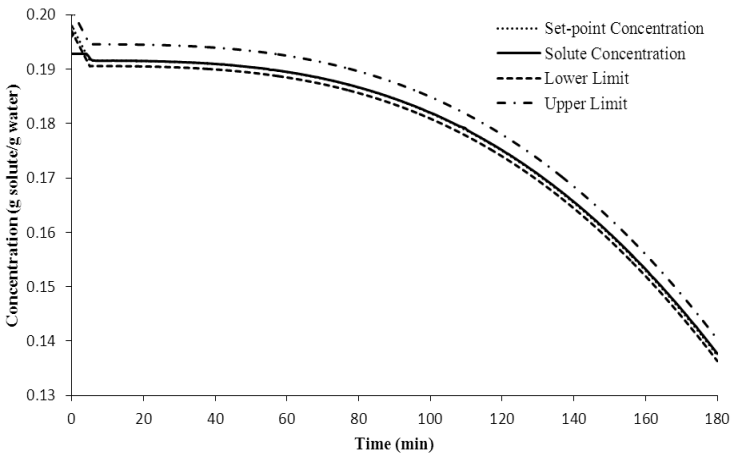


Figure 4.8 Concentration profiles for closed-loop simulation

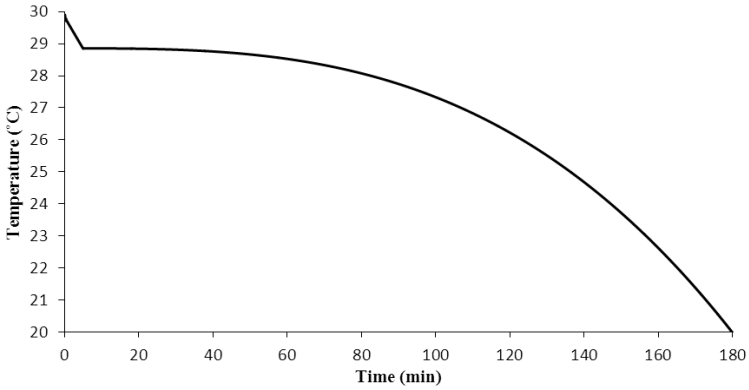


Figure 4.9 Temperature profiles for closed-loop simulation

Figure 4.9 shows the temperature profiles obtained from closed-loop simulation, where the temperature initially is at 30°C, and the liquid is then cooled down to 20°C in 180 minutes. Based on this analysis it was found that the potassium dichromate concentration was maintained at the set point indicating that the generated set point was feasible. Subsequently the performance of the simulated operation is compared with the desired target CSD as highlighted in Figure 4.10. It can be seen that the final CSD obtained from the detailed simulation model is very close to the desired target. The mean and standard deviation obtained for this final CSD are 488.1 μm and 51.83 μm, which is in good agreement with the mean (490 μm) and standard deviation (52 μm) for the target CSD. In terms of total mass obtained, Figure 4.11 shows that a total crystal mass of approximately 6.73 g is obtained from an initial seed mass of 1.2 g used in this study. Based on this analysis, it is shown that the analytical CSD estimator has the ability to provide the set point profiles for producing the desired target CSD. This has been confirmed through the PAT system implementation for potassium dichromate which indicates that by

maintaining the operation at the generated set point profile, the target CSD is successfully achieved.

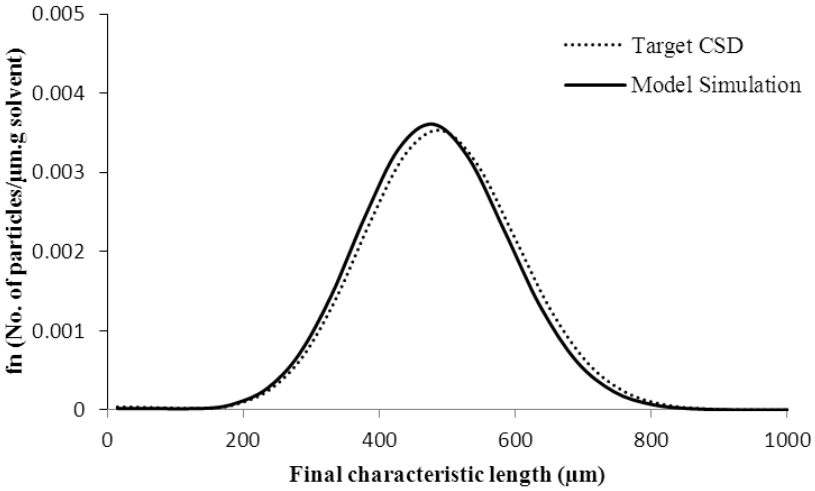


Figure 4.10 Final CSD for potassium dichromate, comparison between the detailed simulation model and the target CSD

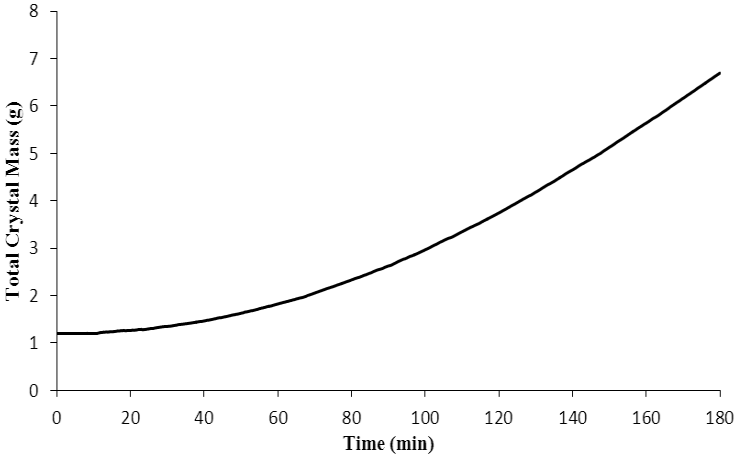


Figure 4.11 Total predicted crystal mass for potassium dichromate crystallization

Finally, a feasible design of the PAT system as shown in Figure 4.12 is obtained. A PI control system is used to control the solute concentration. The concentration is monitored by ATR-FTIR and the temperature is monitored by a thermocouple. The inlet water temperature is manipulated by blending hot and cold water. Meanwhile the CSD is also monitored by Malvern mastersizer. Finally the evolution of the CSD from the initial seed CSD (see Figure 4.5) to the final CSD (see Figure 4.10) is represented in 3-D graphs as shown in Figure 4.13. Figure 4.13(a) shows the initial seed view, were a relatively narrow distribution at the starting point has been grown into the wider distribution at the final time due to the size dependent growth effects included in the model as also shown in Figure 4.13(b).

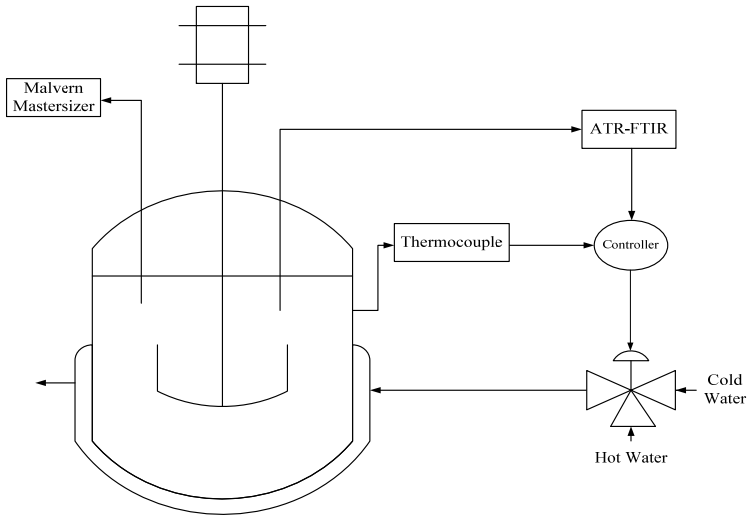


Figure 4.12 Potassium dichromate crystallization process flowsheet with designed PAT system

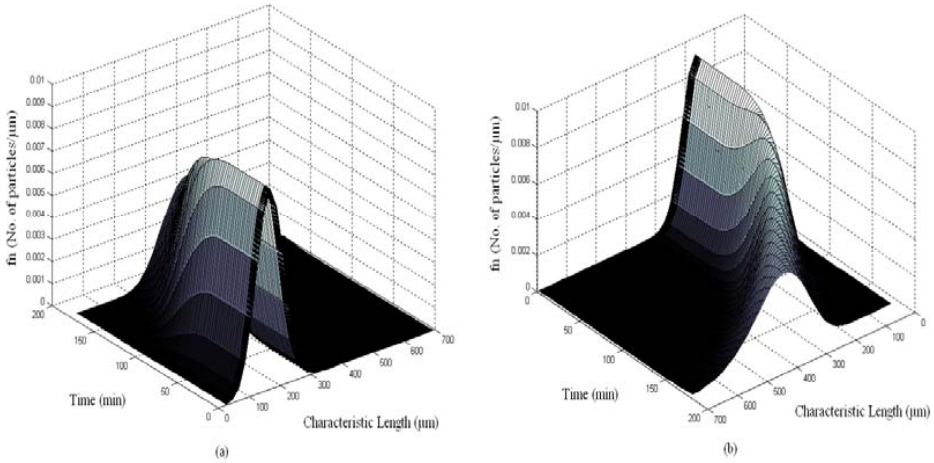


Figure 4.13 Evolution of CSD (a) initial seed view (b) final seed view

## 4.8 Application of the design framework: potassium dihydrogen phosphate (KDP) crystallization case study

In this section, application of the systematic framework for design of PAT systems is highlighted through the chemical system involving crystallization of potassium dihydrogen phosphate (KDP). Relevant data on the crystallization process were taken from Qamar et al. (2007) and Gunawan et al. (2004). The objective of the case study is to generate set point profiles and their implementation to achieve target CSDs for one- as well as two-dimensional crystals of KDP. Note that in the published literature, only the two-dimensional CSD datas could be found for the KDP chemical system. As pointed out earlier, the validation of Process Monitoring and Control (PAT) system using uncertainty and sensitivity analysis (Step 5) is not considered in this paper.

### 4.8.1 Problem definition (Step 1)

The overall objective for this design task is to design a monitoring and control system for the KDP crystallization process in order to achieve a target one- and two-dimensional CSD together with the desired crystal shape, characteristic length, characteristic width (for the two-dimensional case) and total crystal mass. The desired crystal shapes for the one- and two-dimensional cases are cube-shaped and tetragonal prism-shaped crystals, respectively. The desired targets for the one- and two-dimensional cases used in this work are assumed to be a univariate and a bivariate quadratic distribution respectively, and expressed as follows:

For one-dimensional target:

$$\begin{aligned} &\text{if} \quad 56.4 \le L_x \le 65.8 \\ &\quad f_{n,1-D}^{\ target} = -0.0521 L_x^{\ 2} + 6.381 L_x - 194.2 \\ &\text{else} \\ &\quad f_{n,1-D}^{\ target} = 0 \end{aligned} \tag{4.9}$$

For two-dimensional target:

$$\begin{aligned} &\text{if} \quad 56.4 \le L_x \le 65.8; \;\; 24.5 \le L_y \le 30.5 \\ &\quad f_{n,2-D}^{\ target} = -0.0085\left(L_x^{\ 2} + L_y^{\ 2}\right) + 0.3321\left(L_x + L_y\right) - 6.4956 \\ &\text{else} \\ &\quad f_{n,2-D}^{\ target} = 0 \end{aligned} \tag{4.10}$$

The mean characteristic length and standard deviation for the target one-dimensional CSD are 60.85 μm and 2.8 μm, respectively, while the mean characteristic length and width for the two-dimensional CSD are set at 60.85 μm and 27.36 μm with a standard

deviation of 2.8 μm (length) and 1.34 μm (width), respectively. The target one- and two-dimensional CSD are shown in Figure 4.14.

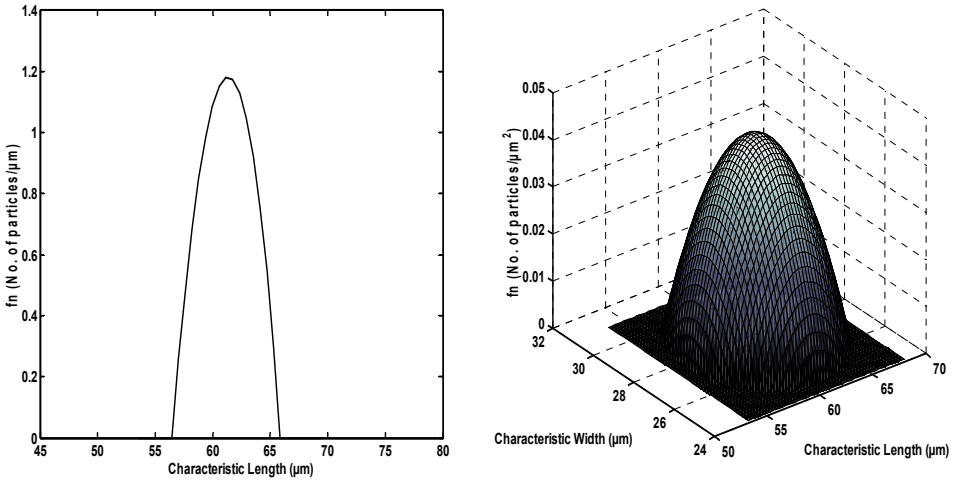


Figure 4.14 Target one- (left) and two-dimensional (right) CSD

## 4.8.2 Crystallization model development (Step 2)

In order to generate a problem-system specific one-dimensional model for KDP crystallization, the generic multi-dimensional model-based framework (Samad et al., 2011a) is employed. In the one-dimensional case, models for size dependent growth, relative supersaturation and a cube-shaped crystal are generated to obtain the problem-system specific model. Table 2 shows the complete problem-system specific one-dimensional model for the KDP crystallization process generated by the generic multi-dimensional model-based framework.

Table 4.5 List of model equations for the one-dimensional model of KDP crystallization

| No. | Type of equations | Equations |
|---|---|---|
| 1 | Population balance equation (size dependent growth) | For $i = 1$;<br>$\frac{dN_1}{dt} + \frac{G_{x1}}{2\Delta Cl_2} N_2 + \frac{G_{x1} - G_{x0}}{2\Delta Cl_1} N_1 = B_{nuc}$,<br>For $1 < i < n$;<br>$\frac{dN_i}{dt} + \frac{G_{xi}}{2\Delta Cl_{i+1}} N_{i+1} + \frac{G_{xi} - G_{xi-1}}{2\Delta Cl_i} N_i + \frac{G_{xi-1}}{2\Delta Cl_{i-1}} N_{i-1} = 0$,<br>For $i = n$;<br>$\frac{dN_n}{dt} + \frac{G_{xn-1}}{2\Delta Cl_n} N_n - \frac{G_{xn-1}}{2\Delta Cl_{n-1}} N_{n-1} = 0$, |
| 2 | Overall mass balance: solute concentration | $\frac{dc}{dt} = -\frac{\rho_c k_v V}{m_w} \left( \sum_{i=1} S_{xi}^3 \frac{dN_i}{dt} \right)$ |
| 3 | Energy balance | $\rho V c_p \frac{dT}{dt} = -\Delta H_c \rho_c k_v V \left( \sum_{i=1} S_{xi}^3 \frac{dN_i}{dt} \right) - U_1 A_1 \left( T - T_w \right)$ |
| 4 | Cooling jacket energy balance | $\rho_w V_w c_{pw} \frac{dT_w}{dt} = \rho_w F_{win} c_{pw} \left( T_{win} - T_w \right) + U_1 A_1 \left( T - T_w \right)$<br>$+ U_2 A_2 \left( T_{ex} - T_w \right)$ |
| 5 | Saturation concentration | $c^{sat} = a_{i1} + b_{i1} T + c_{i1} T^2 + d_{i1} T^3$ |
| 6 | Supersaturation | $S = \frac{c - c^{sat}}{c^{sat}}$ |
| 7 | Nucleation | $B_{nuc} = k_b S^b V$ |
| 8 | Crystal growth rate (Length direction) | $G_{xi} = 0.1 k_{gx} S^{g_x} \left( 1 + \gamma_x L_{xi} \right)^{p_x}$ |
| 9 | Characteristic size | $S_{xi} = \frac{L_{xi} - L_{xi-1}}{2}$ |
| 10 | Total number of particles | $N_c = N_1 + N_2 + N_3 + \ldots + N_n$ |
| 11 | Total crystal mass | $M_c = \rho_c k_v \left( \sum_{i=1} S_{xi}^3 N_i \right)$ |
| 12 | Crystal size distribution | $f_n \left( L_{xi} \right) = \frac{\frac{N_i}{\Delta Cl_i} + \frac{N_{i+1}}{\Delta Cl_{i+1}}}{2}$ |

For the same chemical system and crystallization process, the one-dimensional model can be extended to a two-dimensional model (Samad et al., 2011a,b). The changes needed to develop the two-dimensional model of the KDP crystallization process are mainly the population balance equation (PBE) formulation where the equations are now extended to consider growth in two directions (length and width). In the two-dimensional model, a tetragonal prism-shaped crystal is assumed. The overall mass and energy balances are obtained by substituting the volume occupied by the selected crystal shape. In the constitutive equations, two crystal growth rate equations are now added, as well as equations for calculating the CSD, total number of crystal particles, total crystal mass, mean characteristic length and width. Other than that, the same assumptions, equations and chemical properties used in the one-dimensional model are also used here. The generated problem specific two-dimensional model equations are listed in the Table 4.6. Note that a similar two-dimensional model as published in the literature (Qamar et al., 2007; Gunawan et al., 2004) is generated but in this work, the PBE is solved using the method of classes.

Table 4.6 List of model equations for the two-dimensional model of KDP crystallization

| No. | Type of equations | Equations |
|---|---|---|
| 1 | Population Balance Equation | $\frac{dN_{i,j}}{dt} + f_{i,j} + f_{i,j}^{'} = B_{nuc}, \quad i = 1,\ldots,n; j = 1,\ldots,m$ |
| 2 | Overall Mass Balance: Solute Concentration | $\frac{dc}{dt} = -\frac{\rho_c}{m_w}\left(\sum_{i,j}\left(\frac{1}{3}S_{yj}^3 + \left(S_{xi} - S_{yj}\right)S_{yj}^2\right)\frac{dN_{i,j}}{dt}\right)$ |
| 3 | Energy Balance | $\rho V c_p \frac{dT}{dt} = -\Delta H_c \rho_c V \times\left(\sum_{i,j}\left(\frac{1}{3}S_{yj}^3 + \left(S_{xi} - S_{yj}\right)S_{yj}^2\right)\frac{dN_{i,j}}{dt}\right) - U_1 A_1 \left(T - T_w\right)$ |

| | | |
|---|---|---|
| 4 | Cooling Jacket Energy Balance | $\rho_w V_w c_{pw} \frac{dT_w}{dt} = \rho_w F_{win} c_{pw} \left(T_{win} - T_w\right) + U_1 A_1 \left(T - T_w\right) + U_2 A_2 \left(T_{ex} - T_w\right)$ |
| 5 | Saturation Concentration | $c^{sat} = a_{i1} + b_{i1} T + c_{i1} T^2 + d_{i1} T^3$ |
| 6 | Supersaturation | $S = \frac{c - c^{sat}}{c^{sat}}$ |
| 7 | Nucleation | $B_{nuc} = k_b S^b V$ |
| 8 | Crystal Growth Rate (Length direction) | $G_{xi} = 0.1 k_{gx} S^{g_x} \left(1 + \gamma_x L_{xi}\right)^{p_x}$ |
| 9 | Crystal Growth Rate (Width direction) | $G_{yj} = 0.1 k_{gy} S^{g_y} \left(1 + \gamma_y L_{yj}\right)^{p_y}$ |
| 10 | Tailor development coefficient for length classes | $a_{xi} = \frac{\Delta Cl_{i+1}}{\Delta Cl_i \left(\Delta Cl_{i+1} + \Delta Cl_i\right)}$ |
| 11 | Tailor development coefficient for length classes | $b_{xi} = \frac{\Delta Cl_i}{\Delta Cl_{i+1} \left(\Delta Cl_{i+1} + \Delta Cl_i\right)}$ |
| 12 | Tailor development coefficient for width classes | $c_{yj} = \frac{\Delta Cl_{j+1}}{\Delta Cl_j \left(\Delta Cl_{j+1} + \Delta Cl_j\right)}$ |
| 13 | Tailor development coefficient for width classes | $d_{yj} = \frac{\Delta Cl_j}{\Delta Cl_{j+1} \left(\Delta Cl_{j+1} + \Delta Cl_j\right)}$ |
| 14 | Characteristic length | $S_{xi} = \frac{L_{xi} - L_{xi-1}}{2}$ |
| 15 | Characteristic width | $S_{yj} = \frac{L_{yj} - L_{yj-1}}{2}$ |
| 16 | Outlet crystal flux for length direction | $f_{i,j}^{1,O} = G_{xi} \left(a_{xi} N_{i,j} + b_{xi} N_{i+1,j}\right)$ |
| 17 | Inlet crystal flux for length direction | $f_{i,j}^{1,I} = G_{xi} \left(a_{xi-1} N_{i-1,j} + b_{xi-1} N_{i,j}\right)$ |
| 18 | Outlet crystal flux for width direction | $f_{i,j}^{2,O} = G_{yj} \left(c_{yj} N_{i,j} + d_{yj} N_{i,j+1}\right)$ |
| 19 | Inlet crystal flux for width direction | $f_{i,j}^{2,I} = G_{yj} \left(c_{yj-1} N_{i,j-1} + d_{yj-1} N_{i,j}\right)$ |
| 20 | Inlet flow for length direction | $f_{i,j} = f_{i,j}^{1,O} - f_{i,j}^{1,I}$ |
| 21 | Inlet flow for width direction | $f_{i,j}^{'} = f_{i,j}^{2,O} - f_{i,j}^{2,I}$ |
| 22 | Total number of particles | $N_c = \sum_{i,j} N_{i,j}$ |

| | | |
|---|---|---|
| 23 | Total crystal mass | $M_c = \rho_c \sum_{i,j} \left( \frac{1}{3} S_{yj}^3 + \left( S_{xi} - S_{yj} \right) S_{yj}^2 \right) N_{i,j}$ |
| 24 | Crystal size distribution | $f_n\left(L_{xi}, L_{yj}\right) = \frac{\frac{N_{i,j}}{\Delta Cl_i \Delta Cl_j} + \frac{N_{i+1,j+1}}{\Delta Cl_{i+1} \Delta Cl_{j+1}}}{2}$ |

### 4.8.3 Design of set point profiles (Step 3)

In this section, the set point profiles that guarantee the target one- and two-dimensional CSD are generated using, (i) the analytical CSD estimator, and, (ii) the response surface method (RSM).

#### 4.8.3.1 Generation of set point profiles using analytical CSD estimator

The set point profiles needed to achieve the specified target one- and two-dimensional CSD are generated using the analytical CSD estimator. In order to use the analytical CSD estimator, the initial seed distribution as well as the kinetic growth parameters needs to be specified. The initial seed distribution is acting as a starting point from where the seed is grown until it reaches the final CSD, which in the ideal case should be as close as possible to the target CSD. The initial seed distribution for the one- and the two-dimensional case was taken from Qamar et al. (2007) as follows:

For one-dimensional:

$$\begin{aligned} &\text{if} \quad 18.05 \le L_{x0} \le 21.05 \\ &\quad f_{n0,1-D} = -1.364 L_{x0}{}^2 + 53.54 L_{x0} - 522 \\ &\text{else} \\ &\quad f_{n0,1-D} = 0 \end{aligned} \tag{4.11}$$

For two-dimensional:

$$\begin{aligned} &\text{if} \qquad 18.05 \le L_{x0}, L_{y0} \le 21.05 \\ &\quad f_{n0,2-D} = -0.0348\left(L_{x0}{}^2 + L_{y0}{}^2\right) + 1.36\left(L_{x0} + L_{y0}\right) - 26.6 \\ &\text{else} \\ &\quad f_{n0,2-D} = 0 \end{aligned} \tag{4.12}$$

The CSD of the initial crystal seed is shown in Figure 4.15 for the one- and the two-dimensional cases. For the one-dimensional case, the mean characteristic length of the initial seed is 19.5 μm and the standard deviation is 0.97 μm, while, for the two-dimensional case, the corresponding means and standard deviations for the initial characteristic length and width are assumed to be identical to the one-dimensional case, i.e., 19.5 μm and 0.97 μm respectively. The total number of crystal particles as initial seed is 736 in both cases. The analytical CSD estimator for the case of size dependent growth $\left(\gamma_x = \gamma_y \neq 0;\ p_x = p_y = 1\right)$ is selected from Table 4.1 for the one- and the two-dimensional cases.

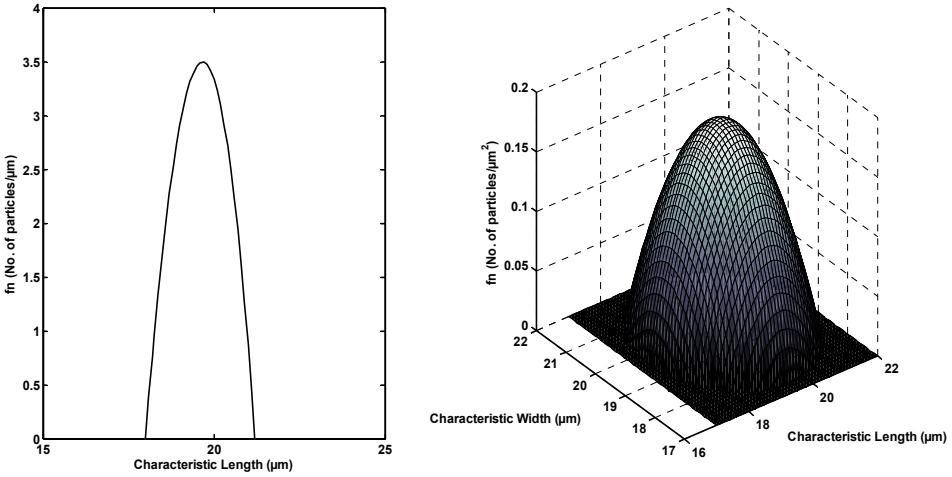


Figure 4.15 Initial seed of the one- (left) and two-dimensional (right) CSD

The kinetic growth parameters for KDP crystallization are taken from Qamar et al. (2007) as indicated in Table 4.7. Using the information of the initial seed, the target CSD and the kinetic growth parameters, the set point profiles candidates are generated using the analytical CSD estimator and subsequently applying Equations (4.1) to (4.4) for the one- and the two-dimensional cases to determine the optimal set point profile. The lower and upper bounds specified for the supersaturation are 0.015 g/g and 0.045 g/g, while a lower bound of 40 seconds and an upper bound of 120 seconds are set for the total crystallization time. The models for both cases are solved using the SQP based solver available in the ICAS-MoT software (Heitzig et al., 2011). The optimal set point profile consisting of the supersaturation set point profile of 0.03 g/g that is to be maintained and the total crystallization time of 80 seconds are obtained for both cases. The total crystallization time generated in this work is consistent with the total

crystallization time used in the published literature which is also 80 seconds (Qamar et al., 2007; Gunawan et al., 2004).

Table 4.7 Kinetic growth parameters of KDP crystallization (Qamar et al., 2007)

| Parameter | Value | Units |
|---|---|---|
| Growth rate constant (length direction), $k_{gx}$ | 100.75 | μm/s |
| Growth rate constant (width direction), $k_{gy}$ | 12.21 | μm/s |
| Growth constant (length direction), $\gamma_x$ | 0.6 | 1/ μm |
| Growth constant (width direction), $\gamma_y$ | 0.6 | 1/ μm |
| Growth constant (length direction), $p_x$ | 1 | Dimensionless |
| Growth constant (width direction), $p_y$ | 1 | Dimensionless |
| Growth order constant (length direction), $g_x$ | 1.74 | Dimensionless |
| Growth order constant (width direction), $g_y$ | 1.48 | Dimensionless |

#### 4.8.3.2 Generation of set point profiles using the response surface method (RSM)

The response surface method (RSM) can alternatively be employed to generate the necessary set point profiles corresponding to the desired target one- or two-dimensional CSD. In this study, the one- and two-dimensional CSD are considered as the response. Therefore the response function (RF) as shown in Equation (4.5) is identified as the sum of squares of relative errors between the final CSD obtained from a simulation of the detailed mathematical model for a combination of set point profiles candidates and the target CSD (generated through Equation (4.9) for the one-dimensional case and Equation (4.10) for the two-dimensional case, respectively).

The response surface study was implemented for the one- and two-dimensional cases using Matlab (R2009). The DoE was performed using a CCD to generate the set

point profile candidates. The range of values for supersaturation set point profile ($S_{sp}$) and total crystallization time ($t_c$) was defined as shown in Table 4.8. These ranges are applicable for both the one- and two-dimensional cases.

Table 4.8 The range of independent variables for experimental design

| Variables | Symbol | Range of independent variables | | | | |
|---|---|---|---|---|---|---|
| | | Lowest | Low | Center | High | Highest |
| Supersaturation set point | $S_{sp}$ | 0.009 | 0.015 | 0.03 | 0.045 | 0.051 |
| Total crystallization time | $t_c$ | 23.431 | 40 | 80 | 120 | 136.568 |

The number of tests (simulation runs) required for CCD is $2^k + 2k + 6 = 14$, for $k$ (the number of considered factors) = 2. However in this specific case, the 6 simulations corresponding to the center point are using the same operating conditions where identical response function values are expected considering that the tests here are conducted through simulations. Therefore, the one- and two-dimensional KDP model was solved for only 9 different set point profiles candidates. Table 6 lists the set point profiles candidates characterizing each of the 9 simulations and the corresponding values of the response function to evaluate the crystallization performance for the one- and two-dimensional cases.

Table 4.9 Central composite design for one- and two-dimensional cases for KDP crystallization

| Test number | Factors | | Response functions (Relative error) | |
|---|---|---|---|---|
| | Supersaturation set point | Total crystallization time | One-dimensional | Two-dimensional |
| 1 | 0.015 | 40 | 5.434 | 8.151 |
| 2 | 0.045 | 40 | 2.771 | 4.184 |
| 3 | 0.015 | 120 | 3.029 | 4.453 |
| 4 | 0.045 | 120 | 11.879 | 17.819 |
| 5 | 0.03 | 80 | 0.112 | 1.021 |
| 6 | 0.009 | 80 | 5.639 | 8.797 |
| 7 | 0.051 | 80 | 9.762 | 14.838 |
| 8 | 0.03 | 23.431 | 4.295 | 6.356 |
| 9 | 0.03 | 136.569 | 4.291 | 6.436 |

Based on the response data from the CCD, a regression analysis is carried out to determine the coefficients of the response model $(b_0, b_1, \ldots, b_n)$. In this study, the coefficients (see Equation 4.6) were estimated by least squares regression in Matlab (R2009). The solutions for the quadratic model for the one- and two-dimensional case are as follows:

One-dimensional:

$$RF = 30.05 - 1281 S_{sp} - 0.3266 t_c + 4.797 S_{sp} t_c + 16620 {S_{sp}}^2 + 0.0012735 {t_c}^2 \quad (4.13)$$

Two-dimensional:

$$RF = 42.79 - 1837 S_{sp} - 0.4426 t_c + 7.222 S_{sp} t_c + 23490 {S_{sp}}^2 + 0.001609 {t_c}^2 \quad (4.14)$$

Figure 4.16 compares the values predicted by the model versus the observed data for the one- and the two-dimensional cases and a good model fit has been obtained. The analysis of variance (ANOVA) test related to this model indicates a predicted $R^2$ value of 0.9448 (one-dimensional) and 0.9441 (two-dimensional).

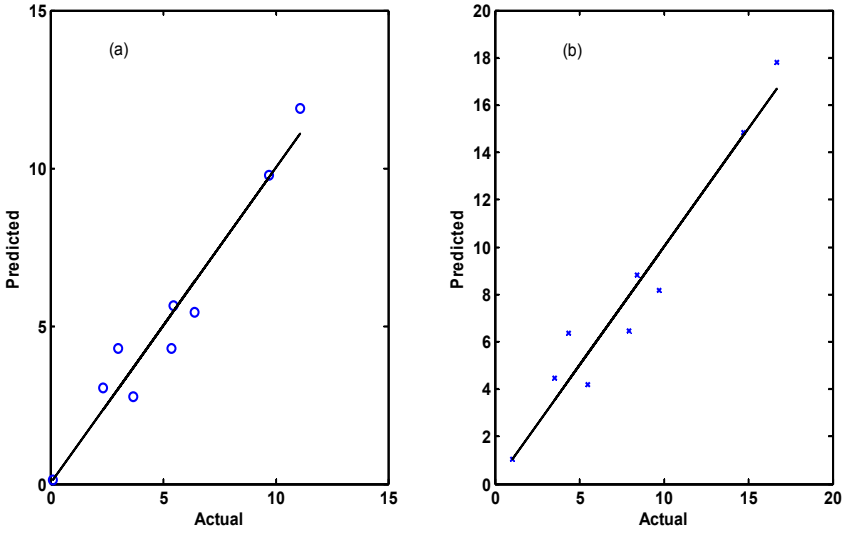


Figure 4.16 Predicted versus actual values of the response function for: (a) one-dimensional case; (b) two-dimensional case

Figure 4.17 presents the response surface as a function of total crystallization time and supersaturation set point profiles for the one-dimensional case. It shows that the relative error is the lowest for a supersaturation set point profile of 0.03 g/g and a total crystallization time of 80 seconds. The lowest relative error indicates that the final CSD obtained using this set point profile is very close to the specified target CSD. However, the relative error tends to increase at the lower supersaturation set point profile (0.015 g/g) and lower crystallization time (40 seconds). When the crystallization is operated at

the lower supersaturation and lower crystallization time, the CSD obtained is far away from the target CSD which explains the large relative error in Figure 4.17. Moreover the relative error also becomes larger for the higher supersaturation set point profile (0.045 g/g) and the higher total crystallization time (120 seconds). This is due to the fact that the crystallization, when operated at the higher supersaturation set point profile and total crystallization time (Figure 4.17, top, right), is influenced by secondary nucleation as well, severely influencing thereby, the final CSD. The set point profiles of the response function model with the lowest relative error is then also selected for generating the optimal set point profiles to achieve the desired target one-dimensional CSD.

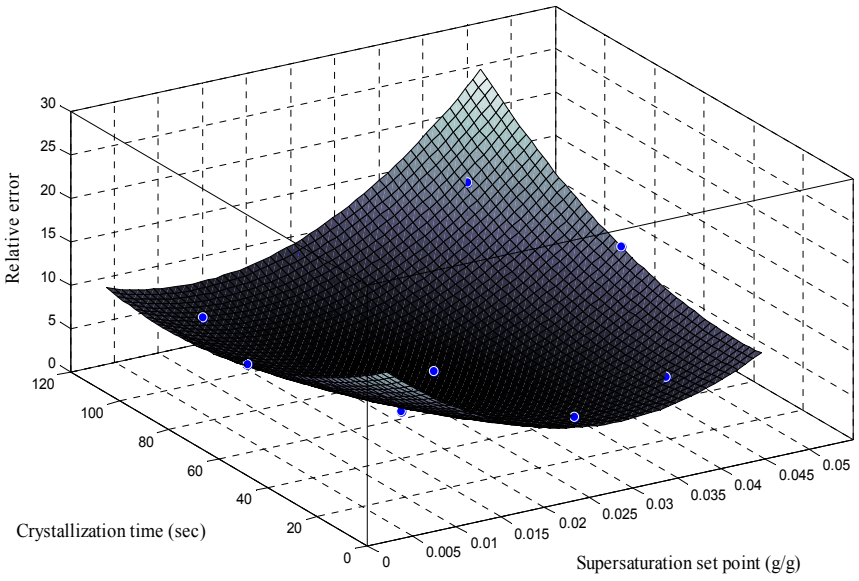


Figure 4.17 Response surface as a function of supersaturation set point and crystallization time for the one-dimensional case

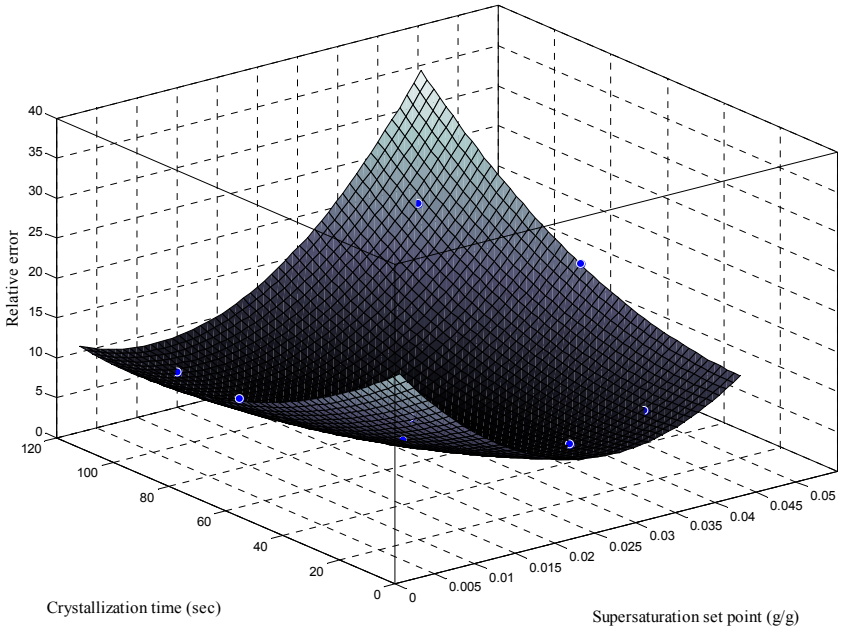


Figure 4.18 Response surface as a function of supersaturation set point and crystallization time for the two-dimensional case

A similar procedure is repeated for the two-dimensional case and a similar trend is observed for the two-dimensional case as highlighted in Figure 4.18. The relative error in the two-dimensional case is a little higher than for the one-dimensional case (see Table 4.9). This is probably due to the fact that a more complex model is used in the simulation with the two-dimensional model compared to the one-dimensional model, resulting in a different type of crystal shape. Similarly, the response function model yields an optimal set point profile which, as expected, is identical to the one-dimensional case (supersaturation set point profile = 0.03 g/g and total crystallization time = 80 seconds). The optimal set point profile obtained from RSM for both cases are also matching with

the optimal set point profiles generated using the analytical CSD estimator and thus, indicating this approach is reliable and able to generate the optimal set point profiles as well. The total crystallization time (80 seconds) obtained through the RSM is also consistent with the published literature (Qamar et al., 2007; Gunawan et al., 2004).

#### 4.8.3.3 Comparison of set point profiles obtained using analytical CSD estimator and response surface method (RSM)

In this work, the optimal set point profiles to produce the desired target CSD have been generated using analytical CSD estimator and RSM approaches for one- and two-dimensional KDP crystallization process. The optimal set point profiles obtained are shown in Table 4.10 where both approaches produced identical set point profiles. This indicates that both approaches can be used to generate the optimal set point profile to achieve the desired target CSD. However it is worth to highlight that the analytical CSD estimator is simpler and computationally more efficient. Furthermore the detailed crystallization model is not needed and therefore the user is able to use this approach to gain some important information about initial seed, set point profiles and the CSD obtained without the need to perform simulations with the detailed model. Meanwhile a higher number of simulations with model are required in the RSM approach in order to provide adequate and reliable data of the response of interest. Nevertheless, the RSM approach is able to generate the necessary set point profile and provides another attractive option for the user to apply in this systematic design framework.

Table 4.10 Comparison of set point profiles obtained using analytical CSD estimator and response surface method (RSM) for both cases

| Cases | Approaches | | | |
|---|---|---|---|---|
| | Analytical CSD estimator | | Response surface method | |
| | Set point profiles (g/g) | Total crystallization time (sec) | Set point profiles (g/g) | Total crystallization time (sec) |
| One-dimensional | 0.03 | 80 | 0.03 | 80 |
| Two-dimensional | 0.03 | 80 | 0.03 | 80 |

### 4.8.4 Design of process monitoring and control (PAT) system (Step 4)

In this section, the process monitoring and control system for the KDP crystallization process is designed for the one-dimensional and the two-dimensional cases using the PAT design methodology developed by Singh et al. (2009) and implemented in the ICAS-PAT software (Singh et al., 2010). The desired product is KDP with the following predefined qualities: target one-dimensional CSD with mean characteristic length of 60.85 μm and cube-shaped crystals; target two-dimensional CSD with mean characteristic length of 60.85 μm; mean characteristic width of 27.36 μm and tetragonal prism-shaped crystals. The basic raw materials required include: Water as a solvent and KDP as a solute assuming that the pure KDP has been isolated with water during the organic synthesis step. The process equipment used is a jacketed batch crystallizer. Furthermore, initial condition, known variable values and model parameters taken from Qamar et al. (2007) and Gunawan et al. (2004) have been used to solve the one- and two-dimensional models in the open- and closed-loop simulations.

The sensitivity analysis based on open-loop simulations is now performed to identify the variables that need to be monitored and controlled in order to assure the predefined end product quality. The KDP concentration is considered as an example of a process variable for the sensitivity analysis. As shown in Figure 4.19, the KDP concentration for both cases was found to violate the operational limits in the open-loop, indicating thereby that this variable needs to be monitored and controlled. Repeating this procedure for all process variables yielded a list of critical process variables which are the KDP concentration and temperature for both cases. The interdependency analysis was performed for each critical process variable to select a suitable actuator. Considering that the same critical process variables were obtained for both cases, and, since the same chemical system is used, only one interdependency analysis was carried out. As shown in Figure 4.20, a critical process variable (KDP concentration) and the corresponding actuator candidates (coolant flow rate and inlet water temperature) were selected for analysis. The analysis indicates that inlet water temperature is the most sensitive based on the large change occur in the KDP concentration when inlet water temperature is perturbed compare to only small change in the KDP concentration when coolant flow rate is perturbed, and therefore, it was selected as an actuator to control the solute concentration in the batch crystallization for both cases.

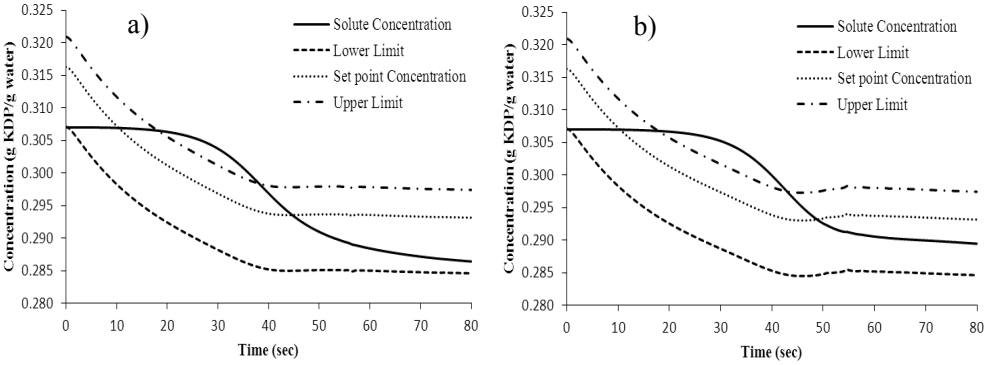


Figure 4.19 KDP concentration profile for a) one-dimensional, b) two-dimensional cases in the open-loop simulation

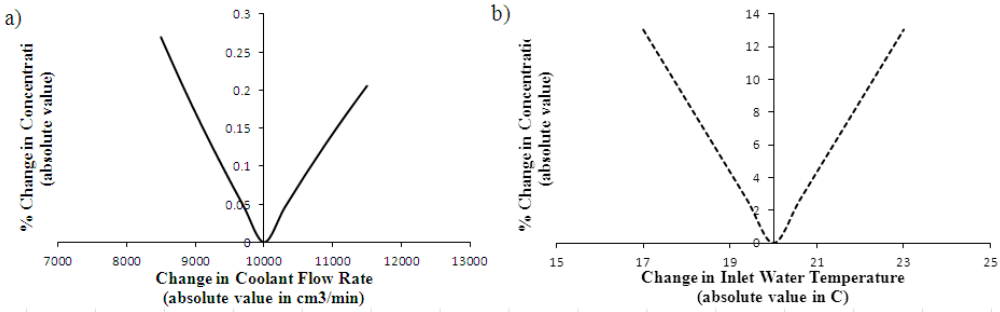


Figure 4.20 Interdependency analysis results for the change in KDP concentration based on a) change in coolant flow rate and b) change in inlet water temperature

The monitoring tools were selected to monitor each identified critical process variable based on a set of monitoring tools performance criteria: accuracy, precision, drift, resolution, response time, operating range and cost. Based on these performance criteria, the attenuated total reflection fourier transform infrared (ATR-FTIR), thermocouple, laser diffraction using Malvern mastersizer (one-dimensional CSD) and in situ video microscopy using particle vision microscope (two-dimensional) are selected as the monitoring techniques to monitor the solute concentration, the temperature and the CSD for both the one- and the two-dimensional cases. The PAT system is proposed based on

the outcomes of the sensitivity analysis, interdependency analysis and performance analysis of monitoring tools as shown in Table 4.11.

Table 4.11 Proposed process monitoring and analysis system for one- and two-dimensional KDP crystallization

| Propose a process monitoring and control system | | | | |
|---|---|---|---|---|
| Critical process points | Critical process variables | Actuators | Monitoring techniques | Monitoring tools |
| Crystallizer | Concentration | Inlet water temperature | ATR-FTIR | ATR-FTIR probe |
| Crystallizer | Temperature | Inlet water temperature | Thermocouple | WZ-08541-28 (E20-gauge thermocouple) |
| Crystallizer | Crystal size distribution (CSD) | - | Laser diffraction (one-dimensional); In situ video microscopy (two-dimensional) | Malvern Mastersizer (one-dimensional); Mettler-Toledo particle vision microscope (two-dimensional) |

### 4.8.5 Implementation of process monitoring and control (PAT) system (Step 6)

For the closed-loop simulation of the PAT system, a PI controller has been considered in order to maintain the KDP concentration at the desired set point profile. The generated supersaturation set point profile at 0.03 g/g is used as a set point profile for the controller for both the one- and the two-dimensional cases. The closed-loop simulation results obtained for one- and two-dimensional cases are shown in Figure 4.21. The KDP concentration for both cases initially started at 0.307 g KDP/g water and once the concentration set point profile was reached the PI controller successfully maintained

the concentration at the set point profile until the end of the operation. As shown in Figure 4.21, approximately 0.2921 g KDP/g water (one-dimensional) and 0.2957 g KDP/g water (two-dimensional) are obtained at the end of the operation. Comparing the predictions from the two models, it can be noted that the one-dimensional model consumes more solute from the solution than the two-dimensional model. This is because there are two different kinetic crystal growth parameters applied to the same crystal growth model in the two-dimensional case. The crystal growth rate for the width direction has a lower rate compared to the crystal growth rate for the length direction. As a consequence, the crystals in the two-dimensional case grow slower, thus explaining why less solute has been consumed compared to the one-dimensional case.

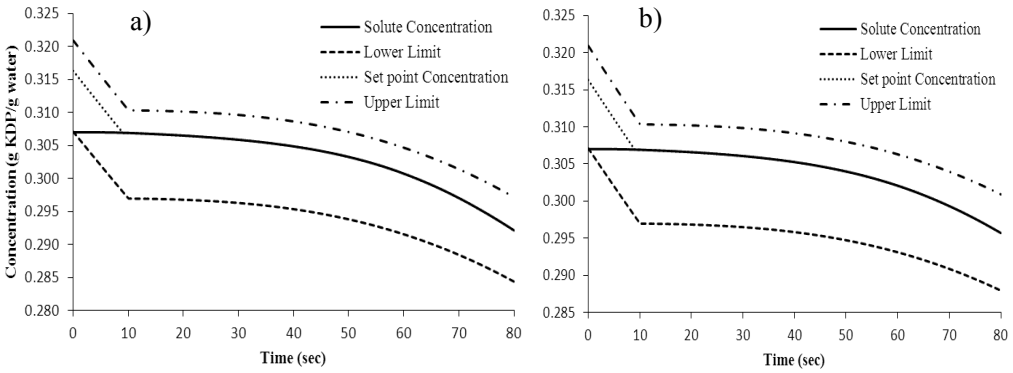


Figure 4.21 KDP concentration profile for: a) one-dimensional; b) two-dimensional cases in the closed-loop simulation

Figure 4.22 shows the temperature profile, for both cases set initially at 32°C and then cooled down to 28°C (one-dimensional) and 28.7°C (two-dimensional), respectively. The temperature in the one-dimensional case is decreasing faster than in the two-dimensional case. The solubility line (lower limit) is temperature dependant. Since the KDP concentration is decreasing, the solubility line must also decrease in order to maintain the

operation at the desired set point profile (constant supersaturation), which results in a decrease of the temperatures.

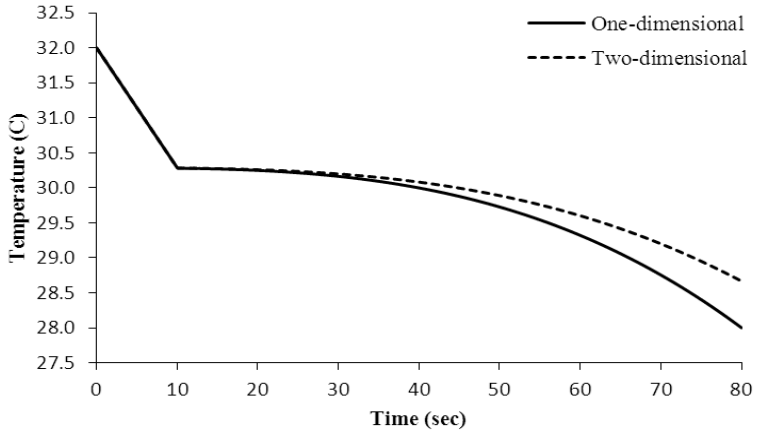


Figure 4.22 Temperature profiles comparison in the closed-loop simulation

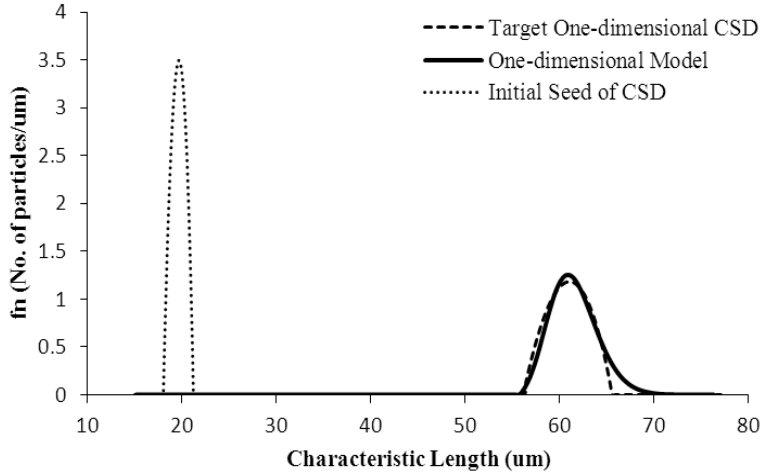


Figure 4.23 Comparison of generated CSD with the target CSD for the one-dimensional case

In terms of CSD, a good agreement with the target CSD was achieved as shown in Figure 4.23, i.e. the detailed one-dimensional simulation model (closed-loop) predicted

a CSD which was almost identical to the target CSD using the generated set point profiles. The cube-shaped seed originally at mean characteristic length of 19.5 μm (standard deviation of 0.97 μm) has been grown to a mean characteristic length of 60.73 μm (standard deviation of 2.79 μm) which is very close to the target mean characteristic length of 60.85 μm (standard deviation of 2.8 μm). Although the good agreement has been achieved between the target and simulated CSD, however the shape of distribution is slightly different as shown in Figure 4.23. This is may be due to the error from the BDF integrator used to solve the method of classes.

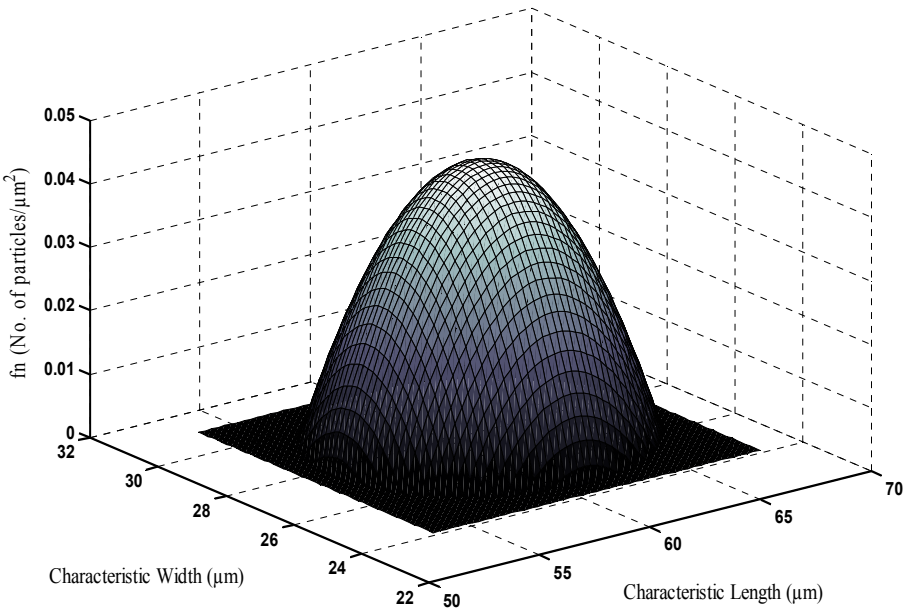


Figure 4.24 Final two-dimensional CSD obtained from the detailed simulation model

Figure 4.24 shows the final two-dimensional CSD with respect to final characteristic length and width obtained from the detailed simulation model based on the

given initial seed of the CSD and the generated set point profiles. The seed has been grown starting from a mean characteristic length and width of 19.5 μm up to a mean characteristic length of approximately 60.6 μm and a mean characteristic width of 26.55 μm. The dimensions obtained from the detailed simulation model are very close to the target mean characteristic length of 60.85 μm and a mean characteristic width of 27.36 μm. Meanwhile the standard deviations obtained from the detailed two-dimensional model for the length and width direction are 2.79 μm and 1.33 μm respectively. Both standard deviations are in good agreement with the target standard deviations of 2.8 μm (length) and 1.34 μm (width). The final two-dimensional CSD obtained in this work is also matched with the two-dimensional CSD obtained from published literature data (Qamar et al., 2007; Gunawan et al., 2004). However, only two-dimensional CSD has been compared with the published literature data due to unavailability of the published one-dimensional CSD data for KDP crystallization. Furthermore, based on the simulation results for the one- and the two-dimensional cases, it was observed that the total number of crystal particles initially at 736 remains unchanged at the end of the operation, indicating no generation of new seeds due to secondary nucleation. Thus it is concluded that by maintaining the operation at the generated set point profiles, the feasible target one- and two-dimensional CSD as well as crystal shapes are achieved, and the undesirable secondary nucleation is avoided. Although the total crystallization time for this case study is rather short, the objective has been to verify the results with published data (Qamar et al., 2007; Gunawan et al., 2004). In principle, operational time can be extended but data would be necessary for verification.

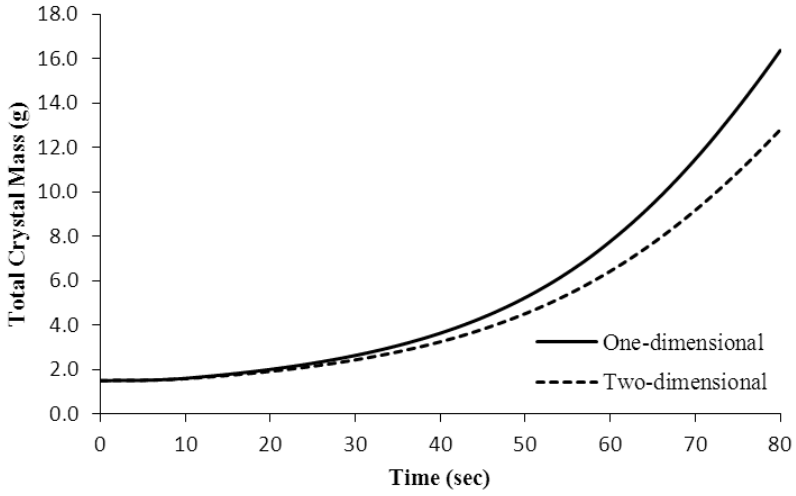


Figure 4.25 Total crystal mass obtained

As highlighted in Figure 4.25, the one-dimensional model yields the highest total crystal mass of approximately 16.4 g starting from an initial seed mass of 1.5 g. The two-dimensional case produced about 12.8 g. The higher total crystal mass obtained in the one-dimensional case is due to the fact that the cube-shaped volume in the one-dimensional case consumes more solute from the solution than the tetragonal-prism volume in the two-dimensional case. Therefore the one-dimensional case produces more crystal mass compared to the two-dimensional case.

Finally the final PAT design flowsheet for one- and two-dimensional KDP crystallization is obtained as shown in Figure 4.26 where PI control is implemented to control the KDP concentration by manipulating the inlet water temperature. The KDP concentration and temperature are monitored by ATR-FTIR and thermocouple respectively. For monitoring CSD in the one dimensional case, the laser diffraction using Malvern mastersizer is employed and in situ video microscopy using particle vision

microscope is used to monitor the two-dimensional CSD respectively. The evolution of the one-dimensional CSD from initial seed to the final one-dimensional CSD is represented in 3-D visual pictures as shown in Figure 4.27. Figure 4.27(a) shows how the initial narrow distribution of the seed has grown into a wider size distribution at the final time, which is due to the size dependent growth effects included in the model, as shown also in Figure 4.27(b). Similarly, the initial seed distribution also becomes wider by the end of the operation for the two-dimensional case as indicated in Figure 4.28.

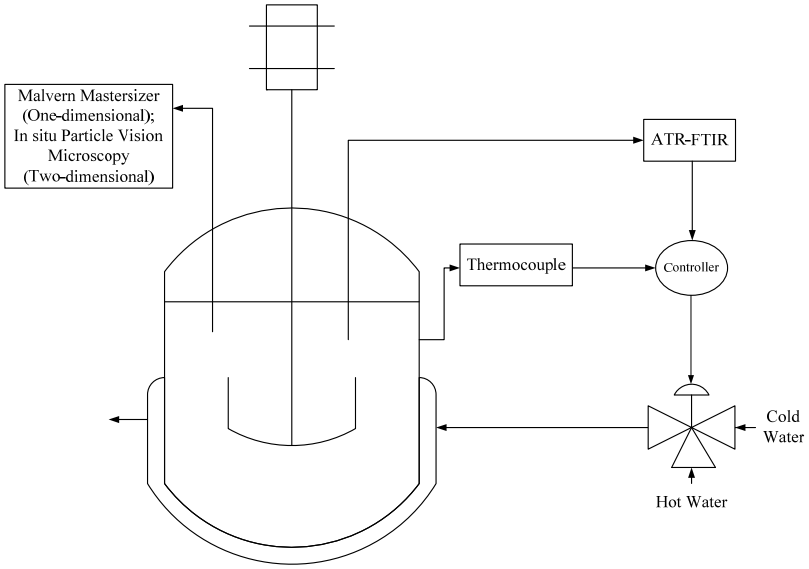


Figure 4.26 KDP crystallization process flowsheet with designed PAT system

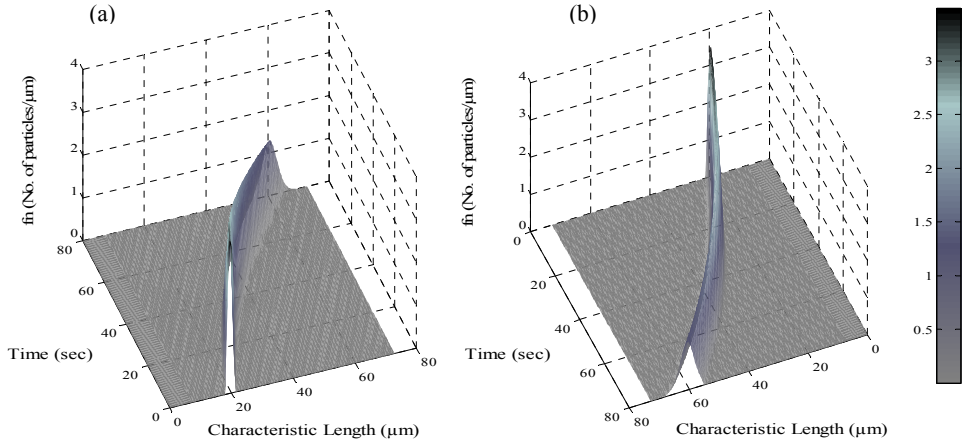


Figure 4.27 Evolution of one-dimensional CSD (a) initial seed view (b) final product view

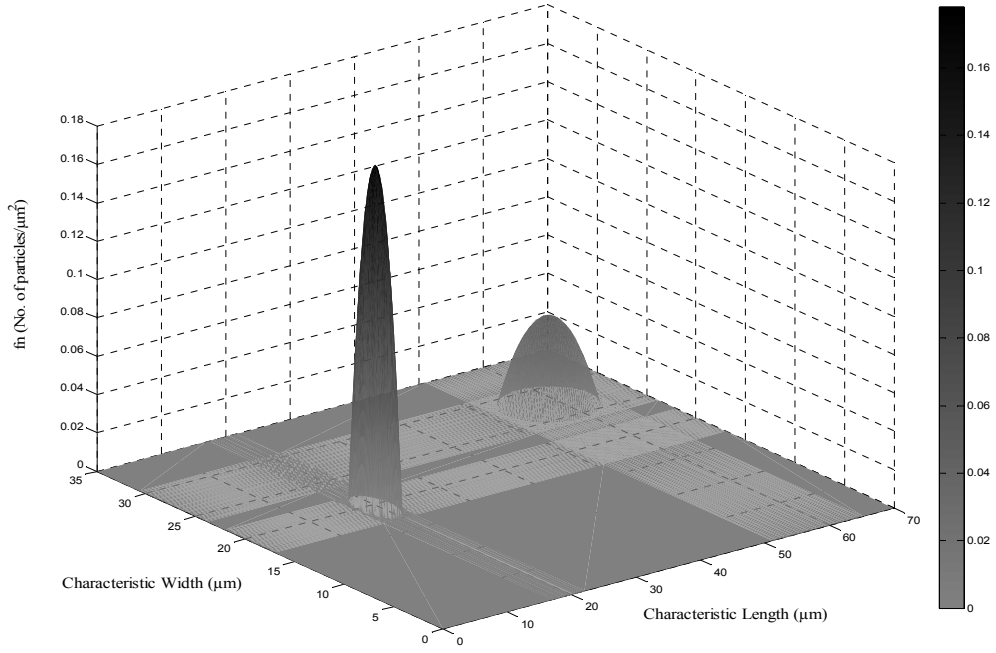


Figure 4.28 Evolution of two-dimensional CSD from initial seed (left) to the final crystal product (right)

## 4.9 Conclusion

A generic and systematic model-based framework for design of process monitoring and control systems to achieve the desired target CSD and shape for a wide range of crystallization processes has been developed and evaluated on a KDP crystallization process. The KDP process was selected because it is the most common two-dimensional case study and the data for nucleation and growth kinetics are available. The generic nature of the framework allows the further development and adaptation of crystallization models to reflect changing product demands (such as one- or two-dimensional CSD). The application of the framework has been highlighted through the KDP crystallization case study where the feature for handling of model complexity, including generation of one-dimensional and two-dimensional models, has been illustrated through the generated models for KDP crystallization. The set point profiles needed for product monitoring and control system design have been generated using the analytical CSD estimator method and the response surface method. The optimal set point profiles obtained from these approaches are comparable, but it is worth pointing out that the analytical CSD estimator provides a more efficient and computationally effective way to generate set point profiles. The results of the simulated CSD achieved through the designed monitoring system show good agreement with the published crystallization data (Qamar et al., 2007; Gunawan et al., 2004), indicating thereby, the power of systematic computer-aided framework for design of PAT systems involving crystallization.

# 5. Uncertainty and sensitivity analysis of process monitoring and control (PAT) system

In this chapter, the generic framework for model-based PAT system design has been expanded with advanced uncertainty and sensitivity analysis tools and methods to comprehensively test and develop reliable PAT system designs. In particular for PAT system design, the objective of this work is to study and analyze the impact of uncertainties in the nucleation and crystal growth parameters on the product-process performances (e.g. CSD) of a crystallization process. The uncertainty and sensitivity analysis is performed under open-loop and closed-loop scenarios with two respective aims: in open-loop, the aim is to understand and identify key parameters that drive crystallization performance metrics (product CSD, etc.) and to form a basis for comparison with the output uncertainties in the closed-loop scenario. In the closed-loop scenario, the aim is to comprehensively test the PAT system design performance in delivering the desired product characteristics under the considered domain of uncertainties. The application of uncertainty and sensitivity analysis is highlighted through the potassium dichromate and potassium dihydrogen phosphate (KDP) crystallization processes where it will be shown that the effect of the input uncertainties on the outputs (product quality) can be minimized and target specifications can indeed be achieved ensuring that the PAT system design is reliable under the considered domain of uncertainties.

## 5.1 Expanding the generic framework for model-based PAT system design with uncertainty and sensitivity analysis

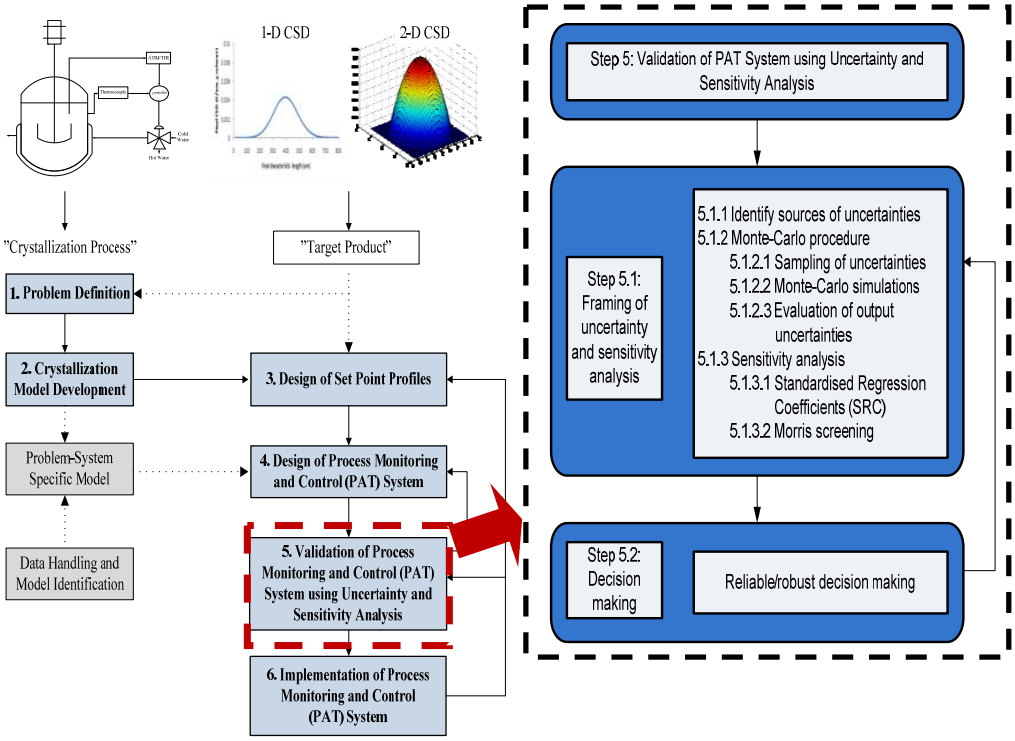


Figure 5.1 Incorporation of a methodology for combined uncertainty and sensitivity analysis in the framework for model-based design of product-process problems

A model-based systematic design framework for monitoring and control (PAT) systems of crystallization processes has been developed earlier in Chapter 4 is shown in Figure 5.1 (left). Through this framework, it is possible to generate a large number of problem-system specific models which can subsequently be used to design a PAT system. In this study, the methodology for performing the uncertainty and sensitivity analysis adopted from Sin et al. (2009b) as shown in Figure 5.1 (right) has been added as a new

feature into the generic framework (Figure 5.1), and will be explained in more detail below.

### 5.1.1 Framing of uncertainty and sensitivity analysis (Step 5.1)

This step deals with the identification, understanding, calculation and analysis of uncertainties in the model predictions, and includes the following sub-steps: (i) identification and characterization of various sources of uncertainties; (ii) Monte-Carlo procedure; and (iii) sensitivity analysis.

#### 5.1.1.1 Identify sources of uncertainties (Step 5.1.1)

Generally, the uncertainties can be classified as: (a) stochastic uncertainty that arises from stochastic components of a simulation model required to describe a stochastic system; (b) input uncertainty that represents incomplete knowledge about the fixed values used as input to the model; and (c) structural uncertainty that relates to the mathematical formulation or the model structure (Sin et al., 2009b). In this study, only input uncertainty is considered, where the effects on the model output prediction of the uncertainty around the parameter values will be investigated.

In this study, we consider uncertainties in the input parameters to the model. To characterise the degree of uncertainty (i.e. range of uncertainties), the expert review process is used (Sin et al., 2009b; Helton and Davis, 2003). In the expert review, the process expertise and knowledge in the crystallization is considered as well as the relevant literature resources to identify uncertain parameters and assign an appropriate

range of uncertainty to each parameter, e.g. what is the upper and lower bound of kinetic parameters. In order to structure the expert review process, all the selected model parameters are assumed to follow a uniform probability distribution and three classes of uncertainty are defined (5, 25 and 50% of variability around the mean values; Sin et al., 2009b). The minimum and maximum values of the uniform distribution can then be calculated as (100% - %variation) x mean and (100% + %variation) x mean respectively. Alternatively and if available, the lower and upper bound values of the kinetic parameters can be obtained from parameter estimation techniques, e.g. by using the 95% confidence interval of the model parameters.

### 5.1.1.2 Monte Carlo procedure (Step 5.1.2)

In order to propagate different sources of uncertainties to the model predictions, the Monte Carlo procedure is applied and it involves three sub-steps: (1) sampling of uncertainties; (2) Monte Carlo simulations; and (3) evaluation of output uncertainties.

#### 5.1.1.2.1 Sampling of uncertainties (Step 5.1.2.1)

The input uncertainties specified in the earlier step are sampled using the Latin-Hypercube sampling method, a commonly used method (Helton and Davis, 2003). Here the user has to specify the number of samples. Based on the specified number of samples, a random combination of the uncertain model parameters is then generated and will be used as input to the Monte Carlo simulations. In case there is a known correlation between the parameters (input uncertainties), for example on the basis of the results of a

parameter estimation on available process data, the Iman and Conover method of correlation control can be used (Iman and Conover, 1982).

#### 5.1.1.2.2 Monte Carlo simulations (Step 5.1.2.2)

The next step in the Monte Carlo procedure is to perform simulations. Here the mathematical model of the crystallization process is simulated for each set of parameter samples obtained in the previous steps. In this work, the model implementation and the Monte Carlo simulations are performed in the ICAS-MoT modelling tool (Heitzig et al, 2011).

#### 5.1.1.2.3 Evaluation of output uncertainties (Step 5.1.2.3)

The results from the Monte Carlo simulations are analyzed in this step by calculating typical statistics such as mean, standard deviation and relevant percentiles of model output distributions. The uncertainty is indicated by the variance of the distribution, which indicates the spread of the data. The larger the spread of the simulated data indicates the larger the uncertainty in that model output. Similarly, the percentiles can also indicate the extent of uncertainties in the outputs, e.g. the further the $10^{th}$ and $90^{th}$ percentiles away from the mean, the larger the uncertainty of the model output.

### 5.1.1.3 Sensitivity analysis (Step 5.1.3)

The sensitivity analysis is performed next to identify the individual contributions of uncertain parameters to the total variance calculated in the step 5.1.2 which provides a

parameter significance ranking for each output. As mentioned above, two methods namely (1) Standardized regression coefficients (SRC) method (Cariboni et al., 2007); and (2) Morris screening method (Morris, 1991) are used.

#### 5.1.1.3.1 Standardized regression coefficients (SRC) (Step 5.1.3.1)

In this method, a linear regression is performed on the Monte Carlo results describing each model output of interest as a multivariate linear function of the model inputs considered in the uncertainty analysis. Here the user selects the model output of interest to the analysis. As for a crystallization process, usually the most important model output is the CSD considering that this is one of the most important product specifications that needs to be achieved. Therefore the mean of the CSD at the final time can be used as a scalar output for the SRC method. The scalar model output matrix can be denoted as $sy$ and has the dimensions of *K*x*N* where *K* is the number of output variables and *N* is the number of samples. The regression model is then fitted to the (scalar) output of the Monte Carlo simulations relating model output, $sy$ to the model inputs considered in the uncertainty analysis, $\theta_{ij}$ as shown in Equation (5.1):

$$sy_{ik} = b_{0k} + \sum_{j=1}^{M} b_{jk}\theta_{ij} + \varepsilon_{ik} \quad \text{for } i = 1,2,\ldots,N \text{ and for } k = 1,2,\ldots,K \tag{5.1}$$

Where, $sy_{ik}$ is the scalar value for the k$^{th}$ output, $b_{jk}$ is the coefficient of the j$^{th}$ input parameter, $\theta_j$, for the k$^{th}$ output, $\theta_{ij}$ is the value of the j$^{th}$ parameter and $\varepsilon_{ik}$ is the error of

the regression model. Equation (5.1) is then written in dimensionless form by scaling the outputs and the parameters using their corresponding mean and standard deviations (Campolongo and Saltelli, 1997) as shown in Equation (5.2):

$$\frac{sy_{ik} - \mu_{sy_k}}{\sigma_{sy_k}} = \sum_{j=1}^{M} \beta_{jk} \cdot \frac{\theta_{ij} - \mu_{\theta j}}{\sigma_{\theta j}} + \varepsilon_{ik} \tag{5.2}$$

The standardized regression coefficients, $\beta_{jk}$, can have values in the range [-1 1] with the following meaning: (i) a high absolute value indicates a large effect of the corresponding parameter on the output, (ii) a negative sign indicates a negative effect and vice versa a positive sign indicates a positive effect on the output, and (iii) coefficients close to zero mean that the output is not sensitive to that parameter (Campolongo and Saltelli, 1997; Helton and Davis, 2003). Furthermore, for these coefficients to be considered a valid measure of sensitivity, the coefficient of determination should be sufficiently high, e.g., $R^2 \geq 0.7$, which implies that the model is sufficiently linear (Campolongo and Saltelli, 1997; Saltelli et al., 2006).

#### 5.1.1.3.2 Morris screening (Step 5.1.3.2)

The Morris screening method relies on estimating the distribution of the elementary effects (EE) of each input parameter on the $k^{th}$ model output called $EE_{jk}$. The $EE_{jk}$ attributable to each input parameter was obtained from the following differentiation of the model output, $sy_k$, with respect to the input, $\theta_j$, as shown in Equation (5.3):

$$EE_{jk} = \frac{\partial sy_k}{\partial \theta_j} = \frac{sy_k\left(\theta_1, \theta_2, \theta_j + \Delta, \ldots, \theta_M\right) - sy_k\left(\theta_1, \theta_2, \theta_j, \ldots, \theta_M\right)}{\Delta} \tag{5.3}$$

Where $\Delta$ is a predetermined perturbation factor of $\theta_j$, $sy_k\left(\theta_1, \theta_2, \theta_j, \ldots, \theta_M\right)$ is the scalar model output evaluated at input parameters $\left(\theta_1, \theta_2, \theta_j, \ldots, \theta_M\right)$, whereas $sy_k\left(\theta_1, \theta_2, \theta_j + \Delta, \ldots, \theta_M\right)$ is the scalar model output corresponding to a $\Delta$ change in $\theta_j$. The distribution function is denoted as $F_{jk}$, which represents the distribution of the effects of the $j^{th}$ input parameter on the $k^{th}$ output. The $F_{jk}$ was estimated by performing calculations of the elementary effects, $EE_{jk}$, at randomly sampled points in the input space and this procedure was repeated a number of times, *r*. In the Morris sampling design, the calculation of one elementary effect for each input requires ($M$ + 1) model simulations (Morris, 1991). Because a number of repetitions, *r*, is needed (typically 10-50), the total number of model simulations needed for the Morris screening becomes $r$*($M$ + 1). Based on the Morris method, there are three degrees of freedom that need to be specified which are the values of $\Delta$, $p$ and $r$, respectively. In this study, the values for $\Delta$, $p$ and $r$ were specified as 2/3, 4 and 10, respectively. Finally, the Morris results can be evaluated by comparing the mean, $\mu_j$ and the standard deviations, $\sigma_j$ of the distribution functions, $F_{jk}$, of each input. The measure of sensitivity for the mean of the distribution functions follows the same concept as the standardized regression coefficients in the SRC method. In this study, the Morris screening is also implemented in the ICAS-MoT modelling tool (Heitzig et al., 2011).

### 5.1.2 Decision making (Step 5.2)

In this step, the robustness of the model-based solution is evaluated by judging on a number of criteria including the probability of failure to meet target product specifications. If the target product specifications are not met due to the input uncertainties, then a solution is to be proposed in order to reduce or eliminate the probability of failure. For example, if the analysis indicates that the proposed PAT system design failed to provide the target product specifications, then appropriate changes to the PAT system need to be made and a new analysis should be performed. Suggestions to modify PAT systems include re-tuning of the controller or the proposal of a new controller structure such as model predictive control (MPC). The modified PAT system with the new controller structure proposal or the new tuning parameters is then tested again in the uncertainty and sensitivity analysis methodology until a reliable PAT system is obtained.

## 5.2 Application of the systematic framework for managing uncertainties: potassium dichromate crystallization case study

It has been assumed during the PAT system design for potassium dichromate crystallization in Chapter 4 that the uncertainty around parameters could be neglected. In this section, the PAT system for potassium dichromate crystallization is validated using uncertainty and sensitivity analysis.

### 5.2.1 Problem definition (Step 1), crystallization model development (Step 2) and design of set point profiles (Step 3)

The main objective of this study is to test and validate a PAT system design using uncertainty and sensitivity analysis in term of its reliability and robustness in the presence of input uncertainties. Here the analysis is carried out on two different scenarios: (1) open-loop, and (2) closed-loop. Specifically for step 2 and 3, the problem-system specific one-dimensional model for the potassium dichromate crystallization process (see Table 4.2) and the optimal set point profiles (supersaturation set point of $1.25\times10^{-4}$ g solute/g water and the total crystallization time of 180 minutes) generated in Chapter 4 are employed in this work.

### 5.2.2 Design of process monitoring and control (PAT) system (Step 4)

The PAT system for potassium dichromate PAT as shown in Figure 4.12 where a PI control system is used to control the solute concentration. The inlet water temperature is manipulated by blending hot and cold water. The concentration, temperature and CSD are monitored by ATR-FTIR, thermocouple and FBRM respectively.

### 5.2.3 Validation of process monitoring and control (PAT) system using uncertainty and sensitivity analysis (Step 5)

In this section, the uncertainty and sensitivity analysis are carried out under open-loop and closed-loop scenarios.

a) Open-loop

The objective here is to quantify the effect of input uncertainties in nucleation and crystal growth parameters on the prediction of the crystallization process. Furthermore, the main reason performing the uncertainty and sensitivity analysis is to check whether the model prediction performance is affected by the input uncertainties. If the input uncertainty is indeed affecting the model prediction then the influential parameter is identified and used as an input in the closed-loop condition. Here the model equations as shown in Table 4.2 have been simulated in the ICAS-MoT modelling tool under open-loop conditions. The open-loop simulation results are shown in Figure 5.2 where the performance in terms of potassium dichromate concentration, temperature, inlet water temperature and final CSD is evaluated based on the assumption of no uncertainty on the process parameters.

Figure 5.2 shows the open-loop reference simulation results for the seeded potassium dichromate crystallization process. The temperature is decreased from 30˚C to 20˚C, and as a result the profiles of the potassium dichromate concentration deviated far from the saturation concentration line. Under these conditions, the high supersaturation is obtained in the beginning of the operation. Therefore secondary nucleation is expected. The final CSD as shown in Figure 5.2 indicates indeed that a secondary peak is obtained in the CSD when the operation is based on the open-loop conditions.

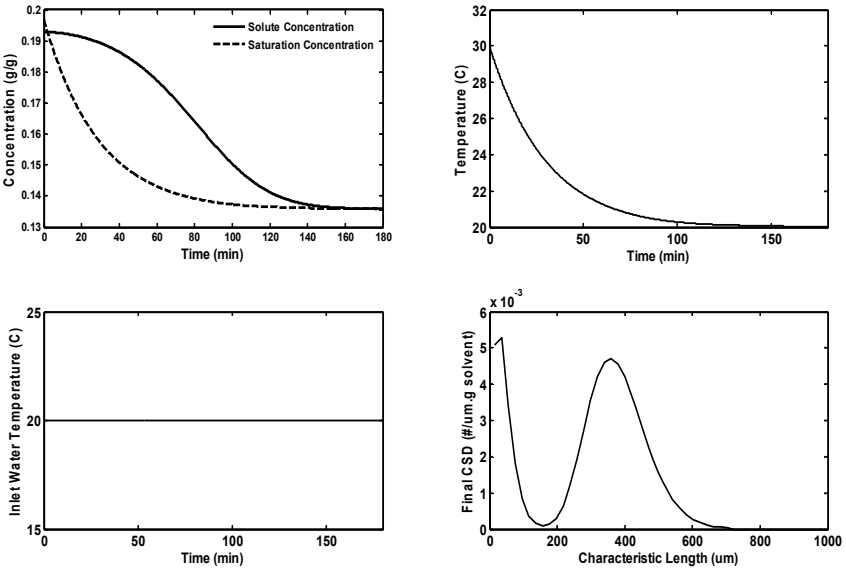


Figure 5.2 Reference simulation results using nominal values for potassium dichromate concentration, temperature, inlet water temperature and final CSD under open-loop operation

### 5.2.3.1 Framing for uncertainty and sensitivity analysis (Step 5.1)

This step involves the development of framing scenario for uncertainty and sensitivity analysis for the potassium dichromate crystallization process.

**Step 5.1.1: Identify sources of uncertainty**

For the one-dimensional potassium dichromate crystallization process, the input uncertainty has been chosen based on the 6 parameters ($k_b$, $b$ , $k_{gx}$, $g_x$, $\gamma_x$ and $p_x$) from the nucleation model and the crystal growth model (see Equation (7) and (8) in Table 4.2). Table 5.1 shows the input uncertainty of nucleation and crystal growth parameters.

The values for lower and upper bound of each parameter are calculated based on the 95% confidence interval taken from Aamir et al. (2010).

Table 5.1 Input uncertainties on nucleation and crystal growth rate parameters for potassium dichromate crystallization

| ID | Parameters | Units | Values | Confidence interval (95%) | Lower bound values | Upper bound values |
|---|---|---|---|---|---|---|
| 1 | Growth rate constant, $k_{gx}$ | μm/s | 9.56 | ±0.0832 | 9.4768 | 9.6432 |
| 2 | Growth order constant, $g_x$ | Dimensionless | 0.8 | ±0.2411 | 0.5589 | 1.0411 |
| 3 | Growth constant, $\gamma_x$ | 1/μm | 0.0075 | ±0.0021 | 0.0054 | 0.0096 |
| 4 | Growth constant, $p_x$ | Dimensionless | 1.24 | ±0.0633 | 1.1767 | 1.3033 |
| 5 | Nucleation rate constant, $k_b$ | No. of particles/$\mu m^3$.s | 0.038 | ±0.0044 | 0.0336 | 0.0424 |
| 6 | Nucleation order constant, $b$ | Dimensionless | 3.4174 | ±0.037 | 3.3804 | 3.4544 |

**Step 5.1.2: Monte Carlo procedure**

There are 3 sub-steps in the Monte Carlo procedure. The first sub-steps is sampling of uncertainties (step 5.1.2.1). The Latin hypercube sampling (LHS) method is employed as a sampling method to sample the parameters. Next task involves the specification of number of samples. In this work, repetitive test using 25, 50, 100 and 150 samples have been implemented in order to obtain a suitable number of samples which can be obtained based on the lowest Monte Carlo errors. Based on the repetitive test, it was shown the 100 and 150 samples have the lowest Monte Carlo errors. Therefore 100 samples are selected as a number of sampling to be used in this work as well as no correlation

between parameters is assumed. Step 5.1.2.2 is the Monte Carlo simulations. Here the open-loop potassium dichromate model is simulated 100 times for each different set of model parameters. The Monte Carlo simulations have been performed in the ICAS-MoT modelling tool.

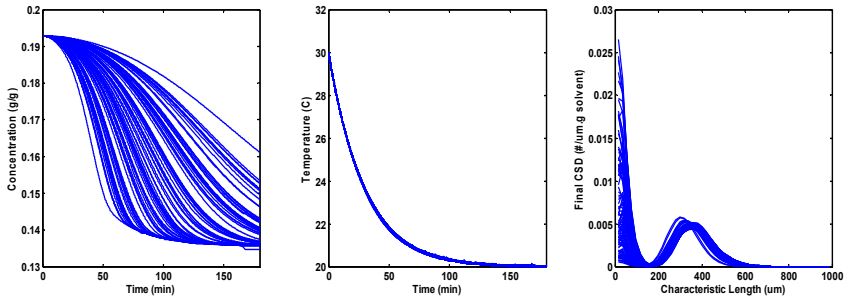


Figure 5.3 Open-loop simulation results for potassium dichromate concentration, temperature, initial CSD and final CSD obtained from the Monte Carlo simulation (in total there are 100 lines, corresponding to 100 samples)

Step 5.1.2.3 concerns the evaluation of output uncertainties based on the Monte Carlo simulations. The Monte Carlo simulation results obtained for potassium dichromate concentration, temperature and final CSD are shown in Figure 5.3. Each output contains 100 lines which represents the dynamic model output obtained based on the 100 sets of parameter values resulting from the sampling. The data are interpreted by evaluating the spread of the simulation results at each time point where a large spread indicate that a high uncertainty is present. In Figure 5.3, it is shown that the highest uncertainty is achieved for the potassium dichromate concentration and final CSD. Meanwhile the temperature shows a low spread, indicating that the uncertain parameters have a low or non-existent effect on the temperature profiles.

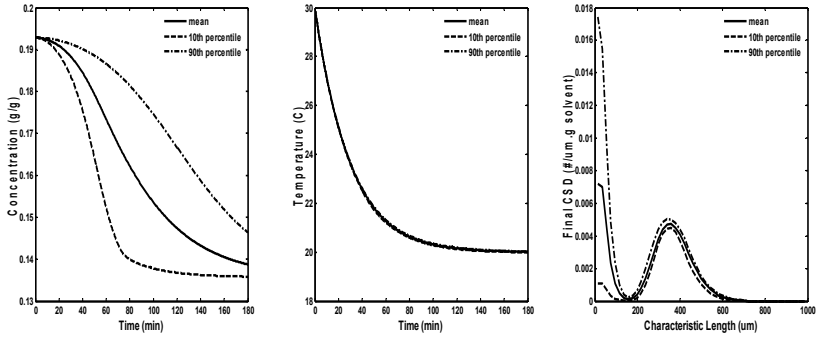


Figure 5.4 Representation of uncertainty using mean, 10$^{th}$ and 90$^{th}$ percentile values of the Monte Carlo simulations under open-loop conditions

Figure 5.4 shows the representation of uncertainty in terms of mean, 10$^{th}$ and 90$^{th}$ percentile values of the Monte Carlo simulations under open-loop conditions. The potassium dichromate concentration and final CSD indicate that the 10$^{th}$ and 90$^{th}$ percentile for both variables are far away from the mean, indicating that the uncertainties for both variables are large. Meanwhile the effect of uncertainty is almost non-existent for the temperature profiles since the 10$^{th}$ and 90$^{th}$ percentile for the temperature profile are very close to the mean. Based on the uncertainty analysis, it can be concluded that the parameters in the nucleation and crystal growth rate model have a strong impact on some of the model outputs, particularly the potassium dichromate concentration and the final CSD.

**Step 5.1.3: Sensitivity analysis**

Two sensitivity analysis techniques are used here: the standardized regression coefficients (SRC) method and the Morris sampling method.

**Step 5.1.3.1: Standardized regression coefficients (SRC) method**

The SRC method is performed on 2 different locations of the one-dimensional CSD data as shown in Figure 5.5. The data taken at point p1) are the CSD data generated by secondary nucleation and the data taken at point p2) correspond to that part of the CSD that corresponds to the seed crystals. The linear regression model is then constructed using Equation (5.1) for the data of points p1) and p2), where the regression coefficients, $\alpha_{jk}$, are calculated using the linear least-squares method. The standardized regression coefficients, $\beta_{jk}$, are then obtained using Equation (5.2). Finally, the $\beta_{jk}$ obtained for each input parameter are arranged in their order of importance for the data corresponding to points p1) and p2). Table 5.2 shows the results of the parameter significance ranking for the open-loop potassium dichromate crystallization.

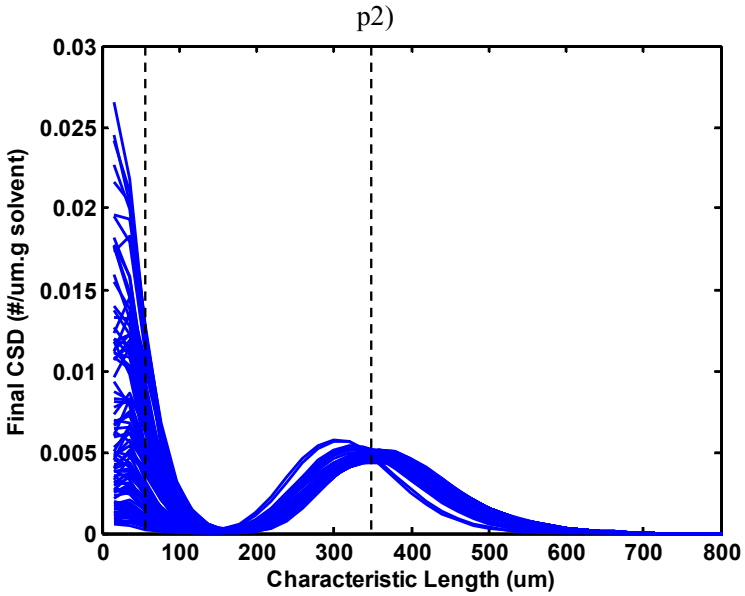


Figure 5.5 Points where the one-dimensional CSD for potassium dichromate crystallization is sampled for sensitivity analysis

Table 5.2 Standardized regression coefficients of linear models and parameters significance ranking for the one-dimensional case

| Location | CSD data taken at p1) | | CSD data taken at p2) | |
|---|---|---|---|---|
| | $R^2 = 0.8626$ | | $R^2 = 0.9269$ | |
| Ranking | Parameter | $\beta_{jk}$ | Parameter | $\beta_{jk}$ |
| 1 | $b$ | -0.9142 | $g_x$ | 0.8908 |
| 2 | $g_x$ | 0.1554 | $\gamma_x$ | -0.3419 |
| 3 | $k_b$ | 0.0592 | $p_x$ | -0.1268 |
| 4 | $\gamma_x$ | -0.0467 | $b$ | -0.0965 |
| 5 | $p_x$ | -0.0382 | $k_{gx}$ | 0.0418 |
| 6 | $k_{gx}$ | -0.0115 | $k_b$ | 0.014 |

The linearized model obtained for data corresponding to points p1) and p2) is indeed reliable. This is because the coefficient of model determination, $R^2$, was above the recommended value 0.7. As shown in Table 5.2, the parameters $b$ (SRC of -0.91) and $g_x$ (SRC of 0.89) were found as the most significant parameters based on the CSD data taken at points p1) and p2), respectively. The parameter $b$ is the nucleation order constant in the nucleation model (see Equation (7) in Table 4.2). The decreasing value of parameter $b$ results into more generation of new crystal indicating thereby a negative impact on the CSD. This is the reason the magnitude of SRC for parameter $b$ is negative. Therefore, it can be concluded that the variation in this parameter affects the production of the new crystal significantly due to the nucleation effects. This explains the large variation of the CSD data taken at point p1) which correspond to that part of the CSD caused by secondary nucleation.

Meanwhile, the nucleation parameters are not affecting the CSD data taken at p2). This is because the CSD data at p2) are directly grown from the seeded crystals. Since no agglomeration and breakage were considered, the seed crystals have grown to

larger sizes due to the effect of crystal growth only. This is also the reason why the parameters for the crystal growth rate are dominant in the parameter significance ranking for CSD data taken at point p2). Here the growth order constant ($g_x$) is the most influential because the distribution of the CSD is usually depending on this parameter. Therefore, at point p2) the higher value of the growth order constant will result into a CSD that is distributed at a higher characteristic length.

**Step 5.1.3.2: Morris screening method**

Alternatively, the Morris screening method can be employed to obtain the parameter significance ranking, and can thus be compared with the the SRC method to see the reliability of both results. The simulations have been implemented in the ICAS-MoT modelling tool and the Morris results are evaluated based on the parameter significance ranking. The parameters have been ranked according to the mean of the distribution function, $\mu_j$. Firstly the parameter significance ranking has been compared based on the one-dimensional CSD data taken at point p1), afterwards followed by a similar analysis for data taken at point p2). Tables 5.3-5.4 show the comparison between the parameter significance rankings obtained using the Morris screening and the SRC method.

Based on Table 5.3, the results of the Morris screening of input parameters were found to be in the good agreement with the ranking obtained by the SRC for the first three parameters. The CSD data taken at point p1) correspond to the secondary nucleation peak. Therefore the most influential parameter is $b$, which is one of the parameters in the nucleation rate equations (see Equation (7) in Table 4.2). However the parameter $g_x$ is also deemed significant since it influences the growth of particles generated by this

secondary nucleation. Although the last three parameters are not in the same order for both methods, the value of the factors is too low and is interpreted as insignificant in this study.

Table 5.3 Method comparison for screening influential factors based on the CSD data taken at point p1) for potassium dichromate crystallization

| | Morris sampling method | | | SRC method | |
|---|---|---|---|---|---|
| Ranking | Parameters | $\mu_j$ | $\sigma_j$ | Parameters | $\beta_{jk}$ |
| 1 | $b$ | -0.8832 | 0.8423 | $b$ | -0.9142 |
| 2 | $g_x$ | 0.2122 | 0.3964 | $g_x$ | 0.1554 |
| 3 | $k_b$ | 0.0611 | 0.1306 | $k_b$ | 0.0592 |
| 4 | $p_x$ | -0.0386 | 0.0563 | $\gamma_x$ | -0.0467 |
| 5 | $\gamma_x$ | -0.0294 | 0.0392 | $p_x$ | -0.0382 |
| 6 | $k_{gx}$ | -0.0083 | 0.0002 | $k_{gx}$ | -0.0115 |

Similarly the first three significant parameters obtained for both methods were found to be in good agreement as shown in Table 5.4 (similar ranking and similar signs for each parameter). The standard deviations obtained for Morris sampling for point p1) shows the non-zero value indicating the all the parameters are involved in non-linear interactions on the outputs. Both methods indicate that the parameters $g_x$, $\gamma_x$ and $p_x$ are the most significant parameters. This result shows that the kinetic growth parameters have a strong influence on the CSD data. Meanwhile the kinetic nucleation parameters are not significant considering that the CSD results obtained at point p2) are dominated by growth effects only. Similarly, the non-zero standard deviations obtained for point p2) indicates the non-linear interaction on the outputs caused by all the parameters.

Table 5.4 Method comparison for screening influential factors based on the CSD data taken at point p2) for potassium dichromate crystallization

| | Morris sampling method | | | SRC method | |
|---|---|---|---|---|---|
| Ranking | Parameters | $\mu_j$ | $\sigma_j$ | Parameters | $\beta_{jk}$ |
| 1 | $g_x$ | 0.7322 | 0.7821 | $g_x$ | 0.8908 |
| 2 | $\gamma_x$ | -0.3218 | 0.4975 | $\gamma_x$ | -0.3419 |
| 3 | $p_x$ | -0.1643 | 0.3038 | $p_x$ | -0.1268 |
| 4 | $k_{gx}$ | 0.0421 | 0.1425 | $b$ | -0.0965 |
| 5 | $b$ | -0.0205 | 0.0184 | $k_{gx}$ | 0.0418 |
| 6 | $k_b$ | 0.0108 | 0.0068 | $k_b$ | 0.014 |

b) Closed-loop

The open-loop analysis based on the uncertainty and sensitivity analysis prove that the input uncertainties in the nucleation and crystal growth parameters clearly affecting the model prediction. In this step, the objective is to perform the PAT system using uncertainty and sensitivity analysis. Here a robustness of the designed PAT system for potassium dichromate crystallization is tested where the controller performance is evaluated in terms of its capability to deal with the presence of uncertainties and obtain the target specifications of the crystal product. Firstly, the closed-loop simulation results are analyzed. Here the closed-loop simulation results are shown in Figure 5.6 where the potassium dichromate concentration initially started at 0.1928 g potassium dichromate/g water and the PI controller successfully maintained the concentration at the set point once the concentration set point was reached. In Figure 5.6 (left, top), approximately 0.1377 g potassium dichromate/g water remains by the end of the operation. Figure 5.6 (right, top)

shows the temperature profiles obtained from closed-loop simulation initially at 30°C and then cooled down to 20°C in 180 minutes. Figure 5.6 (right, bottom) shows the final CSD (mean of 488.1 μm and a standard deviation of 51.83 μm) that has been achieved at the end of the batch crystallization. The final CSD obtained is in good agreement with the mean (490 μm) and standard deviation (52 μm) for the target CSD.

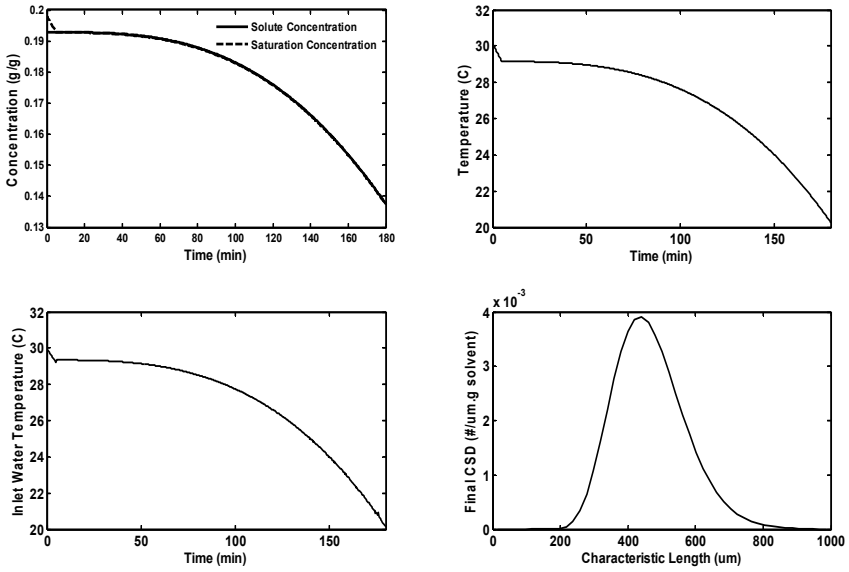


Figure 5.6 Reference simulation results using nominal values for potassium dichromate concentration, temperature, inlet water temperature (manipulated variable) and final CSD under closed-loop operation

Based on the closed-loop simulation results, the uncertainty and sensitivity analysis of the PAT system (step 5) is now repeated again where the same framing scenario and input uncertainties (parameters) used for the open-loop operation are employed. The results from the Monte Carlo simulations for 100 parameter samples are presented in Figure 5.7.

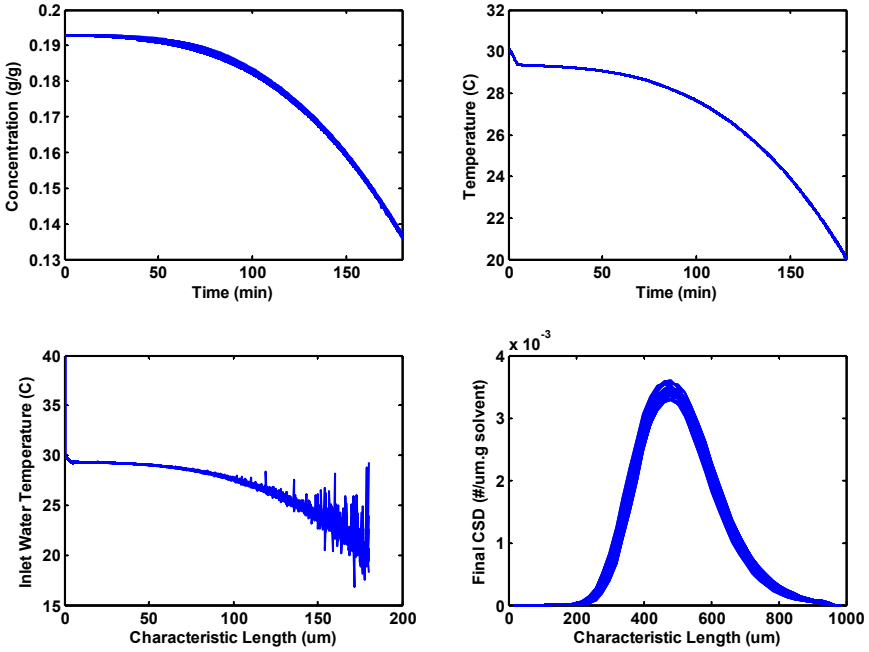


Figure 5.7 Closed-loop simulation results for potassium dichromate concentration, temperature, inlet water temperature (manipulated variable) and final CSD obtained from the Monte Carlo simulation (in total there are 100 simulations)

Based on Figure 5.7, the potassium dichromate concentration (Figure 5.7, left, top) shows only a small variation indicating a low extent of uncertainty. It can be clearly seen that the impact of the uncertain parameters has been minimized for the potassium dichromate concentration when operated under closed-loop conditions. This shows that the PI controller is able to counteract the effect of input uncertainty. The inlet water temperature is used as a manipulated variable in this study. Figure 5.7 (left, bottom) shows the inlet water temperature profile where the profile changes rather vigorously by the end of the operation in order to maintain the concentration at the set point and thus counteract the effects of the input uncertainties. Meanwhile the uncertainty is almost non-

existent in the temperature profiles. Unlike the CSD in the open-loop, the final CSD obtained as shown in Figure 5.7 (right, bottom) indicates that a small variation of the final CSD is achieved. Although it can be observed that there is still a presence of uncertainty in the final CSD, the final CSD obtained from the Monte Carlo simulations is in good agreement with the specified target CSD.

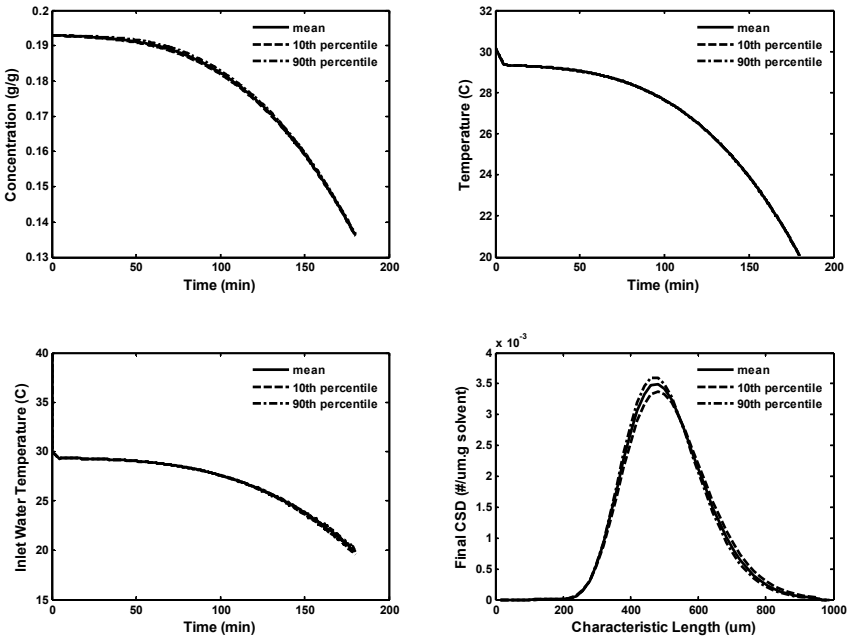


Figure 5.8 Representation of uncertainty using mean, 10$^{th}$ and 90$^{th}$ percentile values of the Monte Carlo simulations under closed-loop potassium dichromate crystallization

Finally the data is analyzed based on the representation of uncertainty using mean, 10$^{th}$ and 90$^{th}$ percentile values of the Monte Carlo simulations as shown in Figure 5.8. The 10$^{th}$ and 90$^{th}$ percentiles for the potassium dichromate concentration (Figure 5.8, left, top) temperature (Figure 5.8, right, top) and inlet water temperature (Figure 5.8, left,

bottom) are very close to the mean respectively indicating that the uncertainty of these model outputs is very low or non-existent. Only the final CSD shows that the $10^{th}$ and $90^{th}$ percentile is a little further away from the mean especially at the top of the CSD peak. Nevertheless it still can be concluded that the final CSD obtained under the presence of uncertainties is in good agreement with the desired target CSD. Through this case study, it also shows that the PAT system for potassium dichormate is robust and reliable to counteract the effect of input uncertainty and thus, obtains the target product specification efficiently.

#### 5.2.3.2 Decision making (Step 5.2)

In this work, the PAT system for potassium dichromate crystallization has been tested using uncertainty and sensitivity analysis. It was carried out on open-loop and closed-loop condition. Based on the open-loop, it has been shown the presence of uncertainties on the model prediction. Therefore, the uncertainty and sensitivity analysis are repeated again under closed-loop condition. Based on the analysis, it is confirmed that the PI controller used in this study is capable to deal with uncertainties indicating a robust PAT system design has been succesfully developed.

## 5.3 Application of the systematic framework for managing uncertainties: potassium dihydrogen phosphate (KDP) crystallization case study

In the previous chapter, the one- and two-dimensional models are generated to represent the crystallization process, and by implementing a controller through PAT system design to maintain the concentration at the required set points, the target one- and two-dimensional CSDs are achieved. However, thus far it has been assumed during the PAT system design that the uncertainty around parameter values can be neglected. In this section, the feature of the systematic design framework to perform uncertainty and sensitivity analysis on the designed PAT system is highlighted through the KDP crystallization process case study: it will be investigated how input (parameter) uncertainty affects the target one- and two-dimensional CSD (see Figure 4.14) and how this uncertainty can be minimized to achieve the desired target CSD.

### 5.3.1 Problem definition (Step 1), crystallization model development (Step 2) and design of set point profiles (Step 3)

The main objective of this study is to develop a reliable and robust PAT system design for the KDP crystallization process by performing uncertainty and sensitivity analysis on the designed PAT system. In this study, the uncertainty and sensitivity analysis are performed under two different scenarios: (1) open-loop, and (2) closed-loop. In step 2, the model equations for the one-dimensional (see Table 4.5) and the two-dimensional (see Table 4.6) KDP crystallization process are used in this section. The optimal set point profile (step 3) that is to be maintained here, consisting of a

supersaturation set point of 0.03 g/g as well as the total crystallization time of 80 seconds is obtained for both cases.

### 5.3.2 Design of process monitoring and control (PAT) system (Step 4)

The PAT system for the KDP crystallization process designed in Chapter 4 is used here. Based on the PAT system design, the ATR-FTIR, thermocouple and FBRM are used to monitor the solute concentration, the temperature and the CSD for both the one- and the two-dimensional cases. The PI control is implemented to control the KDP concentration by manipulating the inlet water temperature.

### 5.3.3 Validation of process monitoring and control (PAT) system using uncertainty and sensitivity analysis (Step 5)

In this study, the uncertainty and sensitivity analysis are performed under two different scenarios: a) open-loop; b) closed-loop.

a) Open-loop

The objective here is to understand the effect of uncertain system parameters such as nucleation and crystal growth parameters on the prediction of the crystallization performance and to identify which parameters are the key driver of variance in the product CSD. Furthermore, the open-loop results will form the basis for comparison with the results obtained from closed-loop simulation using the designed PAT system. The open-loop analysis is conducted where the model equations for the one-dimensional (see

Table 4.5) and two-dimensional (see Table 4.6) KDP crystallization process are simulated in the ICAS-MoT modelling tool. The resulting performance is evaluated here in terms of KDP concentration, temperature profile and final CSD for both cases. The evaluation is first done assuming no uncertainty on the inputs, i.e. only a single output profile is obtained for each output variable. The open-loop reference simulation results for the one- and two-dimensional KDP crystallization process are shown in Figure 5.9.

Figure 5.9 shows the open-loop reference simulation results for the seeded one- and two-dimensional KDP crystallization process. The temperature for both process are cooled from 32ºC to 28 ºC resulting into KDP concentration profiles that are in both cases deviating far from the saturation concentration line. Under such conditions, a too high supersaturation is obtained in the beginning of the operation, and therefore secondary nucleation occurs. The final one- and two-dimensional CSD as shown in Figure 5.9 indeed indicate that the secondary peak consisting of small crystal is obtained as a result of a too high supersaturation.

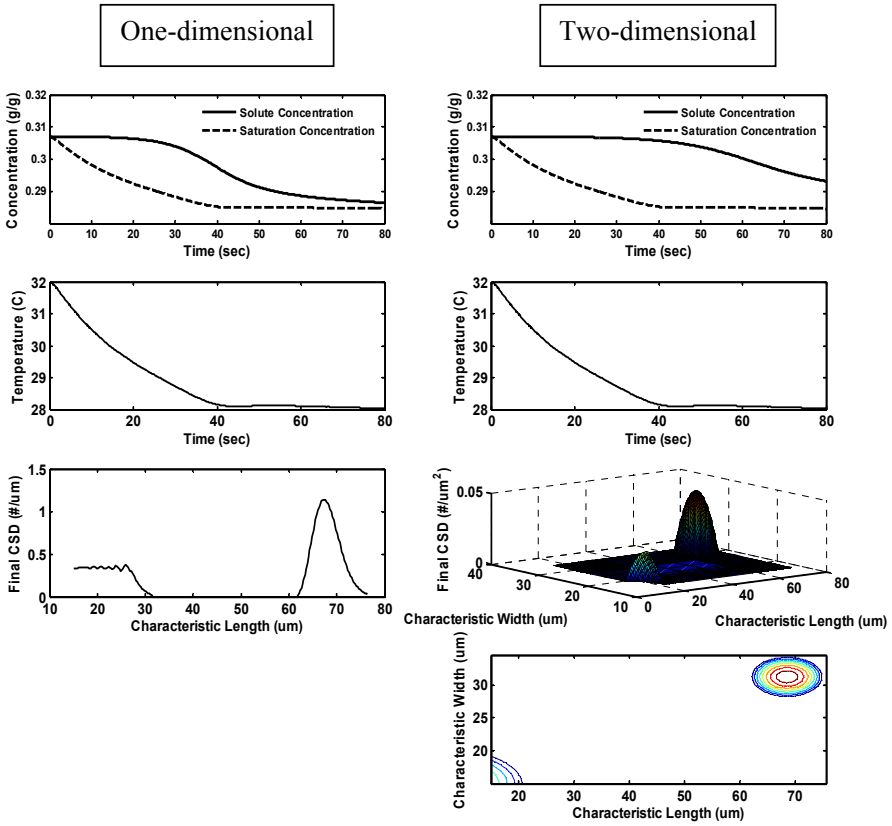


Figure 5.9 Reference simulation results using nominal values for KDP concentration, temperature and final CSD under open-loop operation for the one- and two-dimensional cases

### 5.3.3.1 Framing for uncertainty and sensitivity analysis (Step 5.1)

The framing scenario for uncertainty and sensitivity analysis for KDP crystallization process is as follows:

**Step 5.1.1: Identify sources of uncertainty**

In this work, 5 parameters ($k_b$, $b$ , $k_{gx}$, $g_x$ and $\gamma_x$) from the nucleation and crystal growth model equations (see Equation (7) and (8) in Table 4.5) were investigated for the

one-dimensional case, and 8 parameters ($k_b$, $b$, $k_{gx}$, $g_x$, $\gamma_x$, $k_{gy}$, $g_y$ and $\gamma_y$) from the nucleation and crystal growth models (see Equation (7-9) in Table 4.6) were investigated for the two-dimensional case. All the parameters are assumed to have a uniform probability distribution as shown in Table 5.5 where the reported lower and upper bound values of each parameter are obtained based on the 95% confidence intervals taken from Gunawan et al. (2002).

Table 5.5 Input uncertainties on nucleation and crystal growth rate parameters for KDP crystallization

| ID | Parameters | Units | Values | Confidence interval (95%) | Lower bound values | Upper bound values |
|---|---|---|---|---|---|---|
| 1 | Nucleation rate constant, $k_b$ | No. of particles/μm$^3$.s | 7.49E-08 | ±3.5E-09 | 7.14E-08 | 7.84E-08 |
| 2 | Nucleation order constant, $b$ | Dimensionless | 2.04 | ±0.16 | 1.88 | 2.2 |
| 3 | Growth rate constant, $k_{gx}$ | μm/s | 100.75 | ±12.3833 | 88.3667 | 113.1333 |
| 4 | Growth order constant, $g_x$ | Dimensionless | 1.74 | ±0.07 | 1.67 | 1.81 |
| 5 | Growth constant, $\gamma_x$ | 1/μm | 0.6 | ±0.1 | 0.5 | 0.7 |
| 6 | Growth rate constant, $k_{gy}$ | μm/s | 12.21 | ±3.3167 | 8.8933 | 15.5267 |
| 7 | Growth order constant, $g_y$ | Dimensionless | 1.48 | ±0.06 | 1.42 | 1.54 |
| 8 | Growth constant, $\gamma_y$ | 1/μm | 0.6 | ±0.1 | 0.5 | 0.7 |

**Step 5.1.2: Monte Carlo procedure**

The first step in the Monte Carlo procedure is the sampling of uncertainties (step 5.1.2.1). In this step, a parameter is sampled from a distribution using the Latin hypercube

sampling (LHS) method. In this work, different numbers of samples have been tested repetitively for 25, 50, 100 and 150 samples, and were compared based on the Monte Carlo simulation errors to determine whether the number of samples used is suitable or not. Based on the analysis, the error for 25 and 50 samples are larger than the error for 100 samples. However, the error for 100 and 150 samples is almost identical. Therefore, the number of samples used in this study is 100 samples for both the one- and the two-dimensional cases where no correlation between the parameters is assumed. The next step in the Monte Carlo procedure is to perform simulations (step 5.1.2.2). In this case, the open-loop one- and two-dimensional KDP models are simulated 100 times, i.e. once for each different set of model parameters. The Monte Carlo simulations for both cases have been performed in the ICAS-MoT modelling tool.

The results from the Monte Carlo simulations are then analyzed in the evaluation of output uncertainties step (step 5.1.2.3) as shown in Figure 5.10. Each line in Figure 5.10, for example for the final CSD, corresponds to a dynamic model output obtained by simulating the KDP model with one set of parameter values. The varying spread of the band indicates the extent of uncertainty in the simulated outputs. For both cases, the KDP concentration indicates a large spread indicating a high extent of uncertainty. Meanwhile the uncertainty is at the minimum level in the one- and two-dimensional temperature profiles. The wide spread in the final one- and two-dimensional CSD (shown as contour plot) profiles demonstrates that there is a relatively high extent of uncertainty about the output values. Clearly, the induced variation in the nucleation and crystal growth rate parameters affects the final CSD, as shown in Figure 5.10.

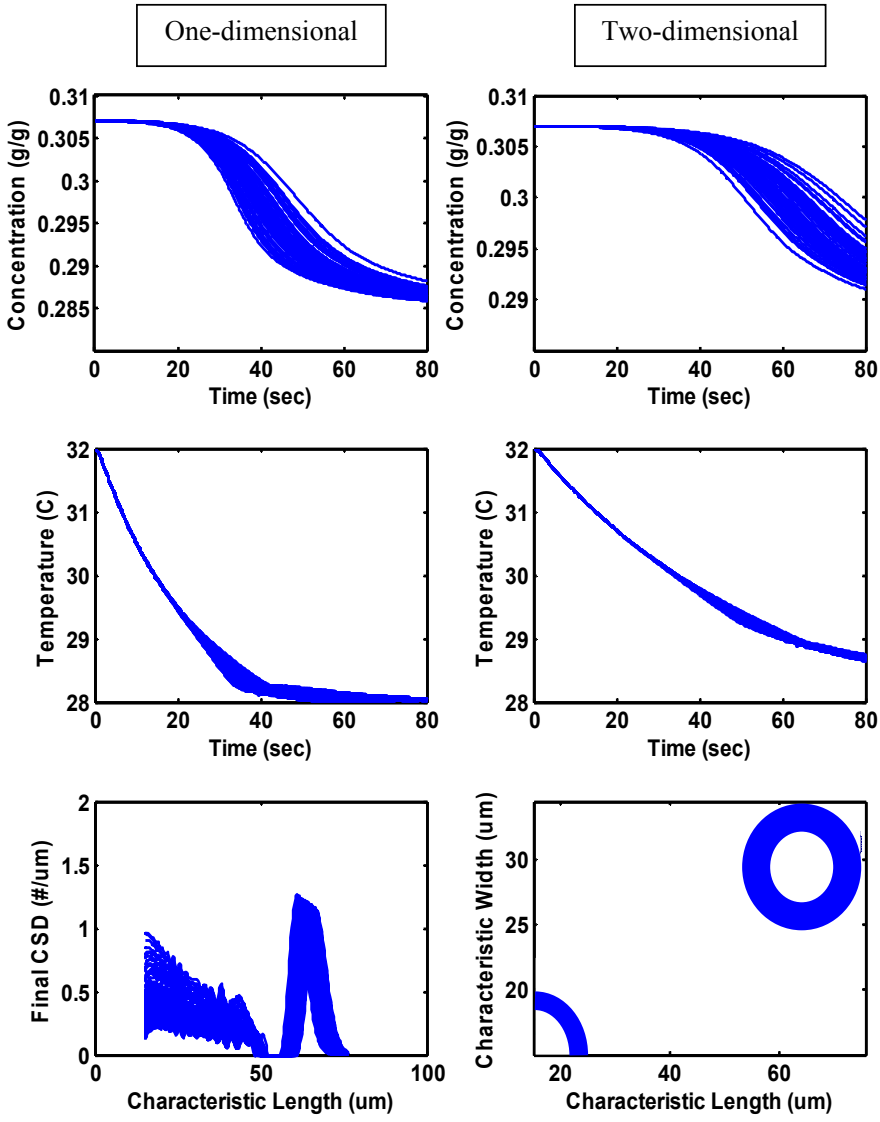


Figure 5.10 Open-loop simulation results for KDP concentration, temperature, and final CSD obtained from the Monte Carlo simulation (in total there are 100 lines) for the one- and two-dimensional cases

Furthermore, the spread of the output variation is larger in the two-dimensional case than the one-dimensional case. This is due to the fact that more parameters are considered for the input uncertainty in the two-dimensional case compared to the one-dimensional case. There are two crystal growth rate models for the two-dimensional case where one crystal growth rate model has the faster growth rate for the characteristic length direction and the other one has a slower rate for the characteristic width direction compared to the single crystal growth model that has been used in the one dimensional case. The crystal growth model is used to grow the crystal and is related with the KDP concentration equation (see Equation (2) in Table 4.6) as well as the CSD through the population balance equation (see Equation (1) in Table 4.6). Therefore the induced variation in parameters used in the two-dimensional case contributes more to the uncertainty in the KDP concentration and CSD model prediction compared to the one-dimensional case.

The data can be assessed further using the mean, $10^{th}$ and $90^{th}$ percentiles of the Monte Carlo output at each simulation time as indicated in Figure 5.11. Based on Figure 5.11, the $10^{th}$ and $90^{th}$ percentile for the temperature in both the one- and the two-dimensional case are very close to the mean, indicating that the uncertainty of this model output is very low or not existing. However, the $10^{th}$ and $90^{th}$ percentiles for the KDP concentration and final CSD for both cases are further away from the mean. Therefore also it is concluded that the uncertainty of the KDP concentration and the final CSD is quite large.

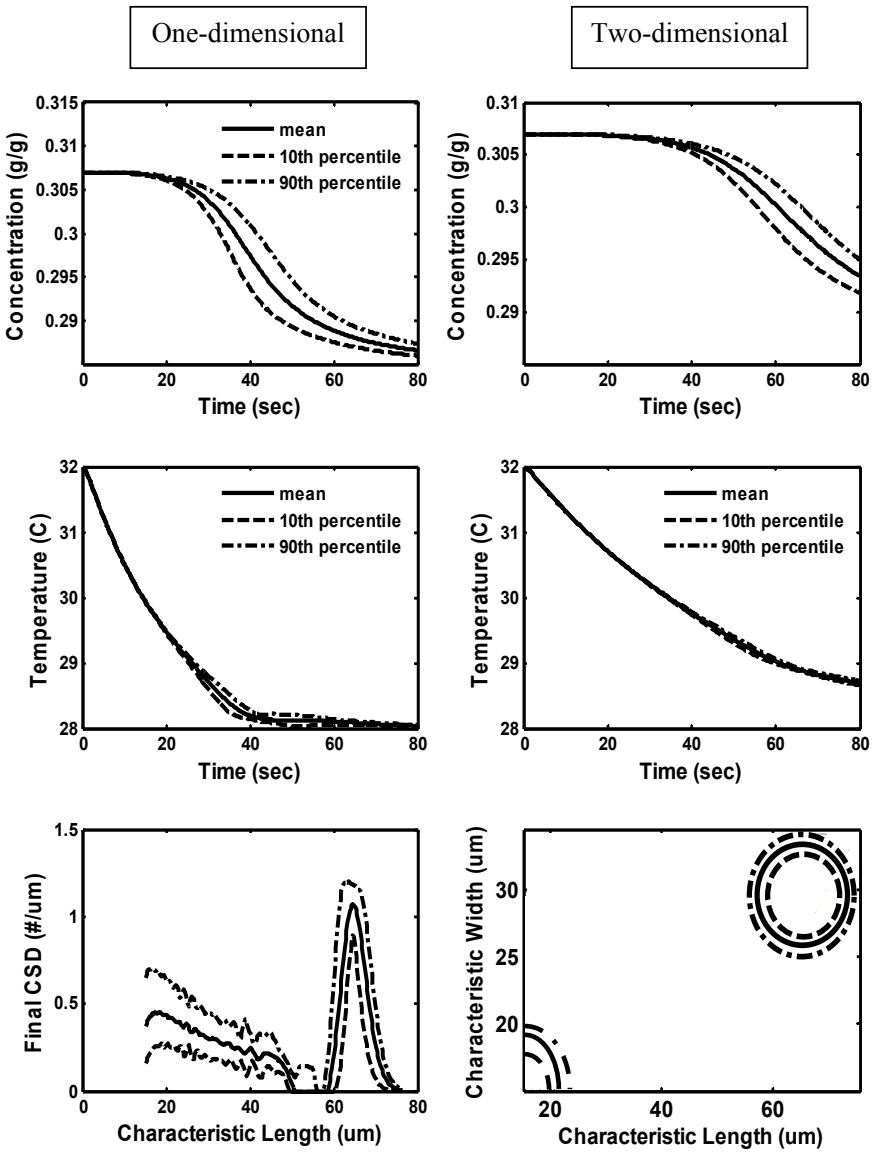


Figure 5.11 Representation of uncertainty using mean, 10$^{th}$ and 90$^{th}$ percentile values of the Monte Carlo simulations under open-loop condition

**Step 5.1.3: Sensitivity analysis**

In this step, the sensitivity analysis is conducted first using the SRC method. Then the reliability of the parameter significance ranking obtained by SRC method is confirmed through the use of the Morris screening method.

**Step 5.1.3.1: Standardized regression coefficients (SRC) method**

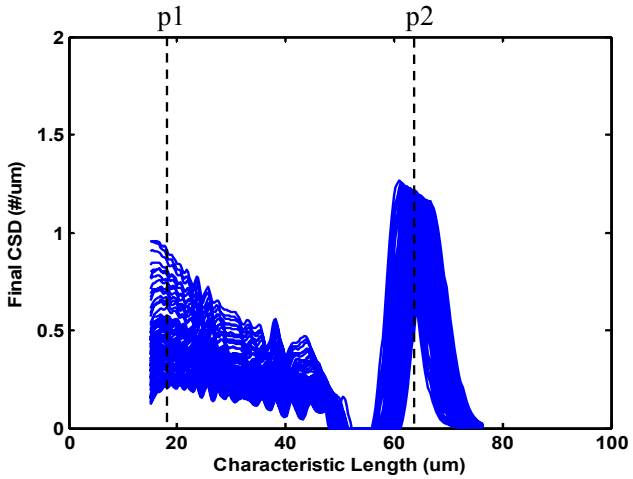


Figure 5.12 Points where the one-dimensional CSD is sampled for sensitivity analysis

The sensitivity analysis is conducted for 2 different points in the simulated one-dimensional CSD data, as shown in Figure 5.12. One data point in the CSD corresponds to the crystals formed due to secondary nucleation (point p1 in Figure 5.12) and the other one corresponds to the CSD from the seeded crystals that have grown (point p2 in Figure 5.12. For each data point, a linear regression model was constructed using Equation (5.1) and the corresponding regression coefficients, $\alpha_{jk}$, were obtained from linear least-squares. The standardized regression coefficients, $\beta_{jk}$, were then calculated using

Equation (5.2), and the resulting summary of the parameter significance ranking for the one-dimensional case is given in Table 5.6.

Table 5.6 Standardized regression coefficients of linear models and parameter significance ranking for the one-dimensional case

| Location | CSD data taken at p1) | | CSD data taken at p2) | |
|---|---|---|---|---|
| | $R^2 = 0.9506$ | | $R^2 = 0.8456$ | |
| Ranking | Parameter | $\beta_{jk}$ | Parameter | $\beta_{jk}$ |
| 1 | $b$ | -0.8241 | $g_x$ | 0.6890 |
| 2 | $g_x$ | 0.4502 | $\gamma_x$ | -0.5804 |
| 3 | $\gamma_x$ | -0.2355 | $k_{gx}$ | 0.3405 |
| 4 | $k_{gx}$ | -0.1734 | $b$ | -0.1603 |
| 5 | $k_b$ | 0.063 | $k_b$ | -0.03 |

The degree of linearization indicated by the coefficient of model determination, $R^2$, was found to be high for all CSD data taken, i.e. the $R^2$ values were above the recommended value of 0.7 (Campolongo and Saltelli, 1997; Saltelli et al., 2006). This indicates that the linearized model is reliable and the corresponding coefficients can be used to assess and rank the importance of the input parameters with respect to the outputs. Based on the one-dimensional CSD data taken at p1, it was shown that the most significant parameter is the nucleation order constant, $b$, which has a SRC of -0.82 and belongs to the nucleation equation (Equation (7) in Table 4.5). This is a reasonable result, considering that the data are taken from the CSD region generated by secondary nucleation. Therefore, the variation of the input parameter, $b$, influences the generation of new crystals due to nucleation effects which explains the large variation of the CSD data taken at p1). In addition, the negative sign for the parameter, $b$, indicates the

negative impact on the CSD where more new crystals are generated when the value of the parameter, $b$, is decreased.

Meanwhile, the parameters, $g_x$ and $\gamma_x$, have a SRC of 0.45 and -0.24 respectively. Both parameters are part of the crystal growth rate equation (Equation (8) in Table 4.5) which also contributes to the large uncertainty on the CSD data prediction at point p1). Both parameters will have an effect on the growth of the new crystals that have been produced due to the secondary nucleation where the parameter, $g_x$, is responsible for driving the CSD towards a larger characteristic length, whereas the parameter, $\gamma_x$, contributes to variation of the secondary peak of the CSD data at point p1). In this case, the parameter $\gamma_x$, has a negative impact, i.e. the lower the value of parameter, $\gamma_x$, the higher the secondary peak that will be obtained which also explains the large variation of the CSD data at point p1). The one-dimensional CSD data taken at p2) correspond to crystal growth of the original seed crystals. Therefore the most significant parameters for the data taken at p2) are $g_x$, $\gamma_x$ and $k_{gx}$ where all three parameters have a SRC of 0.69, -0.58 and 0.34 respectively, and appear in the crystal growth rate equation (Equation (8) in Table 4.5). A higher value of the growth order constant ($g_x$) results into a CSD with a higher characteristic length, which explains the variation in the distribution of the CSD data. Table 5.6 shows that the magnitude of the growth constant ($\gamma_x$) is negative. It means that when the value of the growth constant ($\gamma_x$) is decreased, a higher CSD peak is obtained resulting into a more narrow CSD as well. The nucleation phenomenon has no influence on the CSD data taken at p2) which explains why both parameters for nucleation have the lowest ranking in the table.

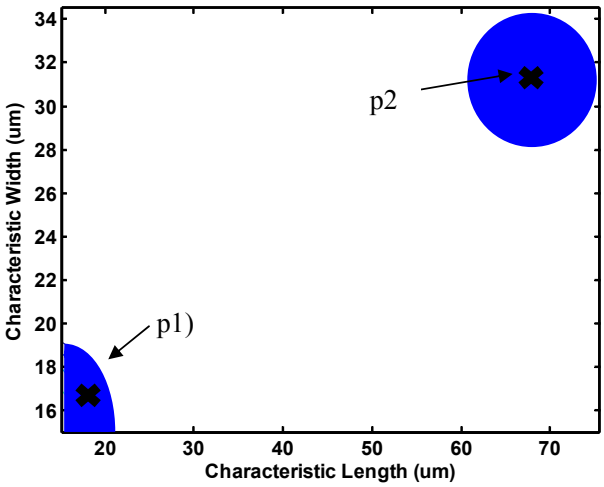


Figure 5.13 Points where the two-dimensional CSD is sampled for sensitivity analysis

Similarly, the sensitivity analysis was also conducted for 2 different parts of the two-dimensional CSD data, which are shown as a contour plot in Figure 5.13: the data of p1) correspond to the CSD generated by secondary nucleation, and the data of p2) are located in the center of the CSD that has originated from the growth of the seeded crystals. The sensitivity analysis showed that the most significant parameters obtained for the 2 different locations in the two-dimensional case are identical to the most significant parameters of the one-dimensional case. The main difference is that there are two different crystal growth rates used in the two-dimensional case.

Based on Table 5.7, it is clear that the parameters corresponding to the crystal growth rate for the characteristic length direction are more significant than the parameters corresponding to the crystal growth rate for the characteristic width direction. For example, the most significant parameter for data taken at p2), the parameter $g_x$ for the characteristic length direction is more influential compared to the parameter $g_y$ for the

characteristic width direction. This is because the parameters in the crystal growth expression for the characteristic length direction have a higher value than the parameters in the crystal growth model for the characteristic width direction and, thereby, contribute more uncertainty to the model prediction. This is due to the fact that usually the high characteristic length is favorable in the two-dimensional case in order to achieve a desired aspect ratio (average characteristic length over average characteristic width) around 1.5-2.2 (Lee et al., 2002). Therefore, the parameter value of crystal growth for characteristic length usually has a higher value compared to the parameter value of crystal growth for characteristic width in order to obtain the desired aspect ratio.

Table 5.7 Standardized regression coefficients of linear models and parameter significance ranking for the two-dimensional case

| Location | CSD data taken at p1) | | CSD data taken at p2) | |
|---|---|---|---|---|
| | $R^2 = 0.9212$ | | $R^2 = 0.8443$ | |
| Ranking | Parameter | $\beta_{jk}$ | Parameter | $\beta_{jk}$ |
| 1 | $b$ | -0.9032 | $g_x$ | 0.6641 |
| 2 | $g_x$ | 0.2312 | $g_y$ | 0.5395 |
| 3 | $g_y$ | 0.1932 | $\gamma_x$ | -0.3781 |
| 4 | $\gamma_x$ | -0.1671 | $\gamma_y$ | -0.3021 |
| 5 | $\gamma_y$ | -0.0921 | $k_{gx}$ | 0.1643 |
| 6 | $k_b$ | 0.0851 | $k_{gy}$ | 0.1296 |
| 7 | $k_{gx}$ | -0.0212 | $b$ | -0.0403 |
| 8 | $k_{gy}$ | -0.0128 | $k_b$ | -0.0276 |

**Step 5.1.3.2: Morris screening method**

In this work, the parameter significance ranking obtained from the Morris screening method has been compared with the one obtained from the SRC method to investigate the

reliability of both sensitivity analysis results. Firstly the parameter significance ranking has been compared based on the one-dimensional CSD data taken at p1) and p2) (refer to Figure 5.12). The results of the Morris method were found to be in good agreement for all the parameters with the ranking obtained by the SRC method as shown in Tables 5.8-5.9. Moreover, the standard deviation, $\sigma_j$ is alco calculated in this method. Here, all the parameters have a non-zero value of $\sigma_j$ with non-zero mean, $\mu_j$ indicating all the parameters are involved in non-linear interactions on the outputs. This observation is clearly correct as the crystallization models are indeed non-linear (Ma et al., 1999). Similarly, for the two-dimensional CSD data, the parameter significance ranking obtained from the Morris screening method is also identical to the ranking obtained by the SRC method as shown in Appendix D. Moreover, all the parameters for the two-dimensional CSD data are also involved in non-linear interactions on the outputs based on the non-zero values obtained for both $\sigma_j$ and $\mu_j$ respectively.

Table 5.8 Method comparison for screening influential factors based on the one-dimensional CSD data taken at point p1)

| | Morris screening method | | | SRC method | |
|---|---|---|---|---|---|
| Ranking | Parameters | $\mu_j$ | $\sigma_j$ | Parameters | $\beta_{jk}$ |
| 1 | $b$ | -0.8213 | 0.7143 | $b$ | -0.8241 |
| 2 | $g_x$ | 0.3912 | 0.2386 | $g_x$ | 0.4502 |
| 3 | $\gamma_x$ | -0.2687 | 0.1308 | $\gamma_x$ | -0.2355 |
| 4 | $k_{gx}$ | -0.1154 | 0.0061 | $k_{gx}$ | -0.1734 |
| 5 | $k_b$ | 0.0294 | 0.0001 | $k_b$ | 0.063 |

Table 5.9 Method comparison for screening influential factors based on the one-dimensional CSD data taken at point p2)

| | Morris screening method | | | SRC method | |
|---|---|---|---|---|---|
| Ranking | Parameters | $\mu_j$ | $\sigma_j$ | Parameters | $\beta_{jk}$ |
| 1 | $g_x$ | 0.6623 | 0.5627 | $g_x$ | 0.6890 |
| 2 | $\gamma_x$ | -0.5456 | 0.5318 | $\gamma_x$ | -0.5804 |
| 3 | $k_{gx}$ | 0.4312 | 0.3954 | $k_{gx}$ | 0.3405 |
| 4 | $b$ | -0.1221 | 0.0175 | $b$ | -0.1603 |
| 5 | $k_b$ | -0.0335 | 0.0006 | $k_b$ | -0.03 |

b) Closed-loop

The open-loop analysis of uncertainties for the one- and two-dimensional KDP crystallization process concluded that significant uncertainty exists in the model outputs for both cases, especially for the KDP concentration and the final CSD. The most significant parameter for that part of the CSD data generated by secondary nucleation is the nucleation order constant, $b$, for both cases. Meanwhile the growth order constant, $g_x$, is identified as the most significant parameter for the part of the CSD corresponding to the seeded crystals for both cases respectively. With this result in mind, in this step we repeat the uncertainty and sensitivity analysis on the PAT system. Here the objective is to comprehensively test the PAT system design performance in achieving the desired target product properties taking into account the under considered domain of uncertainties. For the closed-loop simulation, a PI controller has been developed in order to maintain the KDP concentration at the desired set point. The generated set point profiles consist of a

supersaturation set-point at 0.03 g/g. The closed-loop reference simulation results obtained for the one- and two-dimensional case are shown in Figure 5.14.

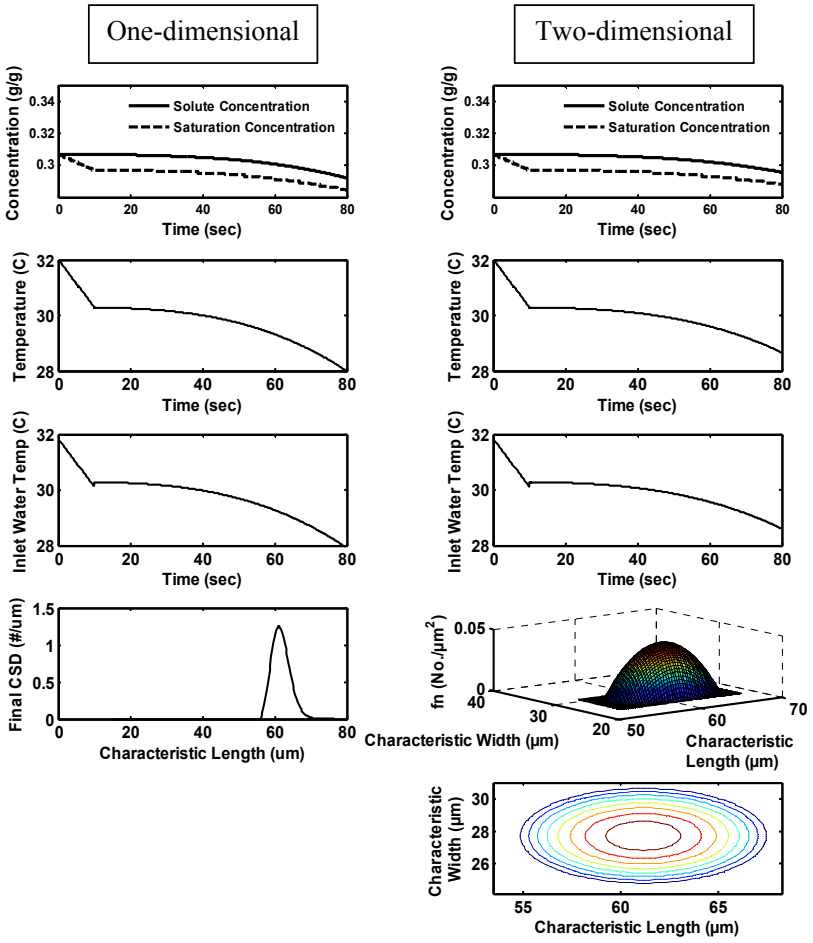


Figure 5.14 Reference one- and two-dimensional simulation results using nominal values for KDP concentration, temperature, inlet water temperature (manipulated variable) and final CSD under closed-loop operation

The KDP concentration for both cases initially started at 0.307 g KDP/g water and once the KDP concentration set point was reached the PI controller successfully maintained the concentration at the set point until the end of the operation. In Figure 5.14, approximately 0.291 g KDP/g water (one-dimensional) and 0.295 g KDP/g water (two-dimensional) remain by the end of the operation. Comparing the predictions from the two models, it can be noted that the KDP concentration profile in the one-dimensional model is decreasing more rapidly than in the two-dimensional model. This is because the cube-shaped volume in the one-dimensional case consumes more solute from the solution than the tetragonal-prism volume in the two-dimensional case, which becomes clear also from the characteristic length data in the two-dimensional case (the crystal growth rate in the width direction is lower in the two-dimensional case, compared to the crystal growth rate in the one-dimensional case).

In terms of CSD, the detailed one-dimensional simulation model predicted an almost identical target CSD. The cube-shaped seed originally at mean characteristic length of 19.5 μm with a standard deviation of 0.97 μm has been grown to the mean characteristic length of 60.73 μm with a standard deviation of 2.79 μm which is very close to the mean characteristic length of 60.85 μm and standard deviation of 2.8 μm for the target CSD. In the two-dimensional case, the final CSD obtained from the detailed simulation model shows that the tetragonal prism shape of the seed has been grown from initially 19.5 μm in the mean characteristic length and width up to approximately 60.6 μm average characteristic length and 26.55 μm mean characteristic width. The length and width obtained from the detailed simulation model are very close to the target values which are the mean characteristic length of 60.85 μm and mean characteristic width of

27.36 μm. Based on the closed-loop operation, it can be concluded that the controller is able to maintain the KDP concentration at its set point for both cases while achieving the target specifications. Therefore the next task is to evaluate the controller performance in terms of its ability to manage the uncertainties and still achieve the desired target specifications.

Here the uncertainty and sensitivity analysis is repeated again where the same framing scenario used in the open-loop operation is applied. Here the same 8 parameters from the nucleation and crystal growth rate models as shown in Table 5.5 as well as the same 100 samples are applied for the one- and two-dimensional case in this analysis. The results from the Monte Carlo simulations are presented in Figure 5.15. The KDP concentration for the one- and two-dimensional cases indicates a small spread indicating a low degree of uncertainty. It can be clearly seen that the impacts of the uncertain parameters have been minimized for the KDP concentration when operated under closed-loop conditions. Meanwhile the uncertainty is almost non-existent in the temperature profiles. In addition, the small spread in the final one- and two-dimensional CSD profiles shows a low extent of uncertainty.

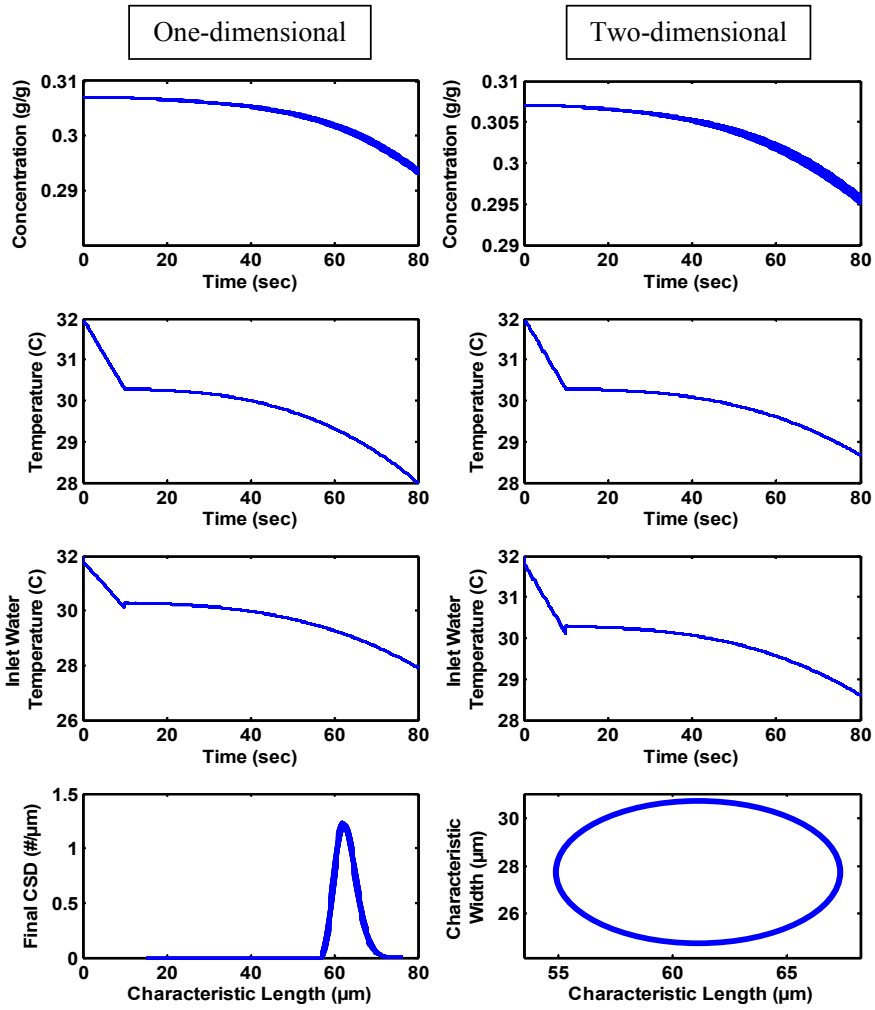


Figure 5.15 Closed-loop simulation results for KDP concentration, temperature, and final CSD obtained from the Monte Carlo simulation (in total there are 100 lines) for one- and two-dimensional cases

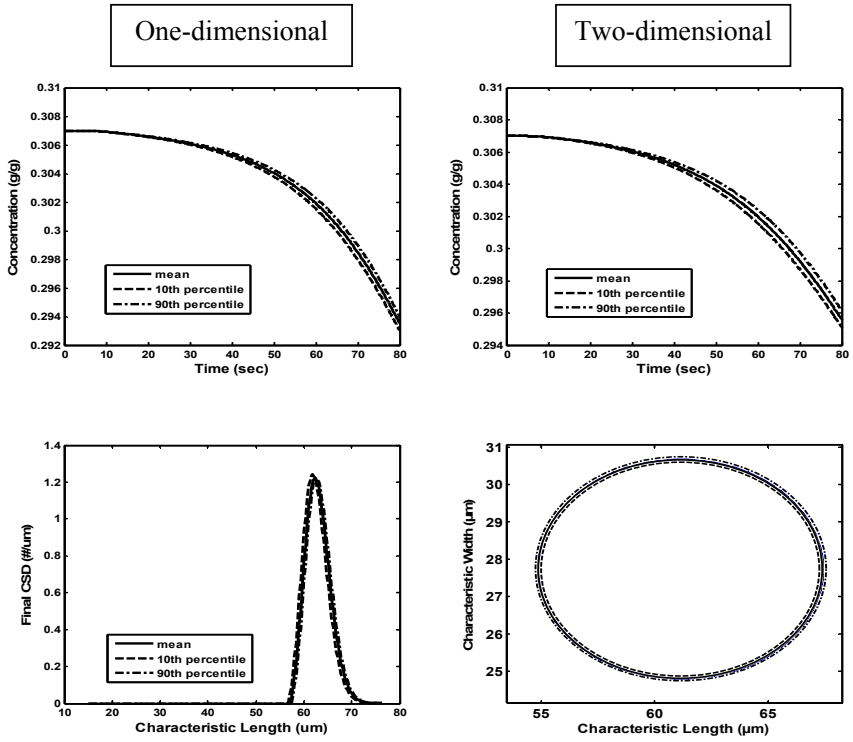


Figure 5.16 Representation of uncertainty using mean, 10$^{th}$ and 90$^{th}$ percentile values of the Monte Carlo simulations under closed-loop for one- and two-dimensional cases

The data are then analysed using the representation of uncertainty using mean, 10$^{th}$ and 90$^{th}$ percentile values of the Monte Carlo simulations. As shown in Figure 5.16, the 10$^{th}$ and 90$^{th}$ percentiles for the KDP concentration and final CSD in the one- and two-dimensional case are very close to the mean, respectively, indicating that the uncertainty of these model outputs is very low. Comparing both cases, it is clearly shown that the uncertainty for both the KDP concentration and the final CSD are slightly higher for the two-dimensional case than for the one-dimensional case. This is due to the fact that more parameters (8 parameters) have been used as input uncertainty in the two-dimensional case compared to only 5 parameters in the one-dimensional case.

Nevertheless, both CSDs obtained under the presence of uncertainty are in good agreement with the specified target CSD. Thus, it can be concluded that the PAT system design using the simple PI control structure and proper controller tuning applied in this study is indeed reliable and robust enough to deal with the presence of uncertainties, and is able to deliver target properties.

#### 5.3.3.2 Decision making (Step 5.2)

Based on the validation of the PAT system using uncertainty and sensitivity analysis, it is concluded that the designed PAT system used in this study is able to achieve the target properties under the considered domain of uncertainties. Therefore this PAT system design is now ready to be implemented in the next step.

### 5.3.4 Implementation of process monitoring and control (PAT) system (Step 6)

In this work, the PAT system has been designed for KDP crystallization. So far the designed PAT system has been implemented only in a simulation (Samad et al., 2012a) and was shown to achieve the target crystal product for the one- and two-dimensional cases. In order to have a practical application, the simulation results need to be supported by results from laboratory experiments. However, this is beyond the scope of this contribution but will be subject of future work.

## 5.4 Concluding remark

The methodology for implementing uncertainty and sensitivity analysis has been successfully incorporated in the model-based systematic design framework for monitoring and control (PAT) systems of crystallization processes. The application of uncertainty and sensitivity analysis has been highlighted through a one- and two-dimensional KDP crystallization process in the frame of the model-based design of a PAT system for both open-loop and closed-loop scenarios. In this work, the input uncertainty of the parameters of the nucleation and the crystal growth rate was propagated using the Monte Carlo procedure. In open-loop, the output uncertainty was found large for the KDP concentration and the CSD obtained for both cases, which confirms the influence of input uncertainties on the model predictions. Subsequently global sensitivity analysis has been performed using SRC and the Morris screening method. Both methods showed a good agreement in terms of the ranking of significant parameters, which helps to identify the main causes of the output uncertainty. The analysis for the closed-loop condition was carried out next to test the reliability of the PAT system design and it was demonstrated that the PAT system using a PI controller with proper tuning developed for the KDP crystallization is reliable and sufficiently robust to produce the desired one- and two-dimensional CSD under a wide range of uncertainties.

# 6. Conclusions and future work

This chapter summarizes the overall achievements of this work and the recommendations for future work.

## 6.1 Achievements

A generic framework for systematic design of a process monitoring and control (PAT) system for crystallization processes has been developed to study various aspects of crystallization operations. The main achievements that have been obtained from this work are summarized as follows:

1. The overall framework is a step-by-step procedure. Each step of the overall framework has its specific purpose. The procedure has been structured in an efficient way, and the generic nature of the framework allows its wide application to crystallization processes.
2. The generic multi-dimensional model-based framework has been developed and succesfully integrated in the overall framework for systematic design of a process monitoring and control (PAT) system. The generic multi-dimensional model-based framework allows the user to generate any problem-system specific model to be studied for a wide range of crystallization processes. This is due to the fact that the framework contains a set of generic balances and a set of constitutive equations that can be selected and used to represent the

crystallization process. Furthermore, the unique features of the modelling framework are that it allows the user to generate a problem-system specific model and further extend the model to consider any crystallization phenomena as well as the ability to reuse the model by changing the chemical system to another chemical system and thus, a wide range of chemical systems can be investigated. In addition, the modelling framework is able to handle increased model complexity from a one-dimensional to a two-dimensional case with minimum modelling effort. The application of the modelling framework has been succesfully highlighted, firstly for paracetamol where the problem-system specific model has been generated and further extended to cover agglomeration and breakage effects. Then, by changing the chemical system, the problem-system specific model for paracetamol was reused and applied to the sucrose crystallization process. Secondly, the KDP crystallization process was studied to demonstrate the capability of the modelling framework to generate the one-dimensional model, and then the resulting model was transformed easily into a two-dimensional model.

3. The systematic procedure to design the set point profiles for the crystallization process is also included in the framework, both by using an analytical CSD estimator and the RSM technique. Here the original one-dimensional analytical CSD estimator of Aamir et al. (2010) has been extended to cover both the one- and the two-dimensional case. This is another contribution where the extended analytical CSD estimator is now able to generate a set point profile that guarantees that the target CSD is achieved and is ready to be applied in a range

of systems, covering size independent crystal growth as well as size dependent crystal growth for a one- or two-dimensional case. As an alternative, the RSM can also be employed to generate the set point profiles, and through the highlighted case studies for potassium dichromate and KDP crystallization processes, it has been proved that both analytical CSD estimator and RSM generate identical optimal set point profiles.

4. Previously, the model-based methodology for design of process monitoring and analysis systems developed by Singh et al. (2009) has been tested on tablet manufacturing, fermentation and cheese manufacturing processes. In this work, the methodology has been extended to crystallization process applications where the knowledge base and model library which both serve as supporting tools in the methodology have been extended to include the relevant monitoring tools/techniques, process variables involved and mathematical models for crystallization processes. Furthermore, the methodology has been integrated into the overall systematic design framework and has been succesfully linked with the developed crystallization modelling framework for efficient model generation and PAT system design application. In this work, the application of the PAT system design has been highlighted as part of the overall systematic framework application for potassium dichromate and KDP crystallization processes to achieve the desired target crystal product.

5. The uncertainty and sensitivity analysis is also included in the overall systematic framework. This provides another unique feature of the overall systematic framework where the uncertainty in the crystallization process inputs and its

propagation to the outputs can be quantified through the Monte Carlo procedure. Furthermore, sensitivity analysis can be conducted as well to determine the most significant parameters. Through this analysis, the risk of not obtaining the target product specifications can now be investigated and the solution is then proposed in order to minimize/reduce the uncertainty and achieve the target product specifications. In order to realize this idea in practice, the framework for uncertainty and sensitivity analysis has been integrated in the existing overall systematic design framework. The application of the uncertainty and sensitivity analysis has been demonstrated for both potassium dichromate and KDP crystallization processes.

## 6.2 Recommendations for future work

The work done within this thesis has resulted in the succesful development of a generic framework for systematic design of a process monitoring and control (PAT) system for crystallization processes. However, there are still opportunities for further developments and improvements. The recommendations for future work are summarized as follows:

1. In this work, the generic modelling framework has been developed to generate problem-system specific models for crystallization processes. However, only one- and two-dimensional models can be generated at this moment through the generic modelling framework. However, the one- and two-dimensional models only consider one inner variable (characteristic length) and two inner variables

(characteristic length and width) in the population balance equations as a measure for crystal size, thus limiting the crystal shape only to the description of spherical, cubic, rod and tetragonal prism crystals. Therefore, to fully characterize the crystal particles higher dimensional models are necessary, that is, a three-dimensional population balance modeling approach is needed, where three characteristic directions in terms of length, width and depth of a crystal may be considered. Through the incorporation of three-dimensional models, more complicated crystal shapes than the above-mentioned shapes (for the one- and two-dimensional case) can be incorporated where the accurate information about size-related dimensional evolution of crystals can be simulated as well as morphology of single crystals can also be studied.

2. The modelling framework needs integration with model identification and data handling frameworks (Samad et al., 2012c) where it should be possible to perform the parameter estimation using raw experimental data. However, such a feature has not been highlighted in this work. The future work should be focused on expanding the databases for operational scenarios, data measurement techniques and data translation policies that will allow a broader range of applications of the total modelling framework.

3. In the uncertainty and sensitivity analysis work, only kinetic parameters in the nucleation and crystal growth rate expressions were considered as an input uncertainty. There is also uncertainty present in the initial conditions, for example the seed crystals. Seeding is an efficient approach to stabilize the crystallization process and produce the desired target product. Usually the

amount and size of seeds to be added to the crystallizer is determined from experimental data which contribute to some extent to the uncertainties. Therefore also, it could be interesting in the future to consider the properties of the seed crystals as an input uncertainty as well. As indicated earlier, implementation of the proposed PAT system in a real crystallization process could both be used to verify and confirm the methodology and the results obtained here.

4. In addition, the optimization of the seed crystals has a major effect on the resulting crystal product, and especially the crystal size distribution (CSD). The developed generic framework (a systematic procedure, collection of relevant methods and tools) in this work is flexible and can be extended to include the optimization of seed crystals and it could be interesting work to optimize seed crystals for the one- and two-dimensional problem in the future work.

5. In this work, the validation of the designed crystallization process is presently based on the process models. However, it would be interesting to include extended experimental validations to validate the designed process.

6. So far only the design and implementation of the PAT system step in the overall systematic design framework has been conducted in the ICAS-PAT software (Singh et al., 2010). In order to provide a more flexible, user-friendly and efficient environment, this software should be expanded to include all those features in the overall systematic design framework, especially the crystallization model development and uncertainty and sensitivity analysis.

7. Another way to improve the robustness of PAT system design is to incorporate robustness in the control of crystallization processes (Nagy, 2009; Nagy and Braatz, 2004). Through this approach, parameter uncertainties are taken into account in the problem formulation for robust optimization. Based on evaluation of robust optimization, the product quality has been successfully improved. Through this approach, the control is implemented in the way of hierarchical structure based on two levels. The lower level is a direct design crystallization control methodology where the supersaturation controller is employed to drive the system in the phase diagram. In the higher level, the robust on-line model-based optimization algorithm using the distributional batch nonlinear model predictive control (NMPC), adapts the set-point of the supersaturation controller to counteract the effects of changing operation conditions. This is another interesting area for the future work.

# Appendix A

Table A1 Paracetamol crystallization model incidence matrix

| | | Differential Variables | | | | | | | Algebraic Variables | | | | | | | |
|---|---|---|---|---|---|---|---|---|---|---|---|---|---|---|---|---|
| | | $\mu_0$ | $\mu_1$ | $\mu_2$ | $\mu_3$ | $c$ | $T$ | $T_w$ | $c^{sat}$ | $S$ | $M_c$ | $B_{nuc}$ | $G$ | $S[1,0]$ | $A[2,0]$ | $V[3,0]$ |
| Algebraic Equations | 8 | | | | | | * | | * | | | | | | | |
| | 9 | | | | | * | | | * | * | | | | | | |
| | 10 | | | | * | | | | | | * | | | | | |
| | 11 | | | | | | | | | * | | * | | | | |
| | 12 | | | | | | | | | * | | | * | | | |
| | 13 | * | * | | | | | | | | | | | * | | |
| | 14 | * | | * | | | | | | | | | | | * | |
| | 15 | * | | | * | | | | | | | | | | | * |
| Differential Equations | 1 | * | | | | | | | | | | * | | | | |
| | 2 | * | * | | | | | | | | | | * | | | |
| | 3 | | * | * | | | | | | | | | * | | | |
| | 4 | | | * | * | | | | | | | | * | | | |
| | 5 | | | * | | * | | | | | | | * | | | |
| | 6 | | | | | | * | | | | | | | | | |
| | 7 | | | | | | | * | | | | | | | | |

# Appendix B

Table B1 KDP crystallization model incidence matrix

| | | Differential Variables | | | | | | | | Algebraic Variables | | | | | | | | | | |
|---|---|---|---|---|---|---|---|---|---|---|---|---|---|---|---|---|---|---|---|---|
| | | $\mu_{00}$ | $\mu_{10}$ | $\mu_{01}$ | $\mu_{20}$ | $\mu_{02}$ | $\mu_{11}$ | $\mu_{21}$ | $c$ | $T$ | $c^{sat}$ | $S$ | $B_{nuc}$ | $G_1$ | $G_2$ | $N_c$ | $M_c$ | $\overline{L}_1$ | $\overline{L}_2$ |
| Algebraic Equations | 9 | | | | | | | | | * | | | | | | | | | |
| | 10 | | | | | | | | | * | * | | | | | | | | |
| | 11 | | | | | | | | * | | * | * | | | | | | | |
| | 12 | | | | | | | | | | | * | * | | | | | | |
| | 13 | | | | | | | | | | | * | | * | | | | | |
| | 14 | | | | | | | | | | | * | | | * | | | | |
| | 15 | * | | | | | | | | | | | | | | * | | | |
| | 16 | | | | | | | * | | | | | | | | | * | | |
| | 17 | * | * | | | | | | | | | | | | | | | * | |
| | 18 | * | | * | | | | | | | | | | | | | | | * |
| Differential Equations | 1 | * | | | | | | | | | | | * | | | | | | |
| | 2 | | * | | | | | | | | | | | * | | | | | |
| | 3 | | | * | | | | | | | | | | | * | | | | |
| | 4 | | | | * | | | | | | | | | * | | | | | |
| | 5 | | | | | * | | | | | | | | | * | | | | |
| | 6 | | | | | | * | | | | | | | * | * | | | | |
| | 7 | | | | | | | * | | | | | | * | * | | | | |
| | 8 | | | | * | | * | | * | | | | | | | | | | |

# Appendix C

**Derivation of analytical CSD estimator for the one- and two-dimensional case**

This appendix shows the detailed derivation of the analytical CSD estimator for the one- and two-dimensional case as shown in Table 4.1.

Considering two growth directios with one characteristic length and width in a well-mixed crystallizer with supersaturation control and growth as the only dominating phenomenon, as well as assuming absence of nucleation, agglomeration and breakage, the population balance equation has the form:

$$\frac{\partial f_n\left(L_x,L_y,t\right)}{\partial t}+\frac{\partial G_x\left(L_x,t\right)\partial f_n\left(L_x,L_y,t\right)}{\partial L_x}+\frac{\partial G_y\left(L_y,t\right)\partial f_n\left(L_x,L_y,t\right)}{\partial L_y}=0 \tag{C1}$$

a) Size independent growth rate

In the case of the generic size independent growth rate, Equation (C1) can be rewritten in the form of:

$$\frac{\partial f_n}{\partial t}+G_x\frac{\partial f_n}{\partial L_x}+G_y\frac{\partial f_n}{\partial L_y}=0 \tag{C2}$$

The expression for size independent growth is given by:

$$G_x=k_{gx}S^{gx} \tag{C3}$$

$$G_y=k_{gy}S^{gy} \tag{C4}$$

The supersaturation can be assumed constant which is possible in a controlled crystallization and the supersaturation expression is given by:

$$S = c - c^{sat} \tag{C5}$$

Differentiating Equations (C3) and (C4) with respect to characteristic length and width, respectively gives:

$$\frac{dG_x}{dL_x} = 0 \tag{C6}$$

$$\frac{dG_y}{dL_y} = 0 \tag{C7}$$

Introduce $f_n\left(L_x, L_y, t\right) = f_n\left(L_x(Z), L_y(Z), t(Z)\right)$ and by applying the chain rules give:

$$\frac{dL_x}{dZ}\frac{\partial f_n}{\partial L_x} + \frac{dL_y}{dZ}\frac{\partial f_n}{\partial L_y} + \frac{dt}{dZ}\frac{\partial f_n}{\partial t} = \frac{df_n}{dZ} \tag{C8}$$

Comparing Equation (C8) and (C2), we have:

$$\frac{dt}{dZ} = 1 \tag{C9}$$

$$\frac{dL_x}{dZ} = G_x \tag{C10}$$

$$\frac{dL_y}{dZ} = G_y \tag{C11}$$

$$\frac{df_n}{dZ} = 0 \tag{C12}$$

Integrating Equation (C9) with limits:

$$dt = dZ \tag{C13}$$

$$\int_{t_0}^{t} dt = \int_{Z_0}^{Z} dZ \tag{C14}$$

$$\left(t - t_0\right) = \left(Z - Z_0\right) \tag{C15}$$

By assuming $t_0 = Z_0 = 0$, Equation (C15) can be simplified into:

$$t = Z \tag{C16}$$

Since $dt = dZ$, Equation (C10) becomes:

$$\frac{dL_x}{dt} = G_x \tag{C17}$$

Substitute Equation (C3) into (C17) gives:

$$\frac{dL_x}{dt} = k_{gx} S^{gx} \tag{C18}$$

Integrating Equation (C18) with limits:

$$dL_x = k_{gx} S^{gx} dt \tag{C19}$$

$$\int_{L_{x0}}^{L_x} dL_x = k_{gx} S^{gx} \int_{t_0}^{t} dt \tag{C20}$$

$$\left(L_x - L_{x0}\right) = k_{gx} S^{gx} \left(t - t_0\right) \tag{C21}$$

By assuming $t_0 = 0$, Equation (C21) can be simplified into:

$$\left(L_x - L_{x0}\right) = k_{gx} S^{gx} t \tag{C22}$$

Rearranging Equation (C22) gives:

$$L_x = L_{x0} + k_{gx} S^{gx} t \tag{C23}$$

Equation (C23) represents the final characteristic length which can be applied for the one- or two-dimensional case. A similar derivation is applied in order to obtain the analytical solution for the final characteristic width. Since $dt = dZ$, Equation (C11) becomes:

$$\frac{dL_y}{dt} = G_y \tag{C24}$$

Substituting Equation (C4) into (C24) gives:

$$\frac{dL_y}{dt} = k_{gy} S^{gy} \tag{C25}$$

Integrating Equation (C25) with limits:

$$dL_y = k_{gy} S^{gy} dt \tag{C26}$$

$$\int_{L_{y0}}^{L_y} dL_y = k_{gy} S^{gy} \int_{t_0}^{t} dt \tag{C27}$$

$$\left(L_y - L_{y0}\right) = k_{gy} S^{gy} \left(t - t_0\right) \tag{C28}$$

By assuming $t_0 = 0$, Equation (C28) can be simplified into:

$$\left(L_y - L_{y0}\right) = k_{gy} S^{gy} t \tag{C29}$$

Rearranging Equation (C29) gives:

$$L_y = L_{y0} + k_{gy} S^{gy} t \tag{C30}$$

Equation (C30) represents the final characteristic width for the two-dimensional case. In order to obtain the analytical solution for the crystal size distribution, since $dt = dZ$, Equation (C12) becomes:

$$\frac{df_n}{dt} = 0 \tag{C31}$$

Integrating Equation (C31) with limits:

$$\int_{f_{n0}}^{f_n} df_n = 0 \tag{C32}$$

$$\left(f_n - f_{n0}\right) = 0 \tag{C33}$$

$$f_n = f_{n0} \tag{C34}$$

Equation (34) represents the final crystal size distribution for the two- and one-dimensional case assuming size independent growth rates.

b) Size dependent growth rate $\left(\gamma_x = \gamma_y \neq 0; p_x = p_y \neq 1\right)$

Revisiting Equation (C1):

$$\frac{\partial f_n\left(L_x, L_y, t\right)}{\partial t} + \frac{\partial G_x\left(L_x, t\right)\partial f_n\left(L_x, L_y, t\right)}{\partial L_x} + \frac{\partial G_y\left(L_y, t\right)\partial f_n\left(L_x, L_y, t\right)}{\partial L_y} = 0 \tag{C1}$$

In the case of the generic size dependent growth rate $\left(\gamma_x = \gamma_y \neq 0; p_x = p_y \neq 1\right)$, Equation (C1) can be expanded and rewritten in the form:

$$\frac{\partial f_n}{\partial t} + f_n \frac{\partial G_x}{\partial L_x} + G_x \frac{\partial f_n}{\partial L_x} + f_n \frac{\partial G_y}{\partial L_y} + G_y \frac{\partial f_n}{\partial L_y} = 0 \tag{C35}$$

The expressions for the size dependent growth in the length and width direction are given by:

$$G_x = k_{gx} S^{gx} \left(1 + \gamma_x L_x\right)^{p_x} \tag{C36}$$

$$G_y = k_{gy} S^{gy} \left(1 + \gamma_y L_y\right)^{p_y} \tag{C37}$$

Differentiating Equations (C36) and (C37) with respect to characteristic length and width:

$$\frac{dG_x}{dL_x} = k_{gx} S^{gx} \gamma_x p_x \left(1 + \gamma_x L_x\right)^{p_x - 1} \tag{C38}$$

$$\frac{dG_y}{dL_y} = k_{gy} S^{gy} \gamma_y p_y \left(1 + \gamma_y L_y\right)^{p_y - 1} \tag{C39}$$

Introducing $f_n\left(L_x, L_y, t\right) = f_n\left(L_x(Z), L_y(Z), t(Z)\right)$ and by applying the chain rules give:

$$\frac{dL_x}{dZ}\frac{\partial f_n}{\partial L_x} + \frac{dL_y}{dZ}\frac{\partial f_n}{\partial L_y} + \frac{dt}{dZ}\frac{\partial f_n}{\partial t} = \frac{df_n}{dZ} \tag{C40}$$

Comparing Equation (C39) and (C35), we have:

$$\frac{dt}{dZ} = 1 \tag{C41}$$

$$\frac{dL_x}{dZ} = G_x \tag{C42}$$

$$\frac{dL_y}{dZ} = G_y \tag{C43}$$

$$\frac{df_n}{dZ} = -f_n \frac{\partial G_x}{\partial L_x} - f_n \frac{\partial G_y}{\partial L_y} \tag{C44}$$

Integrating Equation (C41) with limits:

$$dt = dZ \tag{C45}$$

$$\int_{t_0}^{t} dt = \int_{Z_0}^{Z} dZ \tag{C46}$$

$$\left(t - t_0\right) = \left(Z - Z_0\right) \tag{C47}$$

By assuming $t_0 = Z_0 = 0$, Equation (C44) can be simplified into:

$$t = Z \tag{C48}$$

Since $dt = dZ$, Equation (C42) becomes:

$$\frac{dL_x}{dt} = G_x \tag{C49}$$

Substituting Equation (C36) into (C49) gives:

$$\frac{dL_x}{dt} = k_{gx} S^{gx} \left(1 + \gamma_x L_x\right)^{p_x} \tag{C50}$$

Integrating Equation (C50) with limits:

$$\frac{dL_x}{\left(1 + \gamma_x L_x\right)^{p_x}} = k_{gx} S^{gx} dt \tag{C51}$$

$$\int_{L_{x0}}^{L_x} \frac{dL_x}{\left(1 + \gamma_x L_x\right)^{p_x}} = \int_{t_0}^{t} k_{gx} S^{gx} dt \tag{C52}$$

By assuming $t_0 = 0$, Equation (C52) can be simplified into:

$$\frac{1}{1-p_x}\left[\left(1+\gamma_x L_x\right)^{1-p_x} - \left(1+\gamma_x L_{x0}\right)^{1-p_x}\right] = k_{gx} S^{gx} \gamma_x t \tag{C53}$$

Rearranging Equation (C53) gives:

$$\left(1+\gamma_x L_x\right)^{1-p_x} - \left(1+\gamma_x L_{x0}\right)^{1-p_x} = k_{gx} S^{gx} \gamma_x t \left(1-p_x\right) \tag{C54}$$

$$\left(1+\gamma_x L_x\right)^{1-p_x} = \left(1+\gamma_x L_{x0}\right)^{1-p_x} + k_{gx} S^{gx} \gamma_x t \left(1-p_x\right) \tag{C55}$$

$$\left(1+\gamma_x L_x\right) = \left[\left(1+\gamma_x L_{x0}\right)^{1-p_x} + k_{gx} S^{gx} \gamma_x t \left(1-p_x\right)\right]^{\frac{1}{1-p_x}} \tag{C56}$$

$$\gamma_x L_x = \left[\left(1+\gamma_x L_{x0}\right)^{1-p_x} + k_{gx} S^{gx} \gamma_x t \left(1-p_x\right)\right]^{\frac{1}{1-p_x}} - 1 \tag{C57}$$

$$L_x = \frac{\left[\left(1+\gamma_x L_{x0}\right)^{1-p_x} + k_{gx} S^{gx} \gamma_x t \left(1-p_x\right)\right]^{\frac{1}{1-p_x}} - 1}{\gamma_x} \tag{C58}$$

Equation (C58) represents the analytical solution for the final characteristic length which can be applied for the two- and the one-dimensional case. In order to obtain the analytical solution for final characteristic width, similarly, since $dt = dZ$, Equation (C43) becomes:

$$\frac{dL_y}{dt} = G_y \tag{C59}$$

Substituting Equation (C37) into (C59) gives:

$$\frac{dL_y}{dt} = k_{gy} S^{gy} \left(1+\gamma_y L_y\right)^{p_y} \tag{C60}$$

Integrating Equation (C60) with limits:

$$\frac{dL_y}{\left(1+\gamma_y L_y\right)^{p_y}} = k_{gy} S^{gy} dt \tag{C61}$$

$$\int_{L_{y0}}^{L_y} \frac{dL_y}{\left(1+\gamma_y L_y\right)^{p_y}} = \int_{t_0}^{t} k_{gy} S^{gy} dt \tag{C62}$$

By assuming $t_0 = 0$, Equation (C62) can be simplified into:

$$\frac{1}{1-p_y}\left[\left(1+\gamma_y L_y\right)^{1-p_y} - \left(1+\gamma_y L_{y0}\right)^{1-p_y}\right] = k_{gy} S^{gy} \gamma_y t \tag{C63}$$

Rearranging Equation (C63):

$$\left(1+\gamma_y L_y\right)^{1-p_y} - \left(1+\gamma_y L_{y0}\right)^{1-p_y} = k_{gy} S^{gy} \gamma_y t \left(1-p_y\right) \tag{C64}$$

$$\left(1+\gamma_y L_y\right)^{1-p_y} = \left(1+\gamma_y L_{y0}\right)^{1-p_y} + k_{gy} S^{gy} \gamma_y t \left(1-p_y\right) \tag{C65}$$

$$\left(1+\gamma_y L_y\right) = \left[\left(1+\gamma_y L_{y0}\right)^{1-p_y} + k_{gy} S^{gy} \gamma_y t \left(1-p_y\right)\right]^{\frac{1}{1-p_y}} \tag{C66}$$

$$\gamma_y L_y = \left[\left(1+\gamma_y L_{y0}\right)^{1-p_y} + k_{gy} S^{gy} \gamma_y t \left(1-p_y\right)\right]^{\frac{1}{1-p_y}} - 1 \tag{C67}$$

$$L_y = \frac{\left[\left(1+\gamma_y L_{y0}\right)^{1-p_y} + k_{gy} S^{gy} \gamma_y t \left(1-p_y\right)\right]^{\frac{1}{1-p_y}} - 1}{\gamma_y} \tag{C68}$$

Equation (C68) is the analytical solution for the final characteristic width in the case of the two-dimensional case only. The next task is to obtain the analytical solution for the crystal size distribution. Since $dt = dZ$, Equation (C44) becomes:

$$\frac{df_n}{dt} = -f_n \frac{\partial G_x}{\partial L_x} - f_n \frac{\partial G_y}{\partial L_y} \tag{C69}$$

Substituting Equations (C38) and (C39) into (C69) yields:

$$\frac{df_n}{dt} = -f_n k_{gx} S^{gx} \gamma_x p_x \left(1+\gamma_x L_x\right)^{p_x - 1} - f_n k_{gy} S^{gy} \gamma_y p_y \left(1+\gamma_y L_y\right)^{p_y - 1} \tag{C70}$$

Rearranging and integrating Equation (C70) with limits:

$$\frac{df_n}{f_n} = -k_{gx}S^{gx}\gamma_x p_x\left(1+\gamma_x L_x\right)^{p_x-1}dt - k_{gy}S^{gy}\gamma_y p_y\left(1+\gamma_y L_y\right)^{p_y-1}dt \tag{C71}$$

$$\int_{f_{n0}}^{f_n}\frac{df_n}{f_n} = \int_{t_0}^{t} -k_{gx}S^{gx}\gamma_x p_x\left(1+\gamma_x L_x\right)^{p_x-1}dt - \int_{t_0}^{t} k_{gy}S^{gy}\gamma_y p_y\left(1+\gamma_y L_y\right)^{p_y-1}dt \tag{C72}$$

$$\int_{f_{n0}}^{f_n}\frac{df_n}{f_n} = \int_{t_0}^{t}\frac{-k_{gx}S^{gx}\gamma_x p_x}{\left(1+\gamma_x L_x\right)^{1-p_x}}dt - \int_{t_0}^{t}\frac{k_{gy}S^{gy}\gamma_y p_y}{\left(1+\gamma_y L_y\right)^{1-p_y}}dt \tag{C73}$$

Substituting Equations (C55) and (C66) into (C73) gives:

$$\int_{f_{n0}}^{f_n}\frac{df_n}{f_n} = \int_{t_0}^{t}\frac{-k_{gx}S^{gx}\gamma_x p_x}{\left(1+\gamma_x L_{x0}\right)^{1-p_x}+k_{gx}S^{gx}\gamma_x t\left(1-p_x\right)}dt - \int_{t_0}^{t}\frac{k_{gy}S^{gy}\gamma_y p_y}{\left(1+\gamma_y L_{y0}\right)^{1-p_y}+k_{gy}S^{gy}\gamma_y t\left(1-p_y\right)}dt \tag{C74}$$

By integrating Equation (C74):

$$\ln\left(\frac{f_n}{f_{n0}}\right) = \frac{-k_{gx}S^{gx}\gamma_x p_x}{k_{gx}S^{gx}\gamma_x\left(1-p_x\right)}\ln\left[\frac{\left(1+\gamma_x L_{x0}\right)^{1-p_x}+k_{gx}S^{gx}\gamma_x t\left(1-p_x\right)}{\left(1+\gamma_x L_{x0}\right)^{1-p_x}}\right]$$

$$-\frac{k_{gy}S^{gy}\gamma_y p_y}{k_{gy}S^{gy}\gamma_y\left(1-p_y\right)}\ln\left[\frac{\left(1+\gamma_y L_{y0}\right)^{1-p_y}+k_{gy}S^{gy}\gamma_y t\left(1-p_y\right)}{\left(1+\gamma_y L_{y0}\right)^{1-p_y}}\right] \tag{C75}$$

Simplifying Equation (C75) yields:

$$\ln\left(\frac{f_n}{f_{n0}}\right) = \frac{-p_x}{\left(1-p_x\right)}\ln\left[\frac{\left(1+\gamma_x L_{x0}\right)^{1-p_x}+k_{gx}S^{gx}\gamma_x t\left(1-p_x\right)}{\left(1+\gamma_x L_{x0}\right)^{1-p_x}}\right]$$

$$-\frac{p_y}{\left(1-p_y\right)}\ln\left[\frac{\left(1+\gamma_y L_{y0}\right)^{1-p_y}+k_{gy}S^{gy}\gamma_y t\left(1-p_y\right)}{\left(1+\gamma_y L_{y0}\right)^{1-p_y}}\right] \tag{C76}$$

Rearranging Equation (C76):

$$\frac{f_n}{f_{n0}} = \left[\frac{\left(1+\gamma_x L_{x0}\right)^{1-p_x}+k_{gx}S^{gx}\gamma_x t\left(1-p_x\right)}{\left(1+\gamma_x L_{x0}\right)^{1-p_x}}\right]^{\frac{p_x}{(p_x-1)}} + \left[\frac{\left(1+\gamma_y L_{y0}\right)^{1-p_y}+k_{gy}S^{gy}\gamma_y t\left(1-p_y\right)}{\left(1+\gamma_y L_{y0}\right)^{1-p_y}}\right]^{\frac{p_y}{(p_y-1)}}$$

(C77)

Rearranging Equation (C77) yields:

$$f_n = f_{n0}\left[\frac{\left(1+\gamma_x L_{x0}\right)^{1-p_x} + k_{gx} S^{gx} \gamma_x t\left(1-p_x\right)}{\left(1+\gamma_x L_{x0}\right)^{1-p_x}}\right]^{\frac{p_x}{(p_x-1)}}$$

$$+ f_{n0}\left[\frac{\left(1+\gamma_y L_{y0}\right)^{1-p_y} + k_{gy} S^{gy} \gamma_y t\left(1-p_y\right)}{\left(1+\gamma_y L_{y0}\right)^{1-p_y}}\right]^{\frac{p_y}{(p_y-1)}} \quad \text{(C78)}$$

Equation (C78) represents the analytical solution for the final crystal size distribution for two-dimensional size dependent growth $\left(\gamma_x = \gamma_y \neq 0; p_x = p_y \neq 1\right)$. In order to obtain the analytical solution for the one-dimensional final crystal size distribution, the width direction term can be neglected and thus, Equation (C78) becomes:

$$f_n = f_{n0}\left[\frac{\left(1+\gamma_x L_{x0}\right)^{1-p_x} + k_{gx} S^{gx} \gamma_x t\left(1-p_x\right)}{\left(1+\gamma_x L_{x0}\right)^{1-p_x}}\right]^{\frac{p_x}{(p_x-1)}} \quad \text{(C79)}$$

Equation (C79) represents the analytical solution for the final crystal size distribution for one-dimensional size dependent growth $\left(\gamma_x = \gamma_y \neq 0; p_x = p_y \neq 1\right)$.

c) Size dependent growth rate $\left(\gamma_x = \gamma_y \neq 0; p_x = p_y = 1\right)$

Revisiting Equation (C1):

$$\frac{\partial f_n\left(L_x, L_y, t\right)}{\partial t} + \frac{\partial G_x\left(L_x, t\right) \partial f_n\left(L_x, L_y, t\right)}{\partial L_x} + \frac{\partial G_y\left(L_y, t\right) \partial f_n\left(L_x, L_y, t\right)}{\partial L_y} = 0 \quad \text{(C1)}$$

In the case of a generic size dependent growth rate $\left(\gamma_x = \gamma_y \neq 0; p_x = p_y = 1\right)$, Equation (C1) can be expanded and rewritten in the form:

$$\frac{\partial f_n}{\partial t} + f_n \frac{\partial G_x}{\partial L_x} + G_x \frac{\partial f_n}{\partial L_x} + f_n \frac{\partial G_y}{\partial L_y} + G_y \frac{\partial f_n}{\partial L_y} = 0 \tag{C80}$$

The expressions for the size dependent growth in the length and width direction are given by:

$$G_x = k_{gx} S^{gx} \left(1 + \gamma_x L_x\right) \tag{C81}$$

$$G_y = k_{gy} S^{gy} \left(1 + \gamma_y L_y\right) \tag{C82}$$

Differentiating Equations (C81) and (C82) with respect to characteristic length and width yields:

$$\frac{dG_x}{dL_x} = k_{gx} S^{gx} \gamma_x \tag{C83}$$

$$\frac{dG_y}{dL_y} = k_{gy} S^{gy} \gamma_y \tag{C84}$$

Introducing $f_n\left(L_x, L_y, t\right) = f_n\left(L_x(Z), L_y(Z), t(Z)\right)$, and by applying the chain rules gives:

$$\frac{dL_x}{dZ}\frac{\partial f_n}{\partial L_x} + \frac{dL_y}{dZ}\frac{\partial f_n}{\partial L_y} + \frac{dt}{dZ}\frac{\partial f_n}{\partial t} = \frac{df_n}{dZ} \tag{C85}$$

Comparing Equation (C85) and (C80), we have:

$$\frac{dt}{dZ} = 1 \tag{C86}$$

$$\frac{dL_x}{dZ} = G_x \tag{C87}$$

$$\frac{dL_y}{dZ} = G_y \tag{C88}$$

$$\frac{df_n}{dZ} = -f_n \frac{\partial G_x}{\partial L_x} - f_n \frac{\partial G_y}{\partial L_y} \tag{C89}$$

Integrating Equation (C86) with limits:

$$dt = dZ \tag{C90}$$

$$\int_{t_0}^{t} dt = \int_{Z_0}^{Z} dZ \tag{C91}$$

$$\left(t - t_0\right) = \left(Z - Z_0\right) \tag{C92}$$

By assuming $t_0 = Z_0 = 0$, Equation (C92) can be simplified into:

$$t = Z \tag{C93}$$

Since $dt = dZ$, Equation (C87) becomes:

$$\frac{dL_x}{dt} = G_x \tag{C94}$$

Substituting Equation (C81) into (C94) gives:

$$\frac{dL_x}{dt} = k_{gx} S^{gx} \left(1 + \gamma_x L_x\right) \tag{C95}$$

Integrating Equation (C95) with limits:

$$\frac{dL_x}{\left(1 + \gamma_x L_x\right)} = k_{gx} S^{gx} dt \tag{C96}$$

$$\int_{L_{x0}}^{L_x} \frac{dL_x}{\left(1 + \gamma_x L_x\right)} = k_{gx} S^{gx} \int_{t_0}^{t} dt \tag{C97}$$

By assuming $t_0 = 0$, Equation (C97) can be simplified into:

$$\frac{1}{\gamma_x} \ln \frac{\left(1 + \gamma_x L_x\right)}{\left(1 + \gamma_x L_{x0}\right)} = k_{gx} S^{gx} t \tag{C98}$$

Rearranging Equation (C98) yields:

$$\ln \frac{\left(1 + \gamma_x L_x\right)}{\left(1 + \gamma_x L_{x0}\right)} = k_{gx} S^{gx} \gamma_x t \tag{C99}$$

Equation (99) is then rearranged in the form of:

$$\frac{\left(1+\gamma_x L_x\right)}{\left(1+\gamma_x L_{x0}\right)} = \exp^{k_{gx} S^{gx} \gamma_x t} \tag{C100}$$

Rearranging Equation (C100) becomes:

$$1+\gamma_x L_x = \left(1+\gamma_x L_{x0}\right) \exp^{k_{gx} S^{gx} \gamma_x t} \tag{C101}$$

$$L_x = \frac{\left(1+\gamma_x L_{x0}\right) \exp^{k_{gx} S^{gx} \gamma_x t} - 1}{\gamma_x} \tag{C102}$$

Equation (C102) represents the analytical solution for the final characteristic length which can be applied for the two- and the one-dimensional case. In order to obtain the analytical solution for final characteristic width, similarly, since $dt = dZ$, Equation (C88) becomes:

$$\frac{dL_y}{dt} = G_y \tag{C103}$$

Substituting Equation (C82) into (C103) gives:

$$\frac{dL_y}{dt} = k_{gy} S^{gy} \left(1+\gamma_y L_y\right) \tag{C104}$$

Integrating Equation (C104) with limits:

$$\frac{dL_y}{\left(1+\gamma_y L_y\right)} = k_{gy} S^{gy} dt \tag{C105}$$

$$\int_{L_{y0}}^{L_y} \frac{dL_y}{\left(1+\gamma_y L_y\right)} = k_{gy} S^{gy} \int_{t_0}^{t} dt \tag{C106}$$

By assuming $t_0 = 0$, Equation (C106) can be simplified into:

$$\frac{1}{\gamma_y} \ln \frac{\left(1+\gamma_y L_y\right)}{\left(1+\gamma_y L_{y0}\right)} = k_{gy} S^{gy} t \tag{C107}$$

Rearranging Equation (C107) yields:

$$\ln \frac{\left(1+\gamma_y L_y\right)}{\left(1+\gamma_y L_{y0}\right)} = k_{gy} S^{gy} \gamma_y t \tag{C108}$$

Equation (108) is then rearranged into the form:

$$\frac{\left(1+\gamma_y L_y\right)}{\left(1+\gamma_y L_{y0}\right)} = \exp^{k_{gy} S^{gy} \gamma_y t} \tag{C109}$$

Rearranging Equation (C109) becomes:

$$1+\gamma_y L_y = \left(1+\gamma_y L_{y0}\right) \exp^{k_{gy} S^{gy} \gamma_y t} \tag{C110}$$

$$L_y = \frac{\left(1+\gamma_y L_{y0}\right) \exp^{k_{gy} S^{gy} \gamma_y t} - 1}{\gamma_y} \tag{C111}$$

Equation (C111) is the analytical solution for final characteristic width in the two-dimensionalc case only. The next task is to obtain the analytical solution for crystal size distribution. Since $dt = dZ$ , Equation (C89) becomes:

$$\frac{df_n}{dt} = -f_n \frac{\partial G_x}{\partial L_x} - f_n \frac{\partial G_y}{\partial L_y} \tag{C112}$$

Substituting Equations (C83) and (C84) into (C112) yields:

$$\frac{df_n}{dt} = -f_n k_{gx} S^{gx} \gamma_x - f_n k_{gy} S^{gy} \gamma_y \tag{C113}$$

Rearranging and integrating Equation (C113) with limits:

$$\frac{df_n}{f_n} = -k_{gx} S^{gx} \gamma_x dt - k_{gy} S^{gy} \gamma_y dt \tag{C114}$$

$$\int_{f_{n0}}^{f_n} \frac{df_n}{f_n} = -k_{gx} S^{gx} \gamma_x \int_{t_0}^{t} dt - k_{gy} S^{gy} \gamma_y \int_{t_0}^{t} dt \tag{C115}$$

$$\ln \frac{f_n}{f_{n0}} = -k_{gx} S^{gx} \gamma_x \left(t - t_0\right) - k_{gy} S^{gy} \gamma_y \left(t - t_0\right) \tag{C116}$$

By assuming $t_0 = 0$, Equation (C106) can be simplified into:

$$\ln \frac{f_n}{f_{n0}} = -k_{gx} S^{gx} \gamma_x t - k_{gy} S^{gy} \gamma_y t \tag{C117}$$

Based on Equation (C117), the analytical solution for crystal size distribution can be obtained by:

$$\frac{f_n}{f_{n0}} = \exp^{-\left(k_{gx} S^{gx} \gamma_x t + k_{gy} S^{gy} \gamma_y t\right)} \tag{C118}$$

Rearranging Equation (C118):

$$f_n = f_{n0} \exp^{-\left(k_{gx} S^{gx} \gamma_x t + k_{gy} S^{gy} \gamma_y t\right)} \tag{C119}$$

Equation (C119) represents the analytical solution for final crystal size distribution in the two-dimensional case with size dependent growth rates $\left(\gamma_x = \gamma_y \neq 0; p_x = p_y = 1\right)$. In order to obtain the analytical solution for the one-dimensional final crystal size distribution, the width direction term can be neglected and thus, Equation (C119) becomes:

$$f_n = f_{n0} \exp^{-k_{gx} S^{gx} \gamma_x t} \tag{C120}$$

Equation (C120) represents the analytical solution for the final crystal size distribution for the one-dimensional case with size dependent growth $\left(\gamma_x = \gamma_y \neq 0; p_x = p_y = 1\right)$.

# Appendix D

**Method comparison for screening influential factors between SRC and Morris screening based on the two-dimensional data**

Table D1 Method comparison for screening influential factors based on the two-dimensional CSD data taken at point p1) in Figure 5.13

| | Morris screening method | | | SRC method | |
|---|---|---|---|---|---|
| Ranking | Parameters | $\mu_j$ | $\sigma_j$ | Parameters | $\beta_{jk}$ |
| 1 | $b$ | -0.8563 | 0.6943 | $b$ | -0.9032 |
| 2 | $g_x$ | 0.2561 | 0.1856 | $g_x$ | 0.2312 |
| 3 | $g_y$ | 0.2043 | 0.1264 | $g_y$ | 0.1932 |
| 4 | $\gamma_x$ | -0.1201 | 0.0043 | $\gamma_x$ | -0.1671 |
| 5 | $\gamma_y$ | -0.1143 | 0.0028 | $\gamma_y$ | -0.0921 |
| 6 | $k_b$ | 0.0495 | 0.0009 | $k_b$ | 0.0851 |
| 7 | $k_{gx}$ | -0.0392 | 0.0005 | $k_{gx}$ | -0.0212 |
| 8 | $k_{gy}$ | -0.0065 | 0.0001 | $k_{gy}$ | -0.0128 |

Table D2 Method comparisons for screening influential factors based on the two-dimensional CSD data taken at point p2) in Figure 5.13

| | Morris sampling method | | | SRC method | |
|---|---|---|---|---|---|
| Ranking | Parameters | $\mu_j$ | $\sigma_j$ | Parameters | $\beta_{jk}$ |
| 1 | $g_x$ | 0.5921 | 0.5296 | $g_x$ | 0.6641 |
| 2 | $g_y$ | 0.5843 | 0.4965 | $g_y$ | 0.5395 |
| 3 | $\gamma_x$ | -0.3094 | 0.2538 | $\gamma_x$ | -0.3781 |
| 4 | $\gamma_y$ | -0.2895 | 0.1932 | $\gamma_y$ | -0.3021 |
| 5 | $k_{gx}$ | 0.1153 | 0.0054 | $k_{gx}$ | 0.1643 |
| 6 | $k_{gy}$ | 0.0843 | 0.0010 | $k_{gy}$ | 0.1296 |
| 7 | $b$ | -0.0201 | 0.0002 | $b$ | -0.0403 |
| 8 | $k_b$ | -0.0184 | 0.0001 | $k_b$ | -0.0276 |

# Nomenclature

| | |
|---|---|
| $A[2,0]$ | mean crystal area ($cm^2$) |
| $A_1$ | crystallizer's internal area ($cm^2$) |
| $A_2$ | crystallizer's external area ($cm^2$) |
| $A_c$ | total area of particles ($cm^2$) |
| $A_{pn}$ | empirical coefficient in primary nucleation |
| $ab$ | production-reduction order |
| $a_i$ | tailor development coefficient |
| $a_{i1}$ | polynomial coefficient for saturation concentration |
| $a_{i2}$ | polynomial coefficient for metastable concentration |
| $a_{i3}$ | polynomial coefficient for heat of crystallization |
| $a_{xi}$ | tailor development coefficient |
| $B$ | birth rate (number of particles/$cm^3$.min) |
| $B_{agg}$ | birth rate due to agglomeration (number of particles/$cm^3$.min) |
| $B_{br}$ | birth rate due to breakage (number of particles/$cm^3$.min) |
| $B_{nuc}$ | birth rate due to nucleation (number of particles/$cm^3$.min) |
| $B_{n,1}$ | primary nucleation (number of particles/$cm^3$.min) |
| $B_{n,2}$ | secondary nucleation (number of particles/$cm^3$.min) |
| $B_{pn}$ | empirical coefficient in primary nucleation |
| $b$ | nucleation order |
| $b_i$ | coefficients of the response model |
| $b_{i1}$ | polynomial coefficient for saturation concentration |
| $b_{i2}$ | polynomial coefficient for metastable concentration |
| $b_{i3}$ | polynomial coefficient for heat of crystallization |
| $b_{xi}$ | tailor development coefficient |
| $c$ | solute concentration (g solute/g solvent) |
| $c^{sat}$ | saturation concentration (g solute/g solvent) |
| $c^{met}$ | metastable concentration (g solute/g solvent) |
| $c_i$ | tailor development coefficient |
| $c_{i1}$ | polynomial coefficient for saturation concentration |
| $c_{i2}$ | polynomial coefficient for metastable concentration |
| $c_{i3}$ | polynomial coefficient for heat of crystallization |
| $c_p$ | heat capacity (J/g.°C) |
| $c_{pw}$ | water heat capacity (J/g.°C) |

| | |
|---|---|
| $c_{yj}$ | tailor development coefficient |
| $D$ | diffusivity of the solute ($cm^2$/min) |
| $Diam$ | stirrer diameter (cm) |
| $Diam_T$ | tank diameter (cm) |
| $D[4,3]$ | mean size diameter (μm) |
| $D_{br}$ | death rate due to breakage (number of particles/$cm^3$.min) |
| $d_i$ | tailor development coefficient |
| $d_{i1}$ | polynomial coefficient for saturation concentration |
| $d_{i2}$ | polynomial coefficient for metastable concentration |
| $d_{i3}$ | polynomial coefficient for heat of crystallization |
| $d_{yj}$ | tailor development coefficient |
| $F_{obj}$ | objective function |
| $F_{win}$ | cooling water flow rate ($cm^3$/min) |
| $f$ | relative shape function of crystals |
| $f_{ij}^{I}$ | inlet crystal number flow in the length direction |
| $f_{ij}^{I'}$ | inlet crystal number flow in the width direction |
| $f_{ij}^{O}$ | outlet crystal number flow in the length direction |
| $f_{ij}^{O'}$ | outlet crystal number flow in the width direction |
| $f_n$ | final population density function (number of particles/μm) |
| $f_{n0}$ | initial population density function (number of particles/μm) |
| $G_x$ | crystal growth rate in length direction (μm /sec) |
| $G_y$ | crystal growth rate in width direction (μm /sec) |
| $g_x$ | growth order in length direction |
| $g_y$ | growth order in width direction |
| $j$ | mass order at nucleation |
| $k$ | number of considered variables (factors) |
| $k_a^{'}$ | agglomeration rate constant in the diffusional growth regime (min) |
| $k_{ab}$ | kinetic coefficient for production-reduction (number of particles/$cm^3$. $cm^2$.min.$(g/cm^3)^k(rpm)^{ab}$) |
| $k_b$ | kinetic coefficient for nucleation (number of particles/$cm^3$.min.$(g/cm^3)^j(rpm)^p$) |
| $k_{b0}$ | frequency factor of nucleation rate |
| $k_d$ | mass transfer coefficient (cm/min) |
| $k_{gx}$ | kinetic coefficient for crystal growth in length direction (μm /sec) |
| $k_{g0}$ | frequency factor of crystal growth rate |
| $k_{gy}$ | kinetic coefficient for crystal growth in width direction (μm /sec) |

| | |
|---|---|
| $k_A$ | crystal shape factor |
| $k_L$ | crystal shape factor |
| $k_{pr}$ | mass order at production-reduction |
| $k_r$ | surface shape factor |
| $k_v$ | crystal shape factor |
| $L_x$ | length of crystal particles (μm) |
| $\overline{L}_x$ | average length of crystal particles (μm) |
| $L_{x0}$ | initial length of crystal particles (μm) |
| $L_y$ | width of crystal particles (μm) |
| $\overline{L}_y$ | average width of crystal particles (μm) |
| $L_{y0}$ | initial width of crystal particles (μm) |
| $L_c$ | total length of crystal particles (μm) |
| $MM$ | molecular weight of the crystal (kg/mol) |
| $M_c$ | total crystal mass (g) |
| $m$ | molal concentration of solute (moles solute/g solvent) |
| $m^{sat}$ | molal concentration of solute at saturated solution (moles solute/g solvent) |
| $m_w$ | mass of solvent (g) |
| $N_c$ | total number of particles (number of particles) |
| $N$ | number of classes |
| $N_i$ | number of crystals per unit volume of suspension for class *i* (number of particles/cm$^3$) |
| $N_{ij}$ | number of crystals per unit volume of suspension for class *i* and *j* (number of particles/cm$^3$) |
| $N_{rpm}$ | agitation rate (rpm) |
| $p$ | agitation order at nucleation |
| $p_x$ | size dependent growth constant for length direction |
| $p_y$ | size dependent growth constant for width direction |
| $q$ | agitation order at crystal growth |
| $R^2$ | regression of the polynomial model |
| $R$ | ideal gas constant (J/mol.K) |
| $r$ | agitation order at production-reduction |
| $r(l)$ | intrinsic rate of agglomeration of rank *l* (1/m$^3$s) |
| $S$ | normal supersaturation (g solute/g solvent) |
| $S_{sp}$ | Supersaturation set point (g solute/g solvent) |
| $S[1,0]$ | mean crystal size (μm) |
| $S_{xi}$ | mean size of class *i* (μm) |
| $S_{yj}$ | mean size of class *j* (μm) |
| $T$ | solution temperature (°C) |

| | |
|---|---|
| $T_{ex}$ | exterior temperature (°C) |
| $T_w$ | cooling water temperature (°C) |
| $T_{win}$ | inlet cooling water temperature (°C) |
| $t_c$ | total crystallization time (sec) |
| $U_1$ | heat transfer coefficient for internal crystallizer (J/°C.min.cm$^2$) |
| $U_2$ | heat transfer coefficient for external crystallizer (J/°C.min.cm$^2$) |
| $V$ | solution volume (cm$^3$) |
| $V[3,0]$ | mean crystal volume (cm$^3$) |
| $V_c$ | crystal volume (cm$^3$) |
| $V_w$ | cooling water volume (cm$^3$) |
| $v$ | kinematic viscosity (m$^2$/s) |
| $v_{est(l,i)}$ | stoichiometric coefficient of class *i* in agglomeration of number *l* |
| $x$ | mole fraction of solute |
| $x^{sat}$ | mole fraction of solute at saturated solution |

Greek letters

| | |
|---|---|
| $\alpha$ | production-reduction rate (number of particles/cm$^3$.min) |
| $\mu_{00}$ | zero$^{th}$ moment for two-dimensional PBE |
| $\mu_0$ | zero$^{th}$ moment for one-dimensional PBE |
| $\mu_{mn}$ | $m^{th}$ and $n^{th}$ moment for two-dimensional PBE |
| $\mu_m$ | $m^{th}$ for one-dimensional PBE |
| $\Delta Cl_i$ | extent of $i^{th}$ classes (μm) |
| $\Delta Cl_j$ | extent of $j^{th}$ classes (μm) |
| $\Delta E_b$ | activation energy for nucleation rate |
| $\Delta E_g$ | activation energy for crystal growth rate |
| $\Delta H_c$ | heat of crystallization (J/g) |
| $\Delta c$ | concentration difference (g solute/g solvent) |
| $\sigma$ | relative supersaturation |
| $\sigma_x$ | standard deviation for length direction |
| $\sigma_y$ | standard deviation for width direction |
| $\zeta$ | activity coefficient |
| $\rho_c$ | crystal density (g/cm$^3$) |
| $\rho_w$ | water density (g/cm$^3$) |
| $\gamma_x$ | size dependent growth constant for length direction |
| $\gamma_y$ | size dependent growth constant for width direction |
| $\eta_r$ | effectiveness factor |
| $\varepsilon$ | power dissipation per unit of mass (W.m$^2$/kg.s$^3$) |
| $\lambda_e$ | Lagrangian microscale (m) |

# Abbreviation

| | |
|---|---|
| AE | Algebraic equation |
| ANOVA | Analysis of variance |
| ATR-FTIR | Attenuated total reflectance fourier transform infrared |
| BDF | Backward differentiation formulas |
| CCD | Central composite design |
| CSD | Crystal size distribution |
| DoE | Design of experiments |
| DOF | Degree of freedom |
| EE | Elementary effect |
| FBRM | Focused beam reflectance measurement |
| GMoP | Good modelling practice |
| ICAS-MoT | Integrated computer-aided system-Modelling testbed |
| ICAS-PAT | Integrated computer-aided system-Process analytical technology |
| KDP | Potassium dihydrogen phosphate |
| LHS | Latin hypercube sampling |
| MPC | Model predictive control |
| NMPC | Nonlinear model predictive control |
| ODE | Ordinary differential equation |
| PAT | Process analytical technology |
| PBE | Population balance equation |
| PID | Proportional-integral-derivative |
| PDE | Partial differential equation |
| RF | Response function |
| RSM | Response surface methodology |
| SRC | Standardized regression coefficient |
| SQP | Sequential quadratic programming |

# References


Aamir, E. (2010). Population balance model-based optimal control of batch crystallization processes for systematic crystal size distribution design. PhD thesis, Department of Chemical Engineering, Loughborough University, United Kingdom.

Aamir, E., Nagy, Z.K., & Rielly, C.D. (2010). Optimal seed recipe design for crystal size distribution control for batch cooling crystallization processes. *Chemical Engineering Science, 65,* 3602-3614.

Aamir, E., Nagy, Z.K., Rielly, C.D., Kleinert, T., & Judat, B. (2009). Combined quadrature method of moments and method of characteristics approach for efficient solution of population balance models for dynamic modeling and crystal size distribution control of crystallization processes. *Industrial and Engineering Chemistry Research, 48,* 8575-8584.

Abbas, A. & Romagnoli, J.A. (2007). Multiscale modeling, simulation and validation of batch cooling crystallization. *Separation and Purification Technology, 53,* 153-163.

Abildskov, J. (2005). Solubility and related properties of large complex chemicals. *DECHEMA Chemistry Data Ser., Part 2,* 15-II, DECHEMA, Frankfurt am Main.

Box, G.E.P. & Hunter, J.S. (1957). Multi-factor experimental design for exploring response surfaces. *The Annals of Mathematical Statistics, 28,* 195-241.

Braatz, R.D. (2002). Advanced control of crystallization processes. *Annual Reviews in Control,* 26, 87-99.

Briesen, H. (2006). Simulation of crystal size and shape by means of a reduced two-dimensional population balance model. *Chemical Engineering Science, 61,* 104-112.

Cariboni, J., Gatelli, D., Liska, R. & Saltelli, A. (2007). The role of sensitivity analysis in ecological modelling. *Ecological Modelling, 203,* 167-182.

Campolongo, F., & Saltelli, A. (1997). Sensitivity analysis of an environmental model: an application of different analysis methods. *Reliability Engineering and System Safety, 57,* 49-69.

Choong, K.L., & Smith, R. (2004). Optimization of batch cooling crystallization. *Chemical Engineering Science, 59,* 313-327.

Costa, C.B.B., Maciel, M.R.W., & Filho, R.M. (2006). Considerations on the crystallization modeling: Population balance solution. *Computers and Chemical Engineering, 31,* 206-218.

Costa, C.B.B., da Costa, A.C., & Filho, R.M. (2005). Mathematical modeling and optimal control strategy development for an adipic acid crystallization process. *Chemical Engineering and Processing, 44,* 737-753.

Farrell, R.J. & Tsai, Y. (1994). Modeling, simulation and kinetic parameter estimation in batch crystallization processes. *American Institute of Chemical Engineers Journal, 40(4),* 586-593.

Flores-Alsina, X., Rodriguez-Roda, I., Sin, G., & Gernaey, K.V. (2009). Uncertainty and sensitivity analysis of control strategies using the benchmark simulation model No1 (BSM1). *Water Science & Technology, 59(3),* 491-499.

Fujiwara, M., Nagy, Z.K., Chew, J.W., & Braatz, R.D. (2005). First-principles and direct

design approaches for the control of pharmaceutical crystallization. *Journal of Process Control, 15,* 493-504.

Fujiwara, M., Chow, P.S., Ma, D.L., & Braatz, R.D. (2002). Paracetamol crystallization using laser backscattering and ATR-FTIR spectroscopy: metastability, agglomeration, and control. *Crystal Growth & Design, 2(5),* 363-370.

Gani, R., Muro-Suñé, N., Sales-Cruz, M., Leibovici, C., & O'Connell, J.P. (2006). Mathematical and numerical analysis of classes of property models. *Fluid Phase Equilibria, 250,* 1-32.

Garcia, E., Veesler, S., Boistelle, R., & Hoff, C. (1999). Crystallization and dissolution of pharmaceutical compounds - An experimental approach. *Journal of Crystal Growth, 198/199,* 1360-1364.

Gimbun, J., Nagy, Z.K., & Rielly, C.D. (2009). Simultaneous quadrature method of moments for the solution of population balance equations, using a differential algebraic equation framework. *Industrial and Engineering Chemistry Research, 48,* 7798-7812.

Gunawan, R., Fusman, I., & Braatz, R.D. (2004). High resolution algorithms for multidimensional population balance equations. *American Institute of Chemical Engineers Journal, 50(11),* 2738-2749.

Gunawan, R., Ma, D.L., Fujiwara, M., & Braatz, R.D. (2002). Identification of kinetic parameters in multidimensional crystallization processes. *International Journal of Modern Physics, 16(1&2),* 367-374.

Haskin, F.E., Staple, B.D., & Ding, C. (1996). Efficient uncertainty analyses using fast probability integration. *Nuclear Engineering and Design, 166,* 225-248.

Heitzig, M., Sin, G., Sales-Cruz, M., Glarborg, P., & Gani, R. (2011). Computer-aided modeling framework for efficient model development, analysis and identification: Combustion and reactor modeling. *Industrial & Engineering Chemistry Research, 50(9),* 5253-5265.

Helton, J.C., & Davis, F.J. (2003). Latin hypercube sampling and the propagation of uncertainty in analyses of complex systems. *Reliability Engineering and System Safety, 81,* 23-69.

Hounslow, M.J., Ryall, R.L. & Marshall, V.R. (1988). A discretized population balance for nucleation, growth, and aggregation. *American Institute of Chemical Engineers Journal, 34(11),* 1821-1832.

Hu, Q., Rohani, S., Wang, D.X., & Jutan, A. (2005). Optimal control of a batch cooling seeded crystallizer. *Powder Technology,156,* 170-176.

Hulburt, H.M. & Katz, S. (1964). Some problems in particle technology: A statistical mechanical formulation. *Chemical Engineering Science, 19,* 555-574.

Iman, R.L., & Conover, W.J. (1982). A distribution-free approach to inducing rank correlation among input variables. *Communications in Statistics Part B – Simulation and Computation, 11(3),* 311-334.

Jones, A.G. (2002). *Crystallization process systems.* Butterworth-Heinimann.

Lee, K., Lee, J.H., Fujiwara, M., Ma, D.L., & Braatz, R.D. (2002). Run-to-run control of multidimensional crystal size distribution in a batch crystallizer. *Proceedings of the American Control Conference, Volumes 1-6,* 1013-1018.

Ma, D.L., Tafti, D.K., & Braatz, R.D. (2002). High-resolution simulation of multidimensional crystal growth. *Industrial and Engineering Chemistry Research,*

*41,* 6217-6223.

Ma, D.L., Chung, S.H., & Braatz, R.D. (1999). Worst-case performance analysis of optimal batch control trajectories. *American Institute of Chemical Engineers Journal, 45(7),* 1469-1476.

Mangin, D., Garcia, E., Gerard, S., Hoff, C., Klein, J.P. & Veesler, S. (2006). Modeling of the dissolution of a pharmaceutical compound. *Journal of Crystal Growth,* 286, 121-125.

Marchal, P., David, R., Klein, J.P., & Villermaux, J. (1988). Crystallization and precipitation engineering - I. An efficient method for solving population balance in crystallization with agglomeration. *Chemical Engineering Science, 43(1),* 59-67.

Modarresi, H., Conte, E., Abildskov, J., Gani, R., & Crafts, P. (2008). Model-based calculation of solid solubility for solvent selection – A review. *Industrial and Engineering Chemistry Research, 47(15),* 5234-5242.

Morris, M.D. (1991). Factorial sampling plans for preliminary computational experiments. *Technometrics, 33,* 161-174.

Mullin, J.W. (2001). *Crystallization (fourth edition)*. Butterworth-Heinimann.

Myers, R.H., Montgomery, D.C., & Anderson-Cook, C.M. (2009). *Response surface methodology: process and product optimization using designed experiments* (Third edition). John Wileys & Sons, Inc.

Myerson, A.S. (2002). *Handbook of industrial crystallization (second edition)*. Butterworth-Heinimann.

Nagy, Z.K., & Aamir E. (2012). Systematic design of supersaturation controlled crystallization processes for shaping the crystal size distribution using an analytical estimator. *Chemical Engineering Science, http://dx.doi.org/10.1016/j.ces.2012.08.048, in press.*

Nagy, Z.K., & Braatz R.D. (2012). Advances and new directions in crystallization control. *Annual Review of Chemical and Biomolecular Engineering, 3, 55-75.*

Nagy, Z.K. (2009). Model based robust control approach for batch crystallization product design. *Computers and Chemical Engineering, 33,* 1685-1691.

Nagy, Z.K., Fujiwara, M., & Braatz, R.D. (2008a). Modelling and control of combined cooling and antisolvent crystallization processes. *Journal of Process Control, 18,* 856-864.

Nagy, Z.K., Chew, J.W., Fujiwara, M., & Braatz, R.D. (2008b). Comparative performance of concentration and temperature controlled batch crystallizations. *Journal of Process Control, 18,* 399-407.

Nagy, Z.K., & Braatz, R.D. (2004). Open-loop and closed-loop robust optimal control of batch processes using distributional and worst-case analysis. *Journal of Process Control, 14,* 411-422.

Nagy, Z.K., & Braatz, R.D. (2003). Robust nonlinear model predictive control of batch processes. *American Institute of Chemical Engineers Journal, 49(7),* 1776-1786.

Omlin, M., & Reichert, P. (1999). A comparison of techniques for the estimation of model prediction uncertainty. *Ecological Modelling, 115,* 45-59.

Ouiazzane, S., Messnaoui, B., Abderafi, S., Wouters, J., & Bounahmidi, T. (2008). Estimation of sucrose crystallization kinetics from batch crystallizer data. *Journal of Crystal Growth, 310,* 798-803.

Paengjuntuek, W., Arpornwichanop, A., & Kittisupakorn, P. (2008). Product quality improvement of batch crystallizers by a batch-to-batch optimization and nonlinear control approach. *Chemical Engineering Journal, 139,* 344-350.

Puel, F., Févotte, G., & Klein, J.P. (2003). Simulation and analysis of industrial crystallization processes through multidimensional population balance equations. Part 1: a resolution algorithm based on the method of classes. *Chemical Engineering Science, 58,* 3715-3727.

Qamar, S., Ashfaq, A., Warnecke, G., Angelov, I., Elsner, M.P., & Seidel-Morgenstern, A. (2007). Adaptive high-resolution schemes for multidimensional population balances in crystallization processes. *Computers and Chemical Engineering, 31,* 1296-1311.

Quintana-Hernández, P, Bolaños-Reynoso, E., Miranda-Castro, B., & Salcedo-Estrada, L. (2004). Mathematical modeling and kinetic parameter estimation in batch crystallization. *American Institute of Chemical Engineers Journal, 50(7),* 1407-1417.

Ramkrishna, D. (2000). *Population balances. Theory and applications to particulate systems in engineering.* Academic Press, San Diego, USA.

Randolph, A.D., & Larson, M.A. (1988). *Theory of particulate processes (second edition)*. Academic Press, San Diego.

Rawlings, J.B., Miller, S.M., & Witkowski, W.R. (1993). Model identification and control of solution crystallization processes: A review. *Industrial and Engineering Chemistry Research, 32,* 1275-1296.

Saengchan, A., Kittisupakorn, P., Paengjuntuek, W., & Arpornwichanop, A. (2011). Improvement of batch crystallization control under uncertain kinetic parameters by model predictive control. *Journal of Industrial and Engineering Chemistry, 17,* 430-438.

Sales-Cruz, A.M. (2006). *Development of a computer aided modeling system for bio and chemical process and product design.* Ph.D. Thesis, Technical University of Denmark, Denmark.

Saltelli, A., Ratto, M., Tarantola, S., & Campolongo, F. (2006). Sensitivity analysis practices: strategies for model-based inference. *Reliability Engineering and System Safety, 91,* 1109-1125.

Samad, N.A.F.A., Sin, G., Gernaey, K.V., & Gani, R. (2012a). A systematic framework for design of process monitoring and control (PAT) systems for crystallization processes. *Computers and Chemical Engineering (Submitted)*.

Samad, N.A.F.A., Meisler, K.T., Sin, G., Gernaey, K.V., & Gani, R. (2012b). A generic framework for systematic design of process monitoring and control system for crystallization processes. *Submitted to the Proceedings of the 22nd European Symposium on Computer Aided Process Engineering*.

Samad, N.A.F.A., Meisler, K.T., Gernaey, K.V., von Solms, N.S., & Gani, R. (2012c). Systematic identification of crystallization kinetics within a generic modelling framework. *Computer-Aided Chemical Engineering, 31,* 945-949.

Samad, N.A.F.A., Sin, G., Gernaey, K.V., & Gani, R. (2012d). Introducing uncertainty analysis of nucleation and crystal growth models in Process Analytical Technology (PAT) sytem design of crystallization processes. *European Journal of Pharmaceutics and Biopharmaceutics (Submitted)*.

Samad, N.A.F.A., Singh, R., Sin, G., Gernaey, K.V., & Gani, R. (2011a). A generic multi-dimensional model-based system for batch cooling crystallization processes. *Computers and Chemical Engineering, 35,* 828-843.

Samad, N.A.F.A., Singh, R., Sin, G., Gernaey, K.V., & Gani, R. (2011b). Integration of generic multi-dimensional model and operational policies for batch cooling crystallization. *Computer-Aided Chemical Engineering, 29,* 86-90.

Samad, N.A.F.A., Singh, R., Sin, G., Gernaey, K.V., & Gani, R. (2010). Control of process operations and monitoring of product qualities through generic model-based in batch cooling crystallization. *Computer-Aided Chemical Engineering, 28,* 613-618.

Shi, D., El-Farra, N.H., Li, M., Mhaskar, P., & Christofides, P.D. (2006). Predictive control of particle size distribution in particulate processes. *Chemical Engineering Science, 61,* 268-281.

Sin, G., Gernaey, K.V., Neumann, M.B., van Loosdrecht, M.C.M., & Gujer, W. (2011). Global sensitivity analysis in wastewater treatment plant model applications: Prioritizing sources of uncertainty. *Water Research, 45,* 639-651.

Sin, G., Gernaey, K.V., & Lantz, A.E. (2009a). Good modeling practice for PAT applications: Propagation of input uncertainty and sensitivity analysis. *Biotechnology Progress, 25(4),* 1043-1053.

Sin, G., Gernaey, K.V., Neumann, M.B., van Loosdrecht, M.C.M., & Gujer, W. (2009b). Uncertainty analysis in WWTP model applications: A critical discussion using an example from design. *Water Research, 43,* 2894-2906.

Singh, R., Gernaey, K.V. & Gani, R. (2010). ICAS-PAT: A software for design, analysis and validation of PAT systems. *Computers and Chemical Engineering, 34,* 1108-1136.

Singh, R., Gernaey, K.V. & Gani, R. (2009). Model-based computer aided framework for design of process monitoring and analysis systems. *Computers and Chemical Engineering, 33,* 22-42.

Smith, R. (2005). *Chemical process design and integration*. John Wiley and Sons limited, West Sussex, UK.

Thomsen, K., Rasmussen, P., & Gani, R. (1998). Simulation and optimization of fractional crystallization processes. *Chemical Engineering Science, 53(8),* 1551-1564.

Wibowo, C., & Ng, K.M. (2001). Operational issues in solids processing plants: systems view. *American Institute of Chemical Engineers Journal, 47(1),* 107-125.

Zhang, G.P., & Rohani, S. (2004). Dynamic optimal control of batch crystallization processes. *Chemical Engineering Communications, 191(3),* 356-372.

Zhang, G.P., & Rohani, S. (2003). On-line optimal control of a seeded batch cooling crystallizer. *Chemical Engineering Science,* 58(9), 1887-1896.

This PhD-project was carried out at CAPEC, the Computer Aided Product-Process Engineering Center.
CAPEC is committed to research, to work in close collaboration with industry and to participate in educational activities. The research objectives of CAPEC are to develop computer-aided systems for product/process simulation, design, analysis and control/operation for chemical, petrochemical, pharmaceutical and biochemical industries. The dissemination of the research results of CAPEC is carried out in terms of computational tools, technology and application. Under computational tools, CAPEC is involved with mathematical models, numerical solvers, process/operation mathematical models, numerical solvers, process simulators, process/product synthesis/design toolbox, control toolbox, databases and many more. Under technology, CAPEC is involved with development of methodologies for synthesis/design of processes and products, analysis, control and operation of processes, strategies for modelling and simulation, solvent and chemical selection and design, pollution prevention and many more. Under application, CAPEC is actively involved with developing industrial case studies, tutorial case studies for education and training, technology transfer studies together with industrial companies, consulting and many more.

Further information about CAPEC can be found at www.capec.kt.dtu.dk.

Computer Aided Process Engineering Center
Department of Chemical and Biochemical Engineering
Technical University of Denmark
Søltofts Plads, Building 229
DK-2800 Kgs. Lyngby
Denmark

Phone: +45 4525 2800
Fax: +45 4525 4588
Web: www.capec.kt.dtu.dk

ISBN : 978-87-92481-87-0